A functional renormalization group approach to interacting disordered electron systems

Zur Erlangung des akademischen Grades eines

DOKTORS DER NATURWISSENSCHAFTEN

von der Fakultät für Physik des
Karlsruher Instituts für Technologie (KIT)
genehmigte

DISSERTATION

von

Dipl. Phys. Christian Seiler
aus Stuttgart

Tag der mündlichen Prüfung: 15.01.2016
Referent: Prof. Dr. Ferdinand Evers
Korreferent: Prof. Dr. Alexander Mirlin

Fakultät für Physik
Institut für Theorie der Kondensierten Materie

A functional renormalization group approach to interacting disordered electron systems

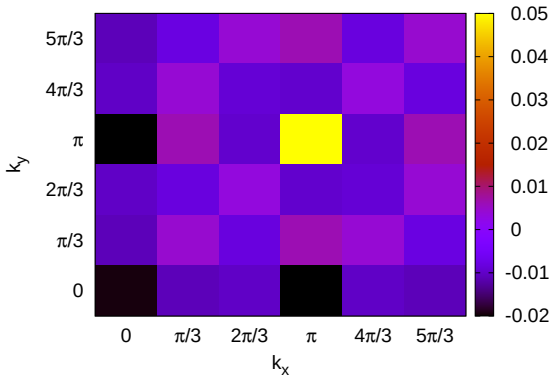

PhD thesis
by
Christian Seiler

Instructor:	Prof. Dr. Ferdinand Evers
2nd Instructor:	Prof. Dr. Alexander Mirlin

Hiermit erkläre ich, dass ich die Dissertation selbständig und nur unter Verwendung der angegebenen Hilfsmittel angefertigt habe.

Karlsruhe, den 19.12.2016

To my parents

for always supporting and encouraging me
in my endeavors

Introduction

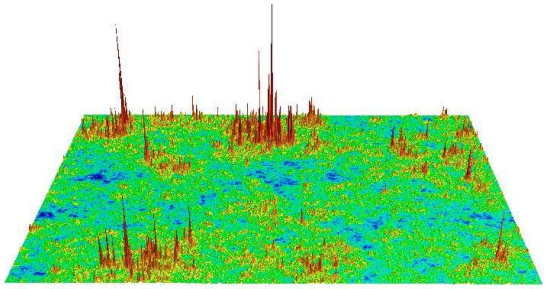

Figure 1: *A numerical simulation of a multifractal wave function at the Quantum Hall transition, courtesy of Achim Mildenberger and Ferdinand Evers, 2003.*

In the past century the study of disordered systems has been a highly fruitful enterprise. Many modern physical effects, such as the Quantum Hall effect, can be fully understood only if the role of disorder is taken into account. One of the earliest contributions was Drude's (classical) model for the electrical conductivity. [1] It explains on a classical level why metals have a finite conductivity: electrons are constantly scattered on disordered ions in the metal, loosing their forward momentum. Else the electrical field along a wire would constantly accelerate the charge carriers. Current models of diffusive transport are more sophisticated in their treatment of the microscopic environment, but the basic idea championed by Drude, that disorder causes electrons to scatter and give up their forward momentum, leading to a finite conductivity, remains valid until today.

Typically metals are weakly disordered systems, well-situated within the diffusive parameter regime. (As long as there is no phase transition to e.g. a superconductor.) But it is possible to increase disorder further, especially in semiconductors. An obvious limit imposed here is through classical percolation: if the disorder is so strong that there are no paths anymore that connect the leads one has attached to the sample, it will not be possible to send a current through the system.[1]

[1] If the sample is large enough, quantum mechanical electron tunneling is suppressed exponentially.

In 1958 P. W. Anderson suggested that quantum mechanics could cause electronic states to localize well before the classical percolation limit, completely suppressing (diffusive) transport in such systems. [2] This phenomenon is known today as "Anderson localization" or "strong localization". It occurs in three dimensions for sufficiently strong disorder (larger than a threshold value) and in two or one dimension for any finite value of disorder. (At least within the model that Anderson treated. See below for exceptions.) We should note that localization means that the quantum mechanical wave functions of the system decay exponentially with on a length scale called the localization length, ξ. This means that even in the localized regime transport through a one- or two-dimensional system may still be possible, provided it is small enough.

Anderson localization arises due to quantum mechanical interference between scattering paths of wave functions, essentially trapping the wave functions in a finite volume. Together with Abrahams, Licciardello, and Ramakrishnan, Anderson later proposed that localization can be understood in terms of scaling, i.e. how the conductivity of a system changes with the system size. [3] They showed that "there is no true metallic behavior" in two dimensions, as the so-called β-function (which is defined as the logarithmic derivative of the conductance, $\beta(g) = \mathrm{d}(\ln G)/\mathrm{d}(\ln L)$) is strictly negative for $d \leq 2$ and only approaches 0 asymptotically for $d = 2$. This approach to understanding localization has been widely successful and is one of the cornerstones of the modern view on disordered systems.

There have been countless developments since, but two of the most important include the symmetry classification of disordered systems (pioneered among others by Zirnbauer, [4]) and the nonlinear σ-model description of disordered systems, which was first introduced by Gell-Mann to describe β decay [5] but has since been adopted in condensed matter theory. It turns out that non-interacting disordered systems can be classified into one of 10 symmetry classes that fully determine the effective low-energy excitations of the system at large length scales. σ-models are the effective field theories associated with each of the symmetry classes. Within these field theories it is possible to calculate corrections to the standard Drude conductivity in the diffusive regime that arise due to quantum interference. Weak localization is one such correction, where the resistivity in the diffusive regime increases due to localization effects of the wave function. This is often considered a precursor to Anderson localization. Research into different symmetry groups has also lead to the opposite effect in certain spin-orbit coupled systems, called weak antilocalization. There the resistivity is reduced due to quantum interference effects.

The study of symmetry groups ties into the concept of topological insulators as well. σ-models of different symmetry groups may allow for the existence of an additional "topological term" in the action in certain dimensions. For example, the quantum spin Hall (QSHE) phase is characterized by an additional topological invariant that distinguishes it from an ordinary insulator. This implies the presence of surface states that

are protected by symmetry (and thus insensitive to edge effects) in a system that is otherwise a bulk insulator. A more complete discussion of the Quantum Spin Hall Effect is available from Kane and Mele. [6] Also characterized by a topological invariant is the standard quantum Hall effect (QHE). [7] The transition between plateaus of the quantum Hall effect is an insulator-insulator transition between two different ground states characterized by different Chern numbers. Wave functions at the critical Anderson transition between these states exhibit multifractal behavior, as can be seen in Fig. 1. Many of these topics are reviewed in [8], which is a good starting point to obtain an overview of the field.

The effects mentioned here are part of a plethora of phenomena that occur in disordered quantum systems. It is important to note that all of these phenomena can be found even when neglecting the interactions between the electrons. At low temperatures, where renormalization effects due to the interaction between the electrons start to play an increasingly important role, [9] it stands to reason that a proper description of some systems is only possible if interactions are included. And while this is a very difficult problem to tackle, there have been plenty of successes in attacking this problem. A good starting point to obtain an overview over some recent developments is [8].

A major issue with many analytical and numerical developments is that they make assumptions that restrict their applicability in terms of the disorder strength. For example, many methods are only valid in the diffusive regime, where the disorder strength is low. Our goal is to develop a new numerical tool that takes disorder into account exactly, but is also capable of analyzing interaction effects beyond the mere mean field level.

Our method of choice is the functional renormalization group. While it has mainly been applied to homogeneous or single impurity systems, it has been very successful at that. The main reason for its success is that it provides an a priori unbiased view on instabilities on the system. It has been applied to determining the leading instabilities in different parameter regimes of the Hubbard model (e.g. [10, 11, 12, 13, 14]), single impurity models (e.g. [15]) and even spin systems (e.g. [16, 17, 18]). A good overview is given by the recent review on the functional renormalization group in [19].

The basic principle begins the functional renormalization group is to introduce an artificial infrared cutoff Λ into the bare propagator of the system by means of a regularization function. This causes all quantities of the system to acquire a dependency on the cutoff. The regularizer is chosen in such a way that at $\Lambda \to \infty$ we may trivially write down what the self-energy and the interaction vertex look like. The derivatives of these quantities form a hierarchy of flow equations that we will integrate numerically. At $\Lambda \to 0$ the modified propagator turns into the physical propagator of the system, so after the numerical integration of the flow equations we have (in principle) obtained the values of the self-energy and the interaction vertex of the interacting system.

Our goal is to formulate the FRG in terms of the eigenbasis of the non-interacting

part of the Hamiltonian that includes disorder exactly. The flow equations will then inform us how interactions play a role for a given disorder configuration; averaging over disorder is performed at the end.

1 Structure of this thesis

The first chapter contains the derivation of all equations related to the FRG procedure: the flow equations, the initial conditions and how to obtain observables, starting from the generic FRG equations found in the literature. Our second chapter will discuss implementation details of our numerics. The focus of the third chapter is to demonstrate the validity of our method by comparing it against other reference methods. We will discuss the central approximation we make to be able to reach larger system sizes. The fourth chapter will apply the methodology we have developed to look into the phase diagram of the model system we study.

Large parts of this thesis have also been published in Ref. 20.

Acknowledgments

There are many people that I'd like to thank and without them this thesis would not have been possible. First and foremost I'm grateful to my thesis advisor Prof. Dr. Ferdinand Evers for all his support and encouragement, and for being a great teacher, always coming up with alternative perspectives on problems. I'd also like to thank Prof. Dr. Alexander Mirlin for agreeing to be my second examiner and for his support throughout my time in Karlsruhe.

My thanks go to Soumya Bera for coming up with the idea of applying the functional renormalization group method to disordered problems. I am also grateful to Prof. Dr. Peter Wölfle and especially Prof. Dr. Johannes Reuther for their insights and discussions on the functional renormalization group at the start of my thesis.

My time at the Institute for Theoretical Condensed Matter physics (TKM) in Karlsruhe was wonderful due to the fantastic atmosphere present, which encouraged discussions and the exchange of ideas, and provided a rich learning environment. The administrative help of Roswitha Schrempp and later Fabienne Flatter was invaluable. I'm also grateful to all of the professors for their outstanding lectures on a large variety of different topics and their excellent selection of invited speakers. Beyond that, discussions with many people at the institute have furthered my understanding of physics, but in particular I'd like to thank Michael Schütt, Sam Carr, Elio König, Stephane Ngo Dinh, Ulf Briskot and Michael Walz. I'd also like to thank the people at the Institute for Nanotechnology (INT) in Karlsruhe for the environment they provided, especially the meeting of different disciplines in a single place, allowing me to look beyond my own nose and broaden my horizon.

I wish to express my gratitude to the members of the Institute for Theoretical Physics in Regensburg, who have graciously welcomed me after my move there. In particular I'd like to thank Robert Hrdina, without whose assistance in administrative matters I would have been at a severe disadvantage.

I am also very grateful to Felix Weiner, who has provided me with the DMRG results used for comparison in Sec. 3.6.1 and was always available for discussions.

Finally, I'd like to acknowledge financial support by the Landesgraduiertenförderung Baden-Württemberg and the Deutsche Forschungsgemeinschaft.

Thank You!

Contents

List of Figures

Chapter 1

1 Methodology: Functional Renormalization Group

In this chapter we give an overview over the basic idea of the functional renormalization group method and derive the equations required for our study of inhomogeneous systems.

1.1 Flow equations

We begin with an interacting Fermionic Hamiltonian H, decomposing it into its non-interacting and interacting parts,

$$H = H_0 + U. \tag{1.1}$$

The non-interacting part may be diagonalized,

$$H_0 |\alpha\rangle = \epsilon_\alpha |\alpha\rangle . \tag{1.2}$$

The entire Hamiltonian may now be written in terms of this basis,

$$H = \sum_\alpha \epsilon_\alpha \hat{c}^\dagger_\alpha \hat{c}_\alpha + \frac{1}{4} \sum_{\alpha\beta\gamma\delta} U_{\alpha\beta\gamma\delta} \hat{c}^\dagger_\alpha \hat{c}^\dagger_\beta \hat{c}_\delta \hat{c}_\gamma, \tag{1.3}$$

where $U_{\alpha\beta\gamma\delta}$ is the antisymmetrized interaction matrix element. (In the following we will assume that higher order interactions are absent.) In the case of a clean system the states α correspond to the quasi-momentum (and possibly the spin of the particles).

The functional renormalization group introduces a cutoff in the bare propagator. While it is also possible to use a cutoff in momentum space in clean systems (see e.g. [10]), we are interested in studying inhomogeneous systems, where there is no regularity

in the single-particle states, hence we use a cutoff in frequency space instead. Following Eq. (57) in Ref. 19, our modified propagator now reads

$$\mathcal{G}^{0,\Lambda}(\mathrm{i}\omega) = \frac{\Theta^{\Lambda}(\omega)}{\mathrm{i}\omega - H_0 + \mu_{\mathrm{chem}}}, \tag{1.4}$$

where $\Theta^{\Lambda}(\omega)$ has the property of vanishing at $\Lambda \to \infty$ and approaching 1 at $\Lambda \to 0$; we will discuss our choice for $\Theta^{\Lambda}(\omega)$ further along.

The introduction of this artificial infrared cutoff Λ into the propagator makes all other quantities of the system depend on Λ. If we take the limit of $\Lambda \to \infty$, it can be shown (see Eq (31) in Ref. 19) that the self-energy is zero and the effective interaction vertex Γ is given by the bare interaction $\hat{U}$. On the other hand, taking the limit of $\Lambda \to 0$, we recover the original system without the introduced cutoff. There is now a continuous variable that connects the real system ($\Lambda \to 0$), where the physical quantities are not known *a priori*, with a trivial system ($\Lambda \to \infty$), where all quantities are known.

It is now possible to calculate the derivatives of the vertex functions (self-energy, two-particle vertex, etc.) with respect to Λ. This gives us a hierarchy of differential equations that give us the physical quantities when integrated. In this sense on can draw a comparison to the classical RG, because in the functional RG we integrate a set of coupled differential equations along a cutoff.

We will defer to Chapter. 4 of [21] for the derivation of the most generic form of the flow equations, as that is quite involved. To summarize: one starts with the generating functional for the vertex functions in a path integral formulation, whose derivative with respect to Λ can be calculated if one replaces the bare propagator in the action with Eq. 1.4. The resulting expression for the derivative can then be expanded in terms of the Grassman fields of the generating functional and comparing the coefficients yields the flow equations.

The flow equation for the self-energy, Eq. (50) in Ref. 19, reads

$$\frac{\mathrm{d}}{\mathrm{d}\Lambda}\Sigma^{\Lambda}(x', x) = \sum_{y,y'} \mathcal{S}^{\Lambda}(y, y')\Gamma^{\Lambda}(x', y'; x, y), \tag{1.5}$$

and that for the vertex, Eq. (52) in Ref. 19,

$$\begin{aligned}
&\frac{\mathrm{d}}{\mathrm{d}\Lambda}\Gamma^{\Lambda}(x_1', x_2'; x_1, x_2) \\
&\quad = \sum_{y_1, y_1'} \sum_{y_2, y_2'} \mathcal{G}^{\Lambda}(y_1, y_1')\mathcal{S}^{\Lambda}(y_2, y_2') \\
&\quad \times \Big\{ \Gamma^{\Lambda}(x_1', x_2'; y_1, y_2)\Gamma^{\Lambda}(y_1', y_2'; x_1, x_2) \\
&\quad - \Big[\Gamma^{\Lambda}(x_1', y_2'; x_1, y_1)\Gamma^{\Lambda}(y_1', x_2'; y_2, x_2) + (y_1 \leftrightarrow y_2, y_1' \leftrightarrow y_2')\Big] \\
&\quad + \Big[\Gamma^{\Lambda}(x_2', y_2'; x_1, y_1) \times \Gamma^{\Lambda}(y_1', x_1'; y_2, x_2) + (y_1 \leftrightarrow y_2, y_1' \leftrightarrow y_2')\Big] \Big\} \\
&\quad - \sum_{y, y'} \mathcal{S}^{\Lambda}(y, y')\Gamma^{(6),\Lambda}(x_1', x_2', y'; x_1, x_2, y).
\end{aligned} \tag{1.6}$$

Furthermore, we adopt the definition of Eq. (47) in Ref. 19 for the so-called single-scale propagator,

$$\mathcal{S}^{\Lambda} = -\mathcal{G}^{\Lambda}\left[\frac{\mathrm{d}}{\mathrm{d}\Lambda}\left(\mathcal{G}^{0,\Lambda}\right)^{-1}\right]\mathcal{G}^{\Lambda}. \tag{1.7}$$

We translate these quantities into our own nomenclature, where we explicitly write out prefactors for sums and integrals, use units of $\hbar = 1$ and $\mathrm{k_B} = 1$, and work in Matsubara space. Furthermore, we separate the generic indices into Matsubara frequencies and Hilbert space indices, $x = (\mu, \omega_n)$.

Since energy is conserved, we may rewrite the self-energy, the single-particle Green's functions, the single-scale propagator and the vertex to include the corresponding δ-function,

$$\Sigma^{\Lambda}_{\alpha\beta}(\omega_n; \omega_{n'}) \rightarrow T^{-1}\delta_{n,n'}\Sigma^{\Lambda}_{\alpha\beta}(\omega_n), \tag{1.8}$$

$$\mathcal{G}^{0,\Lambda}_{\alpha\beta}(\omega_n; \omega_{n'}) \rightarrow T^{-1}\delta_{n,n'}\mathcal{G}^{0,\Lambda}_{\alpha\beta}(\omega_n), \tag{1.9}$$

$$\mathcal{G}^{\Lambda}_{\alpha\beta}(\omega_n; \omega_{n'}) \rightarrow T^{-1}\delta_{n,n'}\mathcal{G}^{\Lambda}_{\alpha\beta}(\omega_n), \tag{1.10}$$

$$\mathcal{S}^{\Lambda}_{\alpha\beta}(\omega_n; \omega_{n'}) \rightarrow T^{-1}\delta_{n,n'}\mathcal{S}^{\Lambda}_{\alpha\beta}(\omega_n), \tag{1.11}$$

$$\begin{aligned}
\Gamma^{\Lambda}_{\alpha\beta\gamma\delta}(\omega_n, \omega_{\tilde{n}}; \omega_{n'}, \omega_{\tilde{n}'}) \rightarrow\ & T^{-1}\delta_{n+\tilde{n},n'+\tilde{n}'} \times \\
& \Gamma^{\Lambda}_{\alpha\beta\gamma\delta}(\omega_n, \omega_{\tilde{n}}; \omega_{n'}, \omega_{\tilde{n}'}).
\end{aligned} \tag{1.12}$$

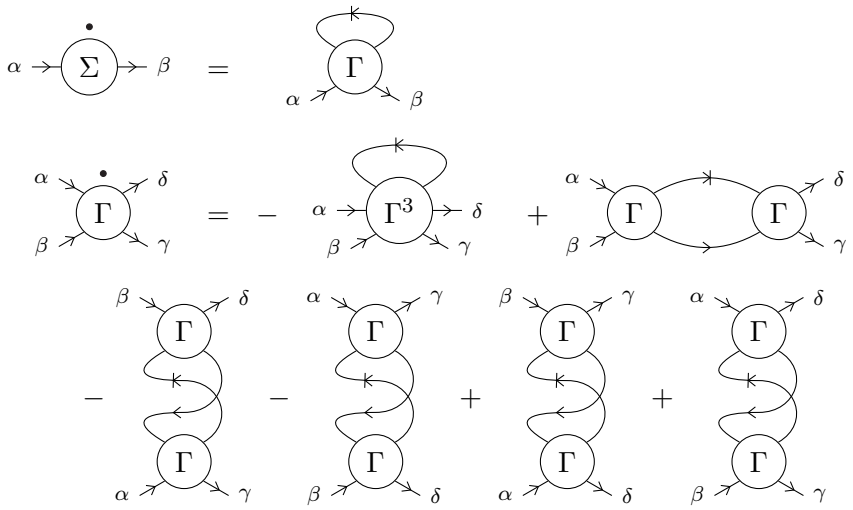

Figure 1.1: *Diagrammatic representation of the FRG flow equations for the self-energy Σ^Λ and the vertex Γ^Λ. An additional bar denotes the single-scale propagator $\mathcal{S}^\Lambda$, the other propagators are $\mathcal{G}^\Lambda$. External legs do not entail a propagator.*

Inserting this into Eq. (1.5), one obtains

$$\begin{aligned}\frac{\mathrm{d}}{\mathrm{d}\Lambda}T^{-1}\delta_{n,n'}\Sigma^\Lambda_{\alpha\beta}(\omega_n) &= T^2\sum_{\omega_m\omega_{m'}}\sum_{\mu\nu}\mathcal{S}^\Lambda_{\mu\nu}(\omega_m)\times \\ &\quad \Gamma^\Lambda_{\alpha\nu\beta\mu}(\omega_n,\omega_{m'};\omega'_n,\omega_m)\times \\ &\quad T^{-1}\delta_{m,m'}T^{-1}\delta_{n+m',n'+m}, \end{aligned} \tag{1.13}$$

and after evaluating the sum over the Matsubara frequency $\omega_{m'}$, one arrives at

$$\begin{aligned}\frac{\mathrm{d}}{\mathrm{d}\Lambda}\Sigma^\Lambda_{\alpha\beta}(\omega_n) &= T\sum_{\omega_m}\sum_{\mu\nu}\mathcal{S}^\Lambda_{\mu\nu}(\omega_m)\times \\ &\quad \Gamma^\Lambda_{\alpha\nu\beta\mu}(\omega_n,\omega_m;\omega_n,\omega_m). \end{aligned} \tag{1.14}$$

Here, we have used that a $\delta_{n,n'}$ appears on both sides and have multiplied the equation by T.

In the same way the equation for the flow of the vertex, Eq. (1.6) may be converted to our notation, again multiplying the equation by T and recognizing that all Kronecker-δs

on the right hand side reduce to the $\delta_{n+\tilde{n},n'+\tilde{n}'}$. We arrive at

$$\begin{aligned}\frac{\mathrm{d}}{\mathrm{d}\Lambda}\Gamma^{\Lambda}_{\alpha\beta\gamma\delta}(\omega_n,\omega_{\tilde{n}};\omega_{n'},\omega_{\tilde{n}'}) &= T\sum_{\omega_m\omega_{\tilde{m}}}\sum_{\mu\nu\rho\sigma}\mathcal{G}^{\Lambda}_{\rho\mu}(\omega_m)\mathcal{S}^{\Lambda}_{\sigma\nu}(\omega_{\tilde{m}})\times\Big\{\\ &\quad\Gamma^{\Lambda}_{\alpha\beta\rho\sigma}(\omega_n,\omega_{\tilde{n}};\omega_m,\omega_{\tilde{m}})\Gamma^{\Lambda}_{\mu\nu\gamma\delta}(\omega_m,\omega_{\tilde{m}};\omega_{n'},\omega_{\tilde{n}'})\delta^{(\mathrm{c})}_{\tilde{m}}\\ &\quad+\Big[\Gamma^{\Lambda}_{\beta\nu\gamma\rho}(\omega_{\tilde{n}},\omega_{\tilde{m}};\omega_{n'},\omega_m)\Gamma^{\Lambda}_{\mu\alpha\sigma\delta}(\omega_m,\omega_n;\omega_{\tilde{m}},\omega_{\tilde{n}'})\delta^{(\mathrm{ph},1)}_{\tilde{m}}\\ &\quad\quad+\Gamma^{\Lambda}_{\beta\mu\gamma\sigma}(\omega_{\tilde{n}},\omega_m;\omega_{n'},\omega_{\tilde{m}})\Gamma^{\Lambda}_{\nu\alpha\rho\delta}(\omega_{\tilde{m}},\omega_n;\omega_m,\omega_{\tilde{n}'})\delta^{(\mathrm{ph},2)}_{\tilde{m}}\Big]\\ &\quad-\Big[\Gamma^{\Lambda}_{\alpha\nu\gamma\rho}(\omega_n,\omega_{\tilde{m}};\omega_{n'},\omega_m)\Gamma^{\Lambda}_{\mu\beta\sigma\delta}(\omega_m,\omega_{\tilde{n}};\omega_{\tilde{m}},\omega_{\tilde{n}'})\delta^{(\mathrm{ph},3)}_{\tilde{m}}\\ &\quad\quad+\Gamma^{\Lambda}_{\alpha\mu\gamma\sigma}(\omega_n,\omega_m;\omega_{n'},\omega_{\tilde{m}})\Gamma^{\Lambda}_{\nu\beta\rho\delta}(\omega_{\tilde{m}},\omega_{\tilde{n}};\omega_m,\omega_{\tilde{n}'})\delta^{(\mathrm{ph},4)}_{\tilde{m}}\Big]\Big\}\\ &\quad-T\sum_{\omega_m}\sum_{\mu\nu}\mathcal{S}^{\Lambda}_{\mu\nu}(\omega_m)\Gamma^{(6),\Lambda}_{\alpha\beta\nu\gamma\delta\mu}(\omega_n,\omega_{\tilde{n}},\omega_m;\omega_{n'},\omega_{\tilde{n}'},\omega_m),\end{aligned}\tag{1.15}$$

where $\delta^{(\mathrm{c})}_{\tilde{m}}$ and $\delta^{(\mathrm{ph},\cdot)}_{\tilde{m}}$ respect the energy conservation of the vertex, e.g. $\delta^{\mathrm{c}}_{\tilde{m}}=\delta_{n+\tilde{n},m+\tilde{m}}$. To simplify the notation, we kept a sum over $\tilde{m}$, even though it may be evaluated immediately. A diagrammatic representation of these flow equations may be found in Fig. 1.1.

We employ the standard truncation scheme described in Ref. 19 by neglecting $\Gamma^{(6),\Lambda}$ and higher order terms, effectively dropping the last term of Eq. (1.15). We note that this precludes us from performing calculations with the bare (unscreened) Coulomb interaction, as a long-range interaction will violate the power counting argument used to neglect these terms.

1.2 Formalism at Zero Temperature

For the most part, we will discuss the Formalism at $T=0$. In that case, sums over Matsubara frequencies are replaced by integrals,

$$T\sum_{\omega_n}\to(2\pi)^{-1}\int\mathrm{d}\omega.\tag{1.16}$$

Accordingly, the Kronecker-δs will be replaced by δ functions,

$$T^{-1}\delta_{n,n'}\to 2\pi\delta(\omega-\omega').\tag{1.17}$$

Eqs. (1.14,1.15) now read

$$\frac{\mathrm{d}}{\mathrm{d}\Lambda}\Sigma^{\Lambda}_{\alpha\beta}(\omega) = \frac{1}{2\pi}\int \mathrm{d}\bar{\omega}\sum_{\mu\nu}\mathcal{S}^{\Lambda}_{\mu\nu}(\bar{\omega})\Gamma^{\Lambda}_{\alpha\nu\beta\mu}(\omega,\bar{\omega};\omega,\bar{\omega}), \tag{1.18}$$

$$\begin{aligned}\frac{\mathrm{d}}{\mathrm{d}\Lambda}\Gamma^{\Lambda}_{\alpha\beta\gamma\delta}(\omega,\tilde{\omega};\omega',\tilde{\omega}') = \frac{1}{2\pi}\int \mathrm{d}\bar{\omega}\mathrm{d}\bar{\omega}'\sum_{\mu\nu\rho\sigma}\mathcal{G}^{\Lambda}_{\rho\mu}(\bar{\omega})\mathcal{S}^{\Lambda}_{\sigma\nu}(\bar{\omega}')\times\Big\{ \\ \Gamma^{\Lambda}_{\alpha\beta\rho\sigma}(\omega,\tilde{\omega};\bar{\omega},\bar{\omega}')\Gamma^{\Lambda}_{\mu\nu\gamma\delta}(\bar{\omega},\bar{\omega}';\omega',\tilde{\omega}')\delta^{(\mathrm{c})}(\bar{\omega}') \\ +\Big[\Gamma^{\Lambda}_{\beta\nu\gamma\rho}(\tilde{\omega},\bar{\omega}';\omega',\bar{\omega})\Gamma^{\Lambda}_{\mu\alpha\sigma\delta}(\bar{\omega},\omega;\bar{\omega}',\tilde{\omega}')\delta^{(\mathrm{ph},1)}(\bar{\omega}') \\ +\Gamma^{\Lambda}_{\beta\mu\gamma\sigma}(\tilde{\omega},\bar{\omega};\omega',\bar{\omega}')\Gamma^{\Lambda}_{\nu\alpha\rho\delta}(\bar{\omega}',\omega;\bar{\omega},\tilde{\omega}')\delta^{(\mathrm{ph},2)}(\bar{\omega}')\Big] \\ -\Big[\Gamma^{\Lambda}_{\alpha\nu\gamma\rho}(\omega,\bar{\omega}';\omega',\bar{\omega})\Gamma^{\Lambda}_{\mu\beta\sigma\delta}(\bar{\omega},\tilde{\omega};\bar{\omega}',\tilde{\omega}')\delta^{(\mathrm{ph},3)}(\bar{\omega}') \\ +\Gamma^{\Lambda}_{\alpha\mu\gamma\sigma}(\omega,\bar{\omega};\omega',\bar{\omega}')\Gamma^{\Lambda}_{\nu\beta\rho\delta}(\bar{\omega}',\tilde{\omega};\bar{\omega},\tilde{\omega}')\delta^{(\mathrm{ph},4)}(\bar{\omega}')\Big]\Big\},\end{aligned} \tag{1.19}$$

where again, $\delta^{(\mathrm{c})}(\bar{\omega}')$ and $\delta^{(\mathrm{ph},\cdot)}(\bar{\omega}')$ respect the energy conservation of the vertex, e.g. $\delta^{(\mathrm{ph},1)}(\bar{\omega}') = \delta(\tilde{\omega}+\bar{\omega}'-\omega'-\bar{\omega})$.

We now proceed to take the static limit, i.e. by projecting all frequencies in these equations to zero. For short-range interactions, power counting of the flow equations demonstrates that the dominant contribution for small Λ comes from zero frequencies and states close to the Fermi energy. This has been discussed extensively in [19], which we will defer to here.

Taking the static limit, we arrive at

$$\frac{\mathrm{d}}{\mathrm{d}\Lambda}\Sigma^{\Lambda}_{\alpha\beta} = \frac{1}{2\pi}\int \mathrm{d}\bar{\omega}\sum_{\mu\nu}\mathcal{S}^{\Lambda}_{\mu\nu}(\bar{\omega})\Gamma^{\Lambda}_{\alpha\nu\beta\mu}, \tag{1.20}$$

$$\begin{aligned}\frac{\mathrm{d}}{\mathrm{d}\Lambda}\Gamma^{\Lambda}_{\alpha\beta} = \frac{1}{2\pi}\int \mathrm{d}\bar{\omega}\sum_{\mu\nu\rho\sigma}\Big\{\mathcal{G}^{\Lambda}_{\rho\mu}(\bar{\omega})\mathcal{S}^{\Lambda}_{\sigma\nu}(-\bar{\omega})\Gamma^{\Lambda}_{\alpha\beta\rho\sigma}\Gamma^{\Lambda}_{\mu\nu\gamma\delta} \\ +\mathcal{G}^{\Lambda}_{\rho\mu}(\bar{\omega})\mathcal{S}^{\Lambda}_{\sigma\nu}(\bar{\omega})\Big[\Gamma^{\Lambda}_{\beta\nu\gamma\rho}\Gamma^{\Lambda}_{\mu\alpha\sigma\delta}+\Gamma^{\Lambda}_{\beta\mu\gamma\sigma}\Gamma^{\Lambda}_{\nu\alpha\rho\delta}\Big] \\ -\mathcal{G}^{\Lambda}_{\rho\mu}(\bar{\omega})\mathcal{S}^{\Lambda}_{\sigma\nu}(\bar{\omega})\Big[\Gamma^{\Lambda}_{\alpha\nu\gamma\rho}\Gamma^{\Lambda}_{\mu\beta\sigma\delta}+\Gamma^{\Lambda}_{\alpha\mu\gamma\sigma}\Gamma^{\Lambda}_{\nu\beta\rho\delta}\Big]\Big\}.\end{aligned} \tag{1.21}$$

Note that the vertex Γ^{Λ} is antisymmetric under exchange of the first or the last pair of indices,

$$\Gamma^{\Lambda}_{\alpha\beta\gamma\delta} = -\Gamma^{\Lambda}_{\beta\alpha\gamma\delta} = -\Gamma^{\Lambda}_{\alpha\beta\delta\gamma} = \Gamma^{\Lambda}_{\beta\alpha\delta\gamma}. \tag{1.22}$$

We now choose our cutoff $\Theta^{\Lambda}(\omega)$ to be a simple step function,

$$\Theta^{\Lambda}(\omega) = \Theta(|\omega|-\Lambda), \tag{1.23}$$

such that its derivative is

$$\frac{\mathrm{d}}{\mathrm{d}\Lambda}\Theta^{\Lambda}(\omega) = -\delta(|\omega| - \Lambda). \tag{1.24}$$

Since the self-energy is not frequency dependent anymore, the frequency integrals may now be solved analytically. For Eq. (1.20), we have to integrate

$$\int \mathrm{d}\bar{\omega}\mathcal{S}^{\Lambda}_{\mu\nu}(\bar{\omega}).$$

For the purpose of the integration, we will drop the indices, but remember that the objects occurring are matrices and hence do not (in general) commute. Inserting Dyson's equation into Eq. (1.7), we have

$$\begin{aligned} \mathcal{S} &= -\mathcal{G}\left(\frac{\mathrm{d}}{\mathrm{d}\Lambda}\left[\mathcal{G}^{0}\right]^{-1}\right)\mathcal{G} = -\mathcal{G}\left(\frac{\mathrm{d}}{\mathrm{d}\Lambda}\left[\mathcal{G}^{-1} + \Sigma\right]\right)\mathcal{G} \\ &= \dot{\mathcal{G}} - \mathcal{G}\dot{\Sigma}\mathcal{G}. \end{aligned} \tag{1.25}$$

We note that $\mathcal{G} = (\mathcal{Q} - \Theta\Sigma)^{-1}\Theta$, where we use the shorthand $\Theta = \Theta(|\omega| - \Lambda)$ and $\mathcal{Q} = \mathrm{i}\omega - H_0 + \mu_{\mathrm{chem}}$. Using $\frac{\mathrm{d}}{\mathrm{d}\Lambda}A^{-1}(\Lambda) = -A^{-1}(\Lambda)\dot{A}(\Lambda)A^{-1}(\Lambda)$, simple algebra yields

$$\mathcal{S} = -\delta\left(\mathbb{1} + \frac{\Theta}{\mathcal{Q} - \Theta\Sigma}\Sigma\right)\frac{1}{\mathcal{Q} - \Theta\Sigma}. \tag{1.26}$$

Since the δ and Θ functions are to be taken at the same argument, we employ Morris's Lemma[22] to resolve this,

$$\mathcal{S} = -\delta\int_0^1 \mathrm{d}t\left(\mathbb{1} + t\frac{1}{\mathcal{Q} - t\Sigma}\Sigma\right)\frac{1}{\mathcal{Q} - t\Sigma}. \tag{1.27}$$

Using the fact that

$$\frac{\mathrm{d}}{\mathrm{d}t}\frac{1}{\mathcal{Q} - t\Sigma} = \frac{1}{\mathcal{Q} - t\Sigma}\Sigma\frac{1}{\mathcal{Q} - t\Sigma}$$

and partial integration, the second summand of the integral yields

$$-\left[\frac{t}{\mathcal{Q} - t\Sigma}\right]_0^1 + \int_0^1 \mathrm{d}t\frac{1}{\mathcal{Q} - t\Sigma},$$

where it can be seen that the remaining integral cancels the first summand of the integral in Eq. (1.27), so we arrive at

$$\mathcal{S}^{\Lambda}_{\mu\nu}(\omega) = -\left.\frac{\delta(|\omega| - \Lambda)}{\mathrm{i}\omega - H_0 + \mu_{\mathrm{chem}} - \Sigma^{\Lambda}}\right|_{\mu\nu}. \tag{1.28}$$

The frequency integral is now trivial, yielding

$$\int \mathrm{d}\bar{\omega}\mathcal{S}^{\Lambda}_{\mu\nu}(\bar{\omega}) = -\sum_{\bar{\omega}=\pm\Lambda} \left.\frac{1}{\mathrm{i}\bar{\omega} - H_0 + \mu_{\mathrm{chem}} - \Sigma^{\Lambda}}\right|_{\mu\nu}. \tag{1.29}$$

As the following quantity will appear also in the flow equation for the vertex, we will define

$$P^{\Lambda}_{\mu\nu}(\bar{\omega}) := \left.\frac{1}{\mathrm{i}\bar{\omega} - H_0 + \mu_{\mathrm{chem}} - \Sigma^{\Lambda}}\right|_{\mu\nu}. \tag{1.30}$$

Inserting Eqs. (1.29,1.30) into Eq. (1.20), the flow equation for the self-energy now reads

$$\frac{\mathrm{d}}{\mathrm{d}\Lambda}\Sigma^{\Lambda}_{\alpha\beta} = -\frac{1}{2\pi}\sum_{\mu\nu}\underbrace{\left(P^{\Lambda}_{\mu\nu}(\Lambda) + P^{\Lambda}_{\mu\nu}(-\Lambda)\right)}_{=:\Pi^{\Sigma,\Lambda}_{\mu\nu}}\Gamma^{\Lambda}_{\alpha\nu\beta\mu}. \tag{1.31}$$

When it comes to the flow equation for the vertex, Eq. (1.21), one must take care that the arguments for the δ and Θ functions are equal, so one may not simply take the result derived for the single-scale propagator in the self-energy flow and apply it, but rather must use the same kind of treatment of the δ and Θ functions for the entire expression, on a term by term basis. Looking at the first term,

$$\int \mathrm{d}\bar{\omega}\sum_{\mu\nu\rho\sigma}\mathcal{G}^{\Lambda}_{\rho\mu}(\bar{\omega})\mathcal{S}^{\Lambda}_{\sigma\nu}(-\bar{\omega})\Gamma^{\Lambda}_{\alpha\beta\rho\sigma}\Gamma^{\Lambda}_{\mu\nu\gamma\delta},$$

it can be seen that by exchanging all traced indices in both vertices that appear, and then renaming the summation indices, the formula may be rewritten as

$$\int \mathrm{d}\bar{\omega}\sum_{\mu\nu\rho\sigma}\mathcal{S}^{\Lambda}_{\rho\mu}(-\bar{\omega})\mathcal{G}^{\Lambda}_{\sigma\nu}(\bar{\omega})\Gamma^{\Lambda}_{\alpha\beta\rho\sigma}\Gamma^{\Lambda}_{\mu\nu\gamma\delta},$$

which is just an exchange of both propagators. Utilizing this, we may write it formulated in terms of matrix products,

$$\frac{1}{2}\mathrm{tr}\int \mathrm{d}\bar{\omega}\Big[\mathcal{S}'\Gamma^{\mathrm{T}}\mathcal{G}^{\mathrm{T}}\Gamma + \mathcal{G}\Gamma^{\mathrm{T}}\mathcal{S}'^{\mathrm{T}}\Gamma\Big].$$

We note that the frequency of the single-scale propagator is negative here, which we denote with prime for $\mathcal{Q}$ and Σ; the Θ and δ-functions only depend on the modulus.

Inserting Eq. (1.26) and using the same representation for $\mathcal{G}$, we can separate four terms,

$$-\frac{\delta}{2}\frac{1}{\mathcal{Q}'-\Theta\Sigma'}\Gamma^{\mathrm{T}}\left(\frac{\Theta}{\mathcal{Q}-\Theta\Sigma}\right)^{\mathrm{T}}\Gamma, \tag{1.32}$$

$$-\frac{\delta}{2}\frac{\Theta}{\mathcal{Q}-\Theta\Sigma}\Gamma^{\mathrm{T}}\left(\frac{1}{\mathcal{Q}'-\Theta\Sigma'}\right)^{\mathrm{T}}\Gamma, \tag{1.33}$$

$$-\frac{\delta}{2}\frac{1}{\mathcal{Q}'-\Theta\Sigma'}\Sigma'\frac{\Theta}{\mathcal{Q}'-\Theta\Sigma'}\Gamma^{\mathrm{T}}\left(\frac{\Theta}{\mathcal{Q}-\Theta\Sigma}\right)^{\mathrm{T}}\Gamma, \tag{1.34}$$

$$-\frac{\delta}{2}\frac{\Theta}{\mathcal{Q}-\Theta\Sigma}\Gamma^{\mathrm{T}}\left(\frac{\Theta}{\mathcal{Q}'-\Theta\Sigma'}\right)^{\mathrm{T}}\Sigma'^{\mathrm{T}}\left(\frac{1}{\mathcal{Q}'-\Theta\Sigma'}\right)^{\mathrm{T}}\Gamma. \tag{1.35}$$

Since all of these terms occur underneath an integral over $\int \mathrm{d}\bar{\omega}\delta(|\omega|-\Lambda)$, we may switch primes within each term, and we note for future use that the terms of Eqs. (1.32,1.33) are equal to each other.

We now apply Morris's Lemma again. In both other terms, Eqs. (1.34,1.35), we can rewrite them in terms of derivatives w.r.t. the integration variable t,

$$-\frac{\delta}{2}\int_0^1 t^2\left(\frac{\mathrm{d}}{\mathrm{d}t}\frac{1}{\mathcal{Q}'-t\Sigma'}\right)\Gamma^{\mathrm{T}}\left(\frac{1}{\mathcal{Q}-t\Sigma}\right)^{\mathrm{T}}\Gamma\mathrm{d}t, \tag{1.36}$$

$$-\frac{\delta}{2}\int_0^1 t^2\frac{1}{\mathcal{Q}-t\Sigma}\Gamma^{\mathrm{T}}\left(\frac{\mathrm{d}}{\mathrm{d}t}\frac{1}{\mathcal{Q}'-t\Sigma'}\right)^{\mathrm{T}}\Gamma\mathrm{d}t. \tag{1.37}$$

Partial integration of Eq. 1.36 yields

$$\begin{aligned}
&-\frac{\delta}{2}\left[t^2\frac{1}{\mathcal{Q}'-t\Sigma'}\Gamma^{\mathrm{T}}\left(\frac{1}{\mathcal{Q}-t\Sigma}\right)^{\mathrm{T}}\Gamma\right]_0^1\\
&+\frac{\delta}{2}\int_0^1 2t\frac{1}{\mathcal{Q}'-t\Sigma'}\Gamma^{\mathrm{T}}\left(\frac{1}{\mathcal{Q}-t\Sigma}\right)^{\mathrm{T}}\Gamma\mathrm{d}t\\
&+\frac{\delta}{2}\int_0^1 t^2\frac{1}{\mathcal{Q}-t\Sigma}\Gamma^{\mathrm{T}}\left(\frac{\mathrm{d}}{\mathrm{d}t}\frac{1}{\mathcal{Q}'-t\Sigma'}\right)^{\mathrm{T}}\Gamma\mathrm{d}t.
\end{aligned} \tag{1.38}$$

One sees that the second term cancels Eqs. (1.32,1.33) and the third term cancels Eq. (1.37), leaving the result

$$-\frac{\delta}{2}\frac{1}{\mathcal{Q}'-\Sigma'}\Gamma^{\mathrm{T}}\left(\frac{1}{\mathcal{Q}-\Sigma}\right)^{\mathrm{T}}\Gamma, \tag{1.39}$$

which can be rewritten in terms of the index notation as

$$-\frac{1}{2}\sum_{\bar{\omega}=\pm\Lambda}\sum_{\mu\nu\rho\sigma} P^{\Lambda}_{\rho\mu}(-\bar{\omega})P^{\Lambda}_{\sigma\nu}(\bar{\omega})\Gamma^{\Lambda}_{\alpha\beta\rho\sigma}\Gamma^{\Lambda}_{\mu\nu\gamma\delta}. \tag{1.40}$$

We note that if one were to keep the frequency dependence of the vertex and the self-energy, two cases need to be distinguished: for the case where all external frequencies are zero, the same derivation applies, so our result holds there. For the case where at least some external frequencies are non-zero, the arguments for the δ and Θ functions differ, so one may directly insert Eq. 1.29 into the flow equations for the vertex.

An analogous treatment is possible for the other four terms in Eq. (1.21), if one remembers that a simultaneous exchange of both pairs of external indices $[\alpha \leftrightarrow \beta, \gamma \leftrightarrow \delta]$ has to give the same expression (due to the symmetry of Γ), so they may be rewritten with a factor of $\frac{1}{2}([\text{original}] + [\text{exchanged}])$.

This allows us to write down the flow equation for the vertex in the static limit,

$$\begin{aligned}
\frac{\mathrm{d}}{\mathrm{d}\Lambda}\Gamma^{\Lambda}_{\alpha\beta\gamma\delta} &= -\frac{1}{2\pi}\sum_{\mu\nu\rho\sigma}\sum_{\bar{\omega}=\pm\Lambda}\Bigg\{\frac{1}{2}P^{\Lambda}_{\mu\nu}(-\bar{\omega})P^{\Lambda}_{\rho\sigma}(\bar{\omega})\Gamma^{\Lambda}_{\alpha\beta\nu\rho}\Gamma^{\Lambda}_{\rho\mu\gamma\delta} \\
&\quad +\frac{1}{2}P^{\Lambda}_{\mu\nu}(\bar{\omega})P^{\Lambda}_{\rho\sigma}(\bar{\omega})\left[\Gamma^{\Lambda}_{\beta\nu\gamma\rho}\Gamma^{\Lambda}_{\alpha\sigma\delta\mu} - \Gamma^{\Lambda}_{\alpha\nu\gamma\rho}\Gamma^{\Lambda}_{\beta\sigma\delta\mu} - \Gamma^{\Lambda}_{\beta\nu\delta\rho}\Gamma^{\Lambda}_{\alpha\sigma\gamma\mu} + \Gamma^{\Lambda}_{\alpha\nu\delta\rho}\Gamma^{\Lambda}_{\beta\sigma\gamma\mu}\right]\Bigg\} \\
&= -\frac{1}{2\pi}\sum_{\mu\nu\rho\sigma}\left\{\Pi^{\mathrm{c},\Lambda}_{\mu\nu\sigma\rho}\Gamma^{\Lambda}_{\nu\rho\gamma\delta}\Gamma^{\Lambda}_{\alpha\beta\sigma\mu} + \Pi^{\mathrm{ph},\Lambda}_{\mu\nu\rho\sigma}\left[\Gamma^{\Lambda}_{\beta\nu\gamma\rho}\Gamma^{\Lambda}_{\alpha\sigma\delta\mu} - \Gamma^{\Lambda}_{\alpha\nu\gamma\rho}\Gamma^{\Lambda}_{\beta\sigma\delta\mu}\right]\right\},
\end{aligned} \tag{1.41}$$

where we have used the symmetries of Γ to simplify the equations and have defined

$$\Pi^{\mathrm{c},\Lambda}_{\mu\nu\sigma\rho} := P^{\Lambda}_{\mu\nu}(\Lambda)P^{\Lambda}_{\sigma\rho}(-\Lambda) \tag{1.42}$$

$$\Pi^{\mathrm{ph},\Lambda}_{\mu\nu\sigma\rho} := P^{\Lambda}_{\mu\nu}(\Lambda)P^{\Lambda}_{\rho\sigma}(\Lambda) + P^{\Lambda}_{\mu\nu}(-\Lambda)P^{\Lambda}_{\rho\sigma}(-\Lambda). \tag{1.43}$$

1.2.1 Initial Conditions

The initial condition for the flow equations are given by Eq (31) in Ref. 19,

$$\underline{\Gamma}^{\Lambda_0}[\chi,\bar{\chi}] = S_{\mathrm{int}}[\chi,\bar{\chi}], \tag{1.44}$$

where $\underline{\Gamma}^{\Lambda_0}$ is the generating functional for all the vertices (the term proportional to $\bar{\chi}\chi$ being the self-energy and the term proportional to $\bar{\chi}\bar{\chi}\chi\chi$ being the effective interaction vertex), whereas S_{int} is the interacting part of the action.

Since that only consists of the quartic term in our setup, the initial conditions at $\Lambda \to \infty$ are given by

$$\Sigma^{\Lambda\to\infty}_{\alpha\beta} = 0 \quad \text{and} \quad \Gamma^{\Lambda\to\infty}_{\alpha\beta\gamma\delta} = U_{\alpha\beta\gamma\delta}. \tag{1.45}$$

In order to solve the equations numerically, we need to start at a Λ_0 that is still finite but larger than all other energy scales in the system. For $\Lambda > \Lambda_0$ one may assume a form of $(\mathrm{i}\omega)^{-1}\mathbb{1}$ for the propagator, allowing us to analytically integrate the flow equations from ∞ to Λ_0. In case of the flow equation for the vertex, power counting in U and Λ_0 immediately yields

$$\Gamma^{\Lambda_0} - U \sim -\int_{\infty}^{\Lambda_0} UU\frac{1}{\Lambda^2} = \frac{1}{\Lambda_0}UU, \tag{1.46}$$

and hence

$$|\Gamma^{\Lambda_0} - U|/|U| \sim |U|/\Lambda_0. \tag{1.47}$$

Because of this we may simply assume that Γ^{Λ_0} does not differ from $\Gamma^{\Lambda\to\infty}$ and use

$$\Gamma^{\Lambda_0}_{\alpha\beta\gamma\delta} = U_{\alpha\beta\gamma\delta}. \tag{1.48}$$

The same does not hold true for the flow equation for the self-energy, where the analytical integral gives a non-negligible contribution,

$$\begin{aligned}
\Sigma^{\Lambda_0}_{\alpha\beta} &= -\frac{1}{2\pi}\sum_{\mu} U_{\alpha\mu\beta\mu} \lim_{\eta\to 0^+} \int_{\infty}^{\Lambda_0} \left(\frac{\mathrm{e}^{\mathrm{i}\Lambda\eta}}{\mathrm{i}\Lambda} - \frac{\mathrm{e}^{-\mathrm{i}\Lambda\eta}}{\mathrm{i}\Lambda}\right) \mathrm{d}\Lambda \\
&= -\frac{1}{\pi}\sum_{\mu} U_{\alpha\mu\beta\mu} \lim_{\eta\to 0^+} \eta \int_{\infty}^{\Lambda_0} \mathrm{sinc}(\eta\Lambda)\mathrm{d}\Lambda \\
&= \frac{1}{\pi}\sum_{\mu} U_{\alpha\mu\beta\mu} \lim_{\eta\to 0^+} \left[\int_0^{\infty} \mathrm{sinc}(x)\mathrm{d}x - \mathcal{O}(\eta)\right] \\
&= \frac{1}{2}\sum_{\mu} U_{\alpha\mu\beta\mu}.
\end{aligned} \tag{1.49}$$

Here we have explicitly included the required convergence factor $\mathrm{e}^{\mathrm{i}\omega 0^+}$ that appears in the Green's function in imaginary frequency space.

1.3 Systems with Spin

In Eqs. (1.31,1.41), the indices designate generic states in the Hilbert space. We will now discuss the case where the system is fully SU(2) symmetric. Here, it is convenient to separate the orbital degrees of freedom from the spin degrees of freedom, $\alpha \to (\alpha, \sigma_1)$. Our derivation will follow Ref. [23], but we will discuss the generic case without the additional particle-hole symmetry. Single-particle quantities (self-energy, propagators)

do not depend on the spin degree of freedom,

$$\Sigma^{\Lambda}_{(\alpha,\sigma_1)(\beta,\sigma_2)} = \Sigma^{\Lambda}_{\alpha\beta}\delta_{\sigma_1\sigma_2}, \tag{1.50}$$

$$\mathcal{G}^{\Lambda}_{(\alpha,\sigma_1)(\beta,\sigma_2)} = \mathcal{G}^{\Lambda}_{\alpha\beta}\delta_{\sigma_1\sigma_2}, \tag{1.51}$$

$$\mathcal{S}^{\Lambda}_{(\alpha,\sigma_1)(\beta,\sigma_2)} = \mathcal{S}^{\Lambda}_{\alpha\beta}\delta_{\sigma_1\sigma_2}. \tag{1.52}$$

The spin structure of the vertex is determined by the fact that two particles may either keep their spin or exchange it, and may thus be decomposed into

$$\begin{aligned}\Gamma^{\Lambda}_{(\alpha,\sigma_1),(\beta,\sigma_2),(\gamma,\sigma_3),(\delta,\sigma_4)} = \quad & c^{\mathrm{I},\Lambda}_{\alpha\beta\gamma\delta}\delta_{\sigma_1\sigma_3}\delta_{\sigma_2\sigma_4} \\ & + c^{\mathrm{II},\Lambda}_{\alpha\beta\gamma\delta}\delta_{\sigma_1\sigma_4}\delta_{\sigma_2\sigma_3},\end{aligned}$$

where c^{I} and c^{II} are the coefficients for each of these processes.

Using the antisymmetry of Γ, Eq. (1.22), we may exchange (γ,σ_3) with (δ,σ_4),

$$\begin{aligned}\Gamma^{\Lambda}_{(\alpha,\sigma_1),(\beta,\sigma_2),(\gamma,\sigma_3),(\delta,\sigma_4)} &= -\Gamma^{\Lambda}_{(\alpha,\sigma_1),(\beta,\sigma_2),(\delta,\sigma_4),(\gamma,\sigma_3)} \\ &= -c^{\mathrm{I},\Lambda}_{\alpha\beta\gamma\delta}\delta_{\sigma_1\sigma_4}\delta_{\sigma_2\sigma_3} - c^{\mathrm{II},\Lambda}_{\alpha\beta\gamma\delta}\delta_{\sigma_1\sigma_3}\delta_{\sigma_2\sigma_4}.\end{aligned}$$

By comparing the coefficients of the Kronecker-δs, we may identify

$$c^{\mathrm{I},\Lambda}_{\alpha\beta\gamma\delta} = -c^{\mathrm{II},\Lambda}_{\alpha\beta\delta\gamma} := -\Gamma^{\mathrm{s},\Lambda}_{\alpha\beta\delta\gamma},$$

and hence write the vertex as

$$\begin{aligned}\Gamma^{\Lambda}_{(\alpha,\sigma_1),(\beta,\sigma_2),(\gamma,\sigma_3),(\delta,\sigma_4)} = \quad & \Gamma^{\mathrm{s},\Lambda}_{\alpha\beta\gamma\delta}\delta_{\sigma_1\sigma_4}\delta_{\sigma_2\sigma_3} \\ & - \Gamma^{\mathrm{s},\Lambda}_{\alpha\beta\delta\gamma}\delta_{\sigma_1\sigma_3}\delta_{\sigma_2\sigma_4}.\end{aligned} \tag{1.53}$$

Using the symmetry of Γ^{Λ}, one can see that $\Gamma^{\mathrm{s},\Lambda}$ is still symmetric under exchange of both pairs of indices,

$$\Gamma^{\mathrm{s},\Lambda}_{\alpha\beta\gamma\delta} = \Gamma^{\mathrm{s},\Lambda}_{\beta\alpha\delta\gamma}, \tag{1.54}$$

but in general it is not antisymmetric with respect to the exchange of a single pair of indices. Instead, one may identify the part of $\Gamma^{\mathrm{s},\Lambda}$ that is antisymmetric under exchange of α and β with the triplet channel of the vertex, whereas the part that is symmetric under the exchange of α and β represents the singlet channel.

Inserting Eqs. (1.50,1.51,1.52,1.53) into Eq. (1.31), we have

$$\begin{aligned}\frac{\mathrm{d}}{\mathrm{d}\Lambda}\Sigma^{\Lambda}_{\alpha\beta}\delta_{\sigma_1\sigma_2} &= -\frac{1}{2\pi}\sum_{\mu\nu}\sum_{\sigma_3}\Pi^{\Sigma,\Lambda}_{\mu\nu}\Big(\Gamma^{\mathrm{s},\Lambda}_{\alpha\nu\beta\mu}\delta_{\sigma_1\sigma_3}\delta_{\sigma_3\sigma_2} - \Gamma^{\mathrm{s},\Lambda}_{\alpha\nu\mu\beta}\delta_{\sigma_1\sigma_2}\delta_{\sigma_3\sigma_3}\Big) \\ &= -\frac{1}{2\pi}\sum_{\mu\nu}\Pi^{\Sigma,\Lambda}_{\mu\nu}\Big(\Gamma^{\mathrm{s},\Lambda}_{\alpha\nu\beta\mu} - 2\Gamma^{\mathrm{s},\Lambda}_{\alpha\nu\mu\beta}\Big)\delta_{\sigma_1\sigma_2},\end{aligned}$$

and hence

$$\frac{\mathrm{d}}{\mathrm{d}\Lambda}\Sigma^{\Lambda}_{\alpha\beta} = -\frac{1}{2\pi}\sum_{\mu\nu}\Pi^{\Sigma,\Lambda}_{\mu\nu}\Big(\Gamma^{\mathrm{s},\Lambda}_{\alpha\nu\beta\mu} - 2\Gamma^{\mathrm{s},\Lambda}_{\alpha\nu\mu\beta}\Big). \tag{1.55}$$

To obtain the flow equation for $\Gamma^{\Lambda,s}$, we must insert Eqs. (1.50,1.51,1.52,1.53) into Eq. (1.41). To simplify our notation, we will use $\delta^{34}_{12} = \delta_{\sigma_1\sigma_2}\delta_{\sigma_3\sigma_4}$. For the first term with $\Pi^{\mathrm{c},\Lambda}$, we have

$$-\frac{1}{2\pi}\sum_{\mu\nu\rho\sigma}\sum_{\sigma_5\sigma_6}\Pi^{\mathrm{c},\Lambda}_{\mu\nu\sigma\rho}\Big(\Gamma^{\mathrm{s},\Lambda}_{\nu\rho\gamma\delta}\delta^{63}_{54} - \Gamma^{\mathrm{s},\Lambda}_{\nu\rho\delta\gamma}\delta^{64}_{53}\Big)\Big(\Gamma^{\mathrm{s},\Lambda}_{\alpha\beta\sigma\mu}\delta^{26}_{15} - \Gamma^{\mathrm{s},\Lambda}_{\alpha\beta\mu\sigma}\delta^{25}_{16}\Big). \tag{1.56}$$

Multiplying out the main product, there are four terms of combinations of $\Gamma^{\mathrm{s},\Lambda}$ that appear,

$$\begin{aligned}
\sum_{\sigma_5\sigma_6}\Gamma^{\mathrm{s},\Lambda}_{\nu\rho\gamma\delta}\Gamma^{\mathrm{s},\Lambda}_{\alpha\beta\sigma\mu}\delta^{63}_{54}\delta^{26}_{15} &= \Gamma^{\mathrm{s},\Lambda}_{\nu\rho\gamma\delta}\Gamma^{\mathrm{s},\Lambda}_{\alpha\beta\sigma\mu}\delta^{23}_{14}.\\
\sum_{\sigma_5\sigma_6} -\Gamma^{\mathrm{s},\Lambda}_{\nu\rho\delta\gamma}\Gamma^{\mathrm{s},\Lambda}_{\alpha\beta\sigma\mu}\delta^{64}_{53}\delta^{26}_{15} &= -\Gamma^{\mathrm{s},\Lambda}_{\nu\rho\delta\gamma}\Gamma^{\mathrm{s},\Lambda}_{\alpha\beta\sigma\mu}\delta^{24}_{13},\\
\\
\sum_{\sigma_5\sigma_6} -\Gamma^{\mathrm{s},\Lambda}_{\nu\rho\gamma\delta}\Gamma^{\mathrm{s},\Lambda}_{\alpha\beta\mu\sigma}\delta^{63}_{54}\delta^{25}_{16} &= -\Gamma^{\mathrm{s},\Lambda}_{\nu\rho\gamma\delta}\Gamma^{\mathrm{s},\Lambda}_{\alpha\beta\mu\sigma}\delta^{24}_{13},\\
\sum_{\sigma_5\sigma_6}\Gamma^{\mathrm{s},\Lambda}_{\nu\rho\delta\gamma}\Gamma^{\mathrm{s},\Lambda}_{\alpha\beta\mu\sigma}\delta^{64}_{53}\delta^{25}_{16} &= \Gamma^{\mathrm{s},\Lambda}_{\nu\rho\delta\gamma}\Gamma^{\mathrm{s},\Lambda}_{\alpha\beta\mu\sigma}\delta^{23}_{14}.
\end{aligned}$$

On the other hand, the left hand side of the flow equation reads

$$\frac{\mathrm{d}}{\mathrm{d}\Lambda}\left(\Gamma^{\mathrm{s},\Lambda}_{\alpha\beta\gamma\delta}\delta^{23}_{14} - \Gamma^{\mathrm{s},\Lambda}_{\alpha\beta\delta\gamma}\delta^{24}_{13}\right). \tag{1.57}$$

We may thus look at the products that contain δ^{23}_{14} to obtain the first term of the flow equation for $\Gamma^{\mathrm{s},\Lambda}$,

$$-\frac{1}{2\pi}\sum_{\mu\nu\rho\sigma}\Pi^{\mathrm{c},\Lambda}_{\mu\nu\sigma\rho}\Big(\Gamma^{\mathrm{s},\Lambda}_{\nu\rho\gamma\delta}\Gamma^{\mathrm{s},\Lambda}_{\alpha\beta\sigma\mu} + \Gamma^{\mathrm{s},\Lambda}_{\nu\rho\delta\gamma}\Gamma^{\mathrm{s},\Lambda}_{\alpha\beta\mu\sigma}\Big)\delta^{23}_{14}. \tag{1.58}$$

We may now proceed in doing the same for the particle-hole channel,

$$\begin{aligned}
&-\frac{1}{2\pi}\sum_{\mu\nu\rho\sigma}\sum_{\sigma_5\sigma_6}\Pi^{\mathrm{ph},\Lambda}_{\mu\nu\rho\sigma}\times\\
&\Big\{\Big(\Gamma^{\mathrm{s},\Lambda}_{\alpha\nu\gamma\rho}\delta^{16}_{53} - \Gamma^{\mathrm{s},\Lambda}_{\alpha\nu\rho\gamma}\delta^{13}_{56}\Big)\Big(\Gamma^{\mathrm{s},\Lambda}_{\beta\sigma\delta\mu}\delta^{25}_{64} - \Gamma^{\mathrm{s},\Lambda}_{\beta\sigma\mu\delta}\delta^{24}_{65}\Big)\\
&+\Big(\Gamma^{\mathrm{s},\Lambda}_{\beta\nu\gamma\rho}\delta^{26}_{53} - \Gamma^{\mathrm{s},\Lambda}_{\beta\nu\rho\gamma}\delta^{23}_{56}\Big)\Big(\Gamma^{\mathrm{s},\Lambda}_{\alpha\sigma\delta\mu}\delta^{15}_{64} - \Gamma^{\mathrm{s},\Lambda}_{\alpha\sigma\mu\delta}\delta^{14}_{65}\Big)\Big\}.
\end{aligned} \tag{1.59}$$

Of the eight products that appear, we again pick out those that appear with a δ_{14}^{23}, where we use that

$$\sum_{\sigma_5\sigma_6} \delta_{53}^{16}\delta_{64}^{25} = \delta_{14}^{23}, \qquad \sum_{\sigma_5\sigma_6} \delta_{56}^{23}\delta_{65}^{14} = 2\delta_{14}^{23},$$
$$\sum_{\sigma_5\sigma_6} \delta_{53}^{26}\delta_{65}^{14} = \delta_{14}^{23}, \qquad \sum_{\sigma_5\sigma_6} \delta_{56}^{23}\delta_{64}^{15} = \delta_{14}^{23},$$

so that we arrive at

$$-\frac{1}{2\pi}\sum_{\mu\nu\rho\sigma} \Pi^{\mathrm{ph},\Lambda}_{\mu\nu\rho\sigma}\Big(2\Gamma^{\mathrm{s},\Lambda}_{\beta\nu\rho\gamma}\Gamma^{\mathrm{s},\Lambda}_{\alpha\sigma\mu\delta} + \Gamma^{\mathrm{s},\Lambda}_{\alpha\nu\gamma\rho}\Gamma^{\mathrm{s},\Lambda}_{\beta\sigma\delta\mu} - \Gamma^{\mathrm{s},\Lambda}_{\beta\nu\rho\gamma}\Gamma^{\mathrm{s},\Lambda}_{\alpha\sigma\delta\mu} - \Gamma^{\mathrm{s},\Lambda}_{\beta\nu\gamma\rho}\Gamma^{\mathrm{s},\Lambda}_{\alpha\sigma\mu\delta}\Big)\delta_{14}^{23}. \quad (1.60)$$

Adding Eq. (1.58) and Eq. (1.60), the flow equation for $\Gamma^{\mathrm{s},\Lambda}$ now reads

$$\frac{\mathrm{d}}{\mathrm{d}\Lambda}\Gamma^{\mathrm{s},\Lambda}_{\alpha\beta\delta\gamma} = -\frac{1}{2\pi}\sum_{\mu\nu\rho\sigma}\Big\{\Pi^{\mathrm{c},\Lambda}_{\mu\nu\sigma\rho}\Big(\Gamma^{\mathrm{s},\Lambda}_{\nu\rho\gamma\delta}\Gamma^{\mathrm{s},\Lambda}_{\alpha\beta\sigma\mu} + \Gamma^{\mathrm{s},\Lambda}_{\nu\rho\delta\gamma}\Gamma^{\mathrm{s},\Lambda}_{\alpha\beta\mu\sigma}\Big)$$
$$+\Pi^{\mathrm{ph},\Lambda}_{\mu\nu\rho\sigma}\Big(2\Gamma^{\mathrm{s},\Lambda}_{\beta\nu\rho\gamma}\Gamma^{\mathrm{s},\Lambda}_{\alpha\sigma\mu\delta} + \Gamma^{\mathrm{s},\Lambda}_{\alpha\nu\gamma\rho}\Gamma^{\mathrm{s},\Lambda}_{\beta\sigma\delta\mu} - \Gamma^{\mathrm{s},\Lambda}_{\beta\nu\rho\gamma}\Gamma^{\mathrm{s},\Lambda}_{\alpha\sigma\delta\mu} - \Gamma^{\mathrm{s},\Lambda}_{\beta\nu\gamma\rho}\Gamma^{\mathrm{s},\Lambda}_{\alpha\sigma\mu\delta}\Big)\Big\}. \quad (1.61)$$

1.4 Finite Temperature

We will now discuss the form of the flow equations at finite temperature. In this case, using a sharp Θ-function is ill-suited. Instead, we utilize the cutoff suggested in Ref. [24], hence we replace $\Theta(|\omega| - \Lambda)$ by $\chi^\Lambda(\omega_n)$, which is given by

$$\chi^\Lambda(\omega_n) = \begin{cases} 0, & |\omega_n| \leq \Lambda - \pi T, \\ \frac{1}{2} + \frac{|\omega_n|-\Lambda}{2\pi T} & \Lambda - \pi T \leq |\omega_n| \leq \Lambda + \pi T, \\ 1, & \Lambda + \pi T \leq |\omega_n|, \end{cases} \quad (1.62)$$

and its derivative with respect to Λ is then given by

$$-\left(\partial_\Lambda \chi^\Lambda(\omega_n)\right) = \begin{cases} \frac{1}{2\pi T} & \Lambda - \pi T \leq |\omega_n| \leq \Lambda + \pi T, \\ 0 & \text{otherwise.} \end{cases} \quad (1.63)$$

We note that $\chi^\Lambda(\omega_n) \to \Theta(|\omega| - \Lambda)$ as $T \to 0$. The full Green's function is now given by

$$\mathcal{G}^\Lambda(\omega_n) = \frac{\chi^\Lambda(\omega_n)}{\mathrm{i}\omega_n - \hat{H}_0 + \mu_{\mathrm{chem}} - \chi^\Lambda(\omega_n)\Sigma^\Lambda(\omega_n)}, \quad (1.64)$$

whereas the single-scale propagator, Eq. 1.7, reads

$$\begin{aligned}\mathcal{S}^{\Lambda}(\omega_n) &= \frac{\partial_\Lambda \chi^\Lambda(\omega_n)}{\mathrm{i}\omega_n - \hat{H}_0 + \mu_{\mathrm{chem}} - \chi^\Lambda(\omega_n)\Sigma^\Lambda(\omega_n)} \times \\ &\quad \left(\mathrm{i}\omega_n - \hat{H}_0 + \mu_{\mathrm{chem}}\right) \frac{1}{\mathrm{i}\omega_n - \hat{H}_0 + \mu_{\mathrm{chem}} - \chi^\Lambda(\omega_n)\Sigma^\Lambda(\omega_n)}.\end{aligned}$$

With this form of a cutoff function, the Matsubara sums that appear may be evaluated analytically. Since Matsubara frequencies have a distance of $2\pi T$ from each other, the derivative of the cutoff is only nonzero for a two Matsubara frequencies, whose magnitude are that closest to the parameter Λ. Any form

$$T\sum_n -(\partial_\Lambda \chi^\Lambda(\omega_n)) f(\omega_n) = \frac{1}{2\pi}\sum_{|\omega_n|\approx\Lambda} f(\omega_n). \tag{1.65}$$

This structure is very similar to the situation at $T = 0$, where we have

$$\frac{1}{2\pi}\int \mathrm{d}\omega \delta(|\omega| - \Lambda) f(\omega) = \frac{1}{2\pi}\sum_{|\omega|=\Lambda} f(\omega). \tag{1.66}$$

Again we drop the frequency-dependence of the self-energy and the vertex. Defining $P^{T,\Lambda}_{\mu\nu}(\omega_n)$ as

$$P^{T,\Lambda}(\omega_n) := \frac{1}{\mathrm{i}\omega_n - H_0 + \mu_{\mathrm{chem}} - \chi^\Lambda(\omega_n)\Sigma^\Lambda}, \tag{1.67}$$

and $P'^{,T,\Lambda}_{\mu\nu}, P''^{,T,\Lambda}_{\mu\nu}$ as

$$P'^{,T,\Lambda}(\omega_n) := P^{T,\Lambda}(\omega_n)(\mathrm{i}\omega_n - H_0 + \mu_{\mathrm{chem}})P^{T,\Lambda}(\omega_n), \tag{1.68}$$

$$P''^{,T,\Lambda}(\omega_n) := P^{T,\Lambda}(\omega_n)\chi^\Lambda(\omega_n), \tag{1.69}$$

the flow equation for the self-energy now reads

$$\frac{\mathrm{d}}{\mathrm{d}\Lambda}\Sigma^\Lambda_{\alpha\beta} = -\frac{1}{2\pi}\sum_{|\omega_n|\approx\Lambda} P'^{,T,\Lambda}_{\mu\nu}(\omega_n)\Gamma^\Lambda_{\alpha\nu\beta\mu}. \tag{1.70}$$

Setting all external frequencies to zero and dropping the frequency dependence of the vertex, its flow equation is now given by

$$\begin{aligned}\frac{\mathrm{d}}{\mathrm{d}\Lambda}\Gamma^\Lambda_{\alpha\beta\gamma\delta} &= -\frac{1}{2\pi}\sum_{|\omega_n|\approx\Lambda}\sum_{\mu\nu\rho\sigma}\Big\{P''^{,T,\Lambda}_{\mu\nu}(\omega_n)P'^{,T,\Lambda}_{\rho\sigma}(-\omega_n)\Gamma^\Lambda_{\alpha\beta\sigma\mu}\Gamma^\Lambda_{\nu\rho\gamma\delta} + \\ &\quad P'^{,T,\Lambda}_{\mu\nu}(\omega_n)P'^{,T,\Lambda}_{\rho\sigma}(\omega_n) \times \\ &\quad \left[\Gamma^\Lambda_{\beta\nu\gamma\rho}\Gamma^\Lambda_{\alpha\mu\delta\sigma} - \Gamma^\Lambda_{\alpha\mu\gamma\sigma}\Gamma^\Lambda_{\beta\nu\delta\rho} + \Gamma^\Lambda_{\beta\mu\gamma\sigma}\Gamma^\Lambda_{\alpha\nu\delta\rho} - \Gamma^\Lambda_{\alpha\nu\gamma\rho}\Gamma^\Lambda_{\beta\mu\delta\sigma}\right]\Big\}.\end{aligned} \tag{1.71}$$

We note that $\chi^\Lambda(\omega_n) \to \frac{1}{2}$ for $\omega_n \to \Lambda$, so if one takes the limit $T \to 0$ and applies the symmetries of the vertex, one recovers Eq. (1.41).

1.5 Observables and Correlators

1.5.1 Zero Temperature

Single-particle Observables at $T = 0$

Within our formalism, we may calculate both single-particle and two-particle observables. Single-particle observables may be expressed by the Green's function, which is given by

$$\mathcal{G}_{\alpha\beta}(\mathrm{i}\omega) = \left.\frac{1}{\mathrm{i}\omega - \hat{H}_0 + \mu - \Sigma} \mathrm{e}^{\mathrm{i}\omega 0^+}\right|_{\alpha\beta}. \tag{1.72}$$

The convergence factor $\mathrm{e}^{\mathrm{i}\omega 0^+}$ is explicitly required here.

For example, the real space density matrix, ρ_{ij}, is given by

$$\rho_{ij} = \sum_{\alpha\beta} V^{\mathrm{rn}}_{i\alpha} \left[\frac{1}{2\pi}\int_{-\infty}^{\infty} \mathrm{d}\omega\, \mathcal{G}_{\alpha\beta}(\mathrm{i}\omega)\mathrm{e}^{\mathrm{i}\omega 0^+}\right] V^{\mathrm{rn},-1}_{\beta j}, \tag{1.73}$$

where $V^{\mathrm{rn}}_{i\alpha}$ is the basis transform from the non-interacting eigenbasis of the inhomogeneous system to the real space basis. The frequency integral may be calculated analytically by going into the basis where $\mathcal{G}$ is diagonal, i.e. the eigenbasis of $H + \Sigma$. We will denote indices in that basis by a tilde, e.g. $\tilde{\mu}$ and the eigenvalues of $H + \Sigma$ with $\tilde{\epsilon}_{\tilde{\mu}}$. The basis transform from that basis into real space will be denoted by $V^{\mathrm{ri}}_{i\tilde{\mu}}$. The integral may now be performed analytically, closing the integration loop around the left half-plane,

$$\begin{aligned}\rho_{ij} &= \sum_{\tilde{\mu}} V^{\mathrm{ri}}_{i\tilde{\mu}} \left[\frac{1}{2\pi}\int_{-\infty}^{\infty} \mathrm{d}\omega\, \frac{\mathrm{e}^{\mathrm{i}\omega 0^+}}{\mathrm{i}\omega - \tilde{\epsilon}_{\tilde{\mu}} + \mu_{\mathrm{chem}}}\right] V^{\mathrm{ri},-1}_{\tilde{\mu} j} \\ &= \sum_{\tilde{\mu}:\,\mathrm{electrons}} V^{\mathrm{ri}}_{i\tilde{\mu}} V^{\mathrm{ri},-1}_{\tilde{\mu} j},\end{aligned} \tag{1.74}$$

where the summation is now only performed over states below the chemical potential.

Single-particle Observables at $T > 0$

In order to obtain the result at finite temperature, $T > 0$, we must replace the integral by a Matsubara sum, performing the inverse of Eq. (1.16). The sum may be performed

analytically, using the well-known result

$$T\sum_{\omega_n}\frac{1}{\mathrm{i}\omega_n-\xi}=n_{\mathrm{F}}(\xi), \tag{1.75}$$

and we obtain

$$\begin{aligned}\rho_{ij} &= \sum_{\tilde{\mu}} V^{\mathrm{ri}}_{i\tilde{\mu}}\left[T\sum_{\omega_n}\frac{1}{\mathrm{i}\omega_n-\tilde{\epsilon}_{\tilde{\mu}}+\mu_{\mathrm{chem}}}\right]V^{\mathrm{ri},-1}_{\tilde{\mu}j}\\ &= \sum_{\tilde{\mu}} V^{\mathrm{ri}}_{i\tilde{\mu}} n_{\mathrm{F}}(\tilde{\epsilon}_{\tilde{\mu}}-\mu_{\mathrm{chem}})V^{\mathrm{ri},-1}_{\tilde{\mu}j},\end{aligned} \tag{1.76}$$

which reproduces Eq. (1.74) for $T\to 0$.

Single-particle Observables in Systems with Spin

In systems that are SU(2)-invariant, single-particle quantities don't differ in spin channels. Using the definition in Eq. (1.51), which defines the single-particle Green's function per spin channel, orbital observables acquire a factor of two, whereas the expectation value for the spin remains trivially zero,

$$\rho_{ij} = 2\begin{cases}\sum_{\tilde{\mu}:\,\mathrm{electrons}} V^{\mathrm{ri}}_{i\tilde{\mu}}V^{\mathrm{ri},-1}_{\tilde{\mu}j}, & T=0\\ \sum_{\tilde{\mu}} V^{\mathrm{ri}}_{i\tilde{\mu}} n_{\mathrm{F}}(\tilde{\epsilon}_{\tilde{\mu}}-\mu_{\mathrm{chem}})V^{\mathrm{ri},-1}_{\tilde{\mu}j}, & T>0\end{cases}, \tag{1.77}$$

$$\left\langle \mathbf{S}_i\right\rangle = 0. \tag{1.78}$$

1.5.2 Density-Density Correlator

Two-particle observables may be rewritten in terms of single- and two-particle Green's functions. In the case of spinless Fermions the density-density correlator, $\mathcal{C}^{\mathrm{dd}}_{ij}$, may be rewritten as

$$\begin{aligned}\mathcal{C}^{\mathrm{dd}}_{ij} &= \left\langle \hat{\mathrm{n}}_i\hat{\mathrm{n}}_j\right\rangle = \left\langle \hat{\mathrm{c}}^\dagger_i\hat{\mathrm{c}}_i\hat{\mathrm{c}}^\dagger_j\hat{\mathrm{c}}_j\right\rangle = \left\langle \hat{\mathrm{c}}^\dagger_j\hat{\mathrm{c}}^\dagger_i\hat{\mathrm{c}}_i\hat{\mathrm{c}}_j\right\rangle + \left\langle \hat{\mathrm{c}}^\dagger_i\hat{\mathrm{c}}_i\right\rangle\delta_{ij}\\ &= \mathcal{C}^{\mathrm{dd},(2)}_{ij} + \left\langle \hat{\mathrm{n}}_i\right\rangle\left\langle \hat{\mathrm{n}}_j\right\rangle - \left\langle \hat{\mathrm{c}}^\dagger_i\hat{\mathrm{c}}_j\right\rangle\left\langle \hat{\mathrm{c}}^\dagger_j\hat{\mathrm{c}}_i\right\rangle + \left\langle \hat{\mathrm{n}}_i\right\rangle\delta_{ij},\end{aligned} \tag{1.79}$$

where $\mathcal{C}^{\mathrm{dd},(2)}_{ij}$ is the part of the correlation function arising from the connected two-particle Green's function and thus the vertex. In the case of spinful Fermions, the density-density correlator includes a sum over the spin degrees of freedom,

$$\mathcal{C}^{\mathrm{dd}}_{ij}=\sum_{\sigma\sigma'}\left\langle \hat{\mathrm{n}}_{i\sigma}\hat{\mathrm{n}}_{j\sigma'}\right\rangle. \tag{1.80}$$

For systems that obey the full SU(2) symmetry, it reads

$$\begin{aligned} \mathcal{C}_{ij}^{\mathrm{dd}} &= \mathcal{C}_{ij}^{\mathrm{dd},(2)} + 4\Big\langle \hat{\mathrm{n}}_{i\sigma} \Big\rangle \Big\langle \hat{\mathrm{n}}_{j\sigma} \Big\rangle - 2\Big\langle \hat{\mathrm{c}}_{i\sigma}^{\dagger} \hat{\mathrm{c}}_{j\sigma} \Big\rangle \Big\langle \hat{\mathrm{c}}_{j\sigma}^{\dagger} \hat{\mathrm{c}}_{i\sigma} \Big\rangle \\ &\quad + 2\Big\langle \hat{\mathrm{n}}_{i\sigma} \Big\rangle \delta_{ij}, \end{aligned} \tag{1.81}$$

where σ is an arbitrary spin index that is not summed over, as the single-particle quantities are proportional to $\delta_{\sigma\sigma'}$.

Density-Density Correlator for Spinless Systems at $T = 0$

We will first derive the expression for $\mathcal{C}_{ij}^{\mathrm{dd},(2)}$ for the spinless case at $T = 0$. Since we are looking at static quantities, but our formalism is derived in Matsubara frequency space, we must perform a Fourier transform,

$$\begin{aligned} \mathcal{C}_{ij}^{\mathrm{dd},(2)} &= \int \frac{\mathrm{d}\omega_1}{2\pi} \int \frac{\mathrm{d}\omega_2}{2\pi} \int \frac{\mathrm{d}\omega_3}{2\pi} \int \frac{\mathrm{d}\omega_4}{2\pi} \times \\ &\quad \mathcal{G}_{ijij}^{(2,c)}(\mathrm{i}\omega_1, \mathrm{i}\omega_2, \mathrm{i}\omega_3, \mathrm{i}\omega_4), \end{aligned} \tag{1.82}$$

where $\mathcal{G}^{(2,c)}$ is the two-particle connected Green's function. Using the well-known relation between the two-particle connected Green's function and the vertex,

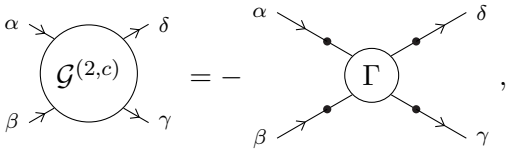

, (1.83)

we arrive at

$$\begin{aligned} \mathcal{G}_{ijij}^{(2,c)}(\mathrm{i}\omega_1, \mathrm{i}\omega_2, \mathrm{i}\omega_3, \mathrm{i}\omega_4) &= -2\pi \sum_{\alpha\beta\gamma\delta} \sum_{\alpha'\beta'\gamma'\delta'} V_{i\alpha'}^{\mathrm{rn}} V_{j\beta'}^{\mathrm{rn}} \times \\ &\mathcal{G}_{\alpha'\alpha}(\mathrm{i}\omega_1) \mathcal{G}_{\beta'\beta}(\mathrm{i}\omega_2) \Gamma_{\alpha\beta\gamma\delta} \delta(\mathrm{i}\omega_1 + \mathrm{i}\omega_2 - \mathrm{i}\omega_3 - \mathrm{i}\omega_4) \times \\ &\mathcal{G}_{\gamma\gamma'}(\mathrm{i}\omega_3) \mathcal{G}_{\delta\delta'}(\mathrm{i}\omega_4) V_{\gamma' i}^{\mathrm{rn},-1} V_{\delta' j}^{\mathrm{rn},-1}. \end{aligned} \tag{1.84}$$

In order to solve the frequency integral analytically, we again transform into the eigenbasis of $H + \Sigma$. Eq. (1.84) now reads

$$\begin{aligned} \mathcal{G}_{ijij}^{(2,c)}(\mathrm{i}\omega_1, \mathrm{i}\omega_2, \mathrm{i}\omega_3, \mathrm{i}\omega_4) &= -2\pi \sum_{\alpha\beta\gamma\delta} \sum_{\tilde{\mu}\tilde{\nu}\tilde{\rho}\tilde{\sigma}} V_{i\tilde{\mu}}^{\mathrm{ri}} V_{j\tilde{\nu}}^{\mathrm{ri}} \times \\ &\mathcal{G}_{\tilde{\mu}\tilde{\mu}}(\mathrm{i}\omega_1) \mathcal{G}_{\tilde{\nu}\tilde{\nu}}(\mathrm{i}\omega_2) V_{\tilde{\mu}\alpha}^{\mathrm{in}} V_{\tilde{\nu}\beta}^{\mathrm{in}} \times \\ &\Gamma_{\alpha\beta\gamma\delta} \delta(\mathrm{i}\omega_1 + \mathrm{i}\omega_2 - \mathrm{i}\omega_3 - \mathrm{i}\omega_4) \times \\ &V_{\gamma\tilde{\rho}}^{\mathrm{in},-1} V_{\delta\tilde{\sigma}}^{\mathrm{in},-1} \mathcal{G}_{\tilde{\rho}\tilde{\rho}}(\mathrm{i}\omega_3) \mathcal{G}_{\tilde{\sigma}\tilde{\sigma}}(\mathrm{i}\omega_4) V_{\tilde{\rho} i}^{\mathrm{ri},-1} V_{\tilde{\sigma} j}^{\mathrm{ri},-1}. \end{aligned} \tag{1.85}$$

For any given $\tilde{\mu}, \tilde{\nu}, \tilde{\rho}, \tilde{\sigma}$, the frequency-dependent part now reads

$$\begin{aligned} & 2\pi \int \frac{\mathrm{d}\omega_1}{2\pi} \int \frac{\mathrm{d}\omega_2}{2\pi} \int \frac{\mathrm{d}\omega_3}{2\pi} \int \frac{\mathrm{d}\omega_4}{2\pi} \mathcal{G}_{\tilde{\mu}\tilde{\mu}}(\mathrm{i}\omega_1)\mathcal{G}_{\tilde{\nu}\tilde{\nu}}(\mathrm{i}\omega_2) \times \\ & \quad \mathcal{G}_{\tilde{\rho}\tilde{\rho}}(\mathrm{i}\omega_3)\mathcal{G}_{\tilde{\sigma}\tilde{\sigma}}(\mathrm{i}\omega_4)\delta(\mathrm{i}\omega_1 + \mathrm{i}\omega_2 - \mathrm{i}\omega_3 - \mathrm{i}\omega_4) \\ = & \int \frac{\mathrm{d}\omega_1}{2\pi} \int \frac{\mathrm{d}\omega_2}{2\pi} \int \frac{\mathrm{d}\omega_3}{2\pi} \mathcal{G}_{\tilde{\mu}\tilde{\mu}}(\mathrm{i}\omega_1)\mathcal{G}_{\tilde{\nu}\tilde{\nu}}(\mathrm{i}\omega_2) \times \\ & \quad \mathcal{G}_{\tilde{\rho}\tilde{\rho}}(\mathrm{i}\omega_3)\mathcal{G}_{\tilde{\sigma}\tilde{\sigma}}(\mathrm{i}(\omega_1 + \omega_2 - \omega_3)). \end{aligned} \tag{1.86}$$

Using the convention that $\tilde{\epsilon}_{\tilde{\mu}}$ is the $\tilde{\mu}$-th eigenvalue of $H + \Sigma$, we may now write

$$\mathcal{G}_{\tilde{\mu}\tilde{\mu}}(\mathrm{i}\omega_1) = \frac{1}{\mathrm{i}\omega_1 - \tilde{\epsilon}_{\tilde{\mu}} + \mu_{\mathrm{chem}}} =: \frac{1}{\mathrm{i}\omega_1 - \tilde{\xi}_{\tilde{\mu}}}. \tag{1.87}$$

All occurring integrals are of similar form and may be solved by simply closing the integration loop around the left complex half-plane,

$$\int \frac{\mathrm{d}\omega}{2\pi} \frac{1}{\mathrm{i}\omega - z} \frac{1}{\mathrm{i}\omega - \xi} = \frac{g(z,\xi)}{z - \xi}. \tag{1.88}$$

The exact result of the integral will depend on the position of each of the poles $\{x, \xi\}$ relative to the integration loop. If both were inside or outside, the integral gives zero (either the residues cancel or there are no poles inside the loop), there is only a contribution if there is just a single pole inside the loop. The residue is always $\pm(z-\xi)^{-1}$. Therefore, we define $g(z,\xi)$ to keep track of the correct sign. It may be represented as

$$\begin{aligned} g(z,\xi) &= -g(\xi,z) \\ &= \Theta_{\Re}(-z)\Theta_{\Re}(\xi) - \Theta_{\Re}(z)\Theta_{\Re}(-\xi), \end{aligned} \tag{1.89}$$

where $\Theta_{\Re}(z)$ is the Heaviside step function of the real part of z.

Performing the first integral over ω_1, we have

$$\begin{aligned} & \int \frac{\mathrm{d}\omega_1}{2\pi} \frac{1}{\mathrm{i}\omega_1 - \tilde{\xi}_{\tilde{\mu}}} \frac{1}{\mathrm{i}\omega_1 - (\tilde{\xi}_{\tilde{\sigma}} - \mathrm{i}\omega_2 + \mathrm{i}\omega_3)} \\ = & \frac{g(\tilde{\xi}_{\tilde{\mu}}, \tilde{\xi}_{\tilde{\sigma}} + \mathrm{i}(\omega_3 - \omega_2))}{\tilde{\xi}_{\tilde{\mu}} - \tilde{\xi}_{\tilde{\sigma}} + \mathrm{i}\omega_2 - \mathrm{i}\omega_3}. \end{aligned} \tag{1.90}$$

The expression $g(\tilde{\xi}_{\tilde{\mu}}, \tilde{\xi}_{\tilde{\sigma}} + \mathrm{i}(\omega_3 - \omega_2))$ may be simplified further, since for real $\omega_{2,3}$, it is equal to $g(\tilde{\xi}_{\tilde{\mu}}, \tilde{\xi}_{\tilde{\sigma}})$.[1] Applying this result sequentially, the integral in Eq. (1.86) has the result

$$\frac{g(\tilde{\xi}_{\tilde{\mu}}, \tilde{\xi}_{\tilde{\sigma}}) g(\tilde{\xi}_{\tilde{\sigma}} - \tilde{\xi}_{\tilde{\mu}}, \tilde{\xi}_{\tilde{\nu}}) g(\tilde{\xi}_{\tilde{\mu}} + \tilde{\xi}_{\tilde{\nu}} - \tilde{\xi}_{\tilde{\sigma}}, \tilde{\xi}_{\tilde{\rho}})}{\tilde{\xi}_{\tilde{\mu}} + \tilde{\xi}_{\tilde{\nu}} - \tilde{\xi}_{\tilde{\rho}} - \tilde{\xi}_{\tilde{\sigma}}}. \tag{1.91}$$

[1] Note that while closing the integrals over $\omega_{2,3}$, those frequencies may obtain an imaginary part, but since those paths have a vanishing contribution, this may be ignored.

Further simplification is possible: if $\Re\tilde{\xi}_{\tilde{\mu}} > 0$, then $\Re\tilde{\xi}_{\tilde{\sigma}}$ must be less than zero, or the contribution vanishes. In that case, it follows that $\Re(\tilde{\xi}_{\tilde{\sigma}} - \tilde{\xi}_{\tilde{\mu}}) < 0$, and we may deduce in the same way that $\Re\tilde{\xi}_{\tilde{\nu}}$ should be greater than zero. Finally, $\Re(\tilde{\xi}_{\tilde{\mu}} + \tilde{\xi}_{\tilde{\nu}} - \tilde{\xi}_{\tilde{\sigma}}) < 0$ leads to the conclusion that $\Re\tilde{\xi}_{\tilde{\rho}} < 0$. On the other hand, if $\Re\tilde{\xi}_{\tilde{\mu}} < 0$, the analogous argument can be made with flipped inequalities. The only non-zero contributions arise from combinations where the real parts of $\tilde{\xi}_{\tilde{\mu}}$ and $\tilde{\xi}_{\tilde{\nu}}$ have the same sign, but have the opposite sign to both $\tilde{\xi}_{\tilde{\rho}}$ and $\tilde{\xi}_{\tilde{\sigma}}$. Using this result, Eq. (1.82) now reads

$$\begin{aligned} \mathcal{C}_{ij}^{\mathrm{dd},(2)} = & \sum_{\alpha\beta\gamma\delta} \left[\sum_{\tilde{\rho},\tilde{\sigma}:\,\mathrm{holes}}^{\tilde{\mu},\tilde{\nu}:\,\mathrm{electrons}} - \sum_{\tilde{\rho},\tilde{\sigma}:\,\mathrm{electrons}}^{\tilde{\mu},\tilde{\nu}:\,\mathrm{holes}} \right] \times \\ & V_{i\tilde{\mu}}^{\mathrm{ri}} V_{j\tilde{\nu}}^{\mathrm{ri}} \frac{1}{\tilde{\epsilon}_{\tilde{\mu}} + \tilde{\epsilon}_{\tilde{\nu}} - \tilde{\epsilon}_{\tilde{\rho}} - \tilde{\epsilon}_{\tilde{\sigma}}} V_{\tilde{\rho}i}^{\mathrm{ri},-1} V_{\tilde{\sigma}j}^{\mathrm{ri},-1} \times \\ & V_{\tilde{\mu}\alpha}^{\mathrm{in}} V_{\tilde{\nu}\beta}^{\mathrm{in}} \Gamma_{\alpha\beta\gamma\delta} V_{\gamma\tilde{\rho}}^{\mathrm{in},-1} V_{\delta\tilde{\sigma}}^{\mathrm{in},-1}. \end{aligned} \tag{1.92}$$

Density-Density Correlator for Spinless Systems at $T > 0$

At finite temperatures $T > 0$, the result is very similar. To derive it, we need to replace the integrals in Eq. (1.86) by Matsubara sums according to the inverse of Eqs. (1.16,1.17),

$$\begin{aligned} & T\sum_{\omega_n} T\sum_{\omega_m} T\sum_{\omega_{n'}} \mathcal{G}_{\tilde{\mu}\tilde{\mu}}(\mathrm{i}\omega_n)\mathcal{G}_{\tilde{\nu}\tilde{\nu}}(\mathrm{i}\omega_m) \times \\ & \mathcal{G}_{\tilde{\rho}\tilde{\rho}}(\mathrm{i}\omega_{n'})\mathcal{G}_{\tilde{\sigma}\tilde{\sigma}}(\mathrm{i}(\omega_n + \omega_m - \omega_{n'})). \end{aligned} \tag{1.93}$$

Inserting Eq. (1.87) into this expression, we may now perform the Matsubara sums analytically, which are of the form

$$T\sum_{\omega_n} \frac{1}{\mathrm{i}\omega_n - z} \frac{1}{\mathrm{i}\omega_n - \xi} = \frac{n_{\mathrm{F}}(z) - n_{\mathrm{F}}(\xi)}{z - \xi}, \tag{1.94}$$

where n_{F} is the Fermi function. We note that due to its periodicity we have $n_{\mathrm{F}}(\tilde{\xi} \pm \mathrm{i}\omega_{n'}) = n_{\mathrm{F}}(\tilde{\xi})$ if $\omega_{n'}$ is a Matsubara function, so we may simplify the numerator again. Eq. (1.93) is thus equal to

$$\begin{aligned} & [n_{\mathrm{F}}(\tilde{\xi}_{\tilde{\mu}}) - n_{\mathrm{F}}(\tilde{\xi}_{\tilde{\sigma}})][n_{\mathrm{F}}(\tilde{\xi}_{\tilde{\sigma}} - \tilde{\xi}_{\tilde{\mu}}) - n_{\mathrm{F}}(\tilde{\xi}_{\tilde{\nu}})] \times \\ & \frac{[n_{\mathrm{F}}(\tilde{\xi}_{\tilde{\mu}} + \tilde{\xi}_{\tilde{\nu}} - \tilde{\xi}_{\tilde{\sigma}}) - n_{\mathrm{F}}(\tilde{\xi}_{\tilde{\rho}})]}{\tilde{\xi}_{\tilde{\mu}} + \tilde{\xi}_{\tilde{\nu}} - \tilde{\xi}_{\tilde{\rho}} - \tilde{\xi}_{\tilde{\sigma}}}. \end{aligned} \tag{1.95}$$

Therefore, we have

$$\begin{aligned}\mathcal{C}_{ij}^{\mathrm{dd},(2)} &= \sum_{\alpha\beta\gamma\delta}\sum_{\tilde{\mu}\tilde{\nu}\tilde{\rho}\tilde{\sigma}} V_{i\tilde{\mu}}^{\mathrm{ri}} V_{j\tilde{\nu}}^{\mathrm{ri}} \frac{1}{\tilde{\epsilon}_{\tilde{\mu}}+\tilde{\epsilon}_{\tilde{\nu}}-\tilde{\epsilon}_{\tilde{\rho}}-\tilde{\epsilon}_{\tilde{\sigma}}} \times \\ &\quad [n_{\mathrm{F}}(\tilde{\xi}_{\tilde{\sigma}})-n_{\mathrm{F}}(\tilde{\xi}_{\tilde{\mu}})][n_{\mathrm{F}}(\tilde{\xi}_{\tilde{\sigma}}-\tilde{\xi}_{\tilde{\mu}})-n_{\mathrm{F}}(\tilde{\xi}_{\tilde{\nu}})] \times \\ &\quad [n_{\mathrm{F}}(\tilde{\xi}_{\tilde{\mu}}+\tilde{\xi}_{\tilde{\nu}}-\tilde{\xi}_{\tilde{\sigma}})-n_{\mathrm{F}}(\tilde{\xi}_{\tilde{\rho}})] V_{\tilde{\rho}i}^{\mathrm{ri},-1} V_{\tilde{\sigma}j}^{\mathrm{ri},-1} \times \\ &\quad V_{\tilde{\mu}\alpha}^{\mathrm{in}} V_{\tilde{\nu}\beta}^{\mathrm{in}} \Gamma_{\alpha\beta\gamma\delta} V_{\gamma\tilde{\rho}}^{\mathrm{in},-1} V_{\delta\tilde{\sigma}}^{\mathrm{in},-1}. \end{aligned} \tag{1.96}$$

For orbitals far away from the Fermi energy, $|\tilde{\xi}| \gg T$, this expression goes over into the expression for $T = 0$ and we arrive at Eq. (1.92) again.

Density-Density Correlator for Systems with Spin

In systems with spin we must also sum over two spin indices when calculating $\mathcal{C}_{ij}^{\mathrm{dd},(2)}$. We replace all orbital indices in Eq. (1.96) by pairs of orbital and spin indices, $\alpha \to (\alpha, \sigma)$. For systems with SU(2) symmetry all single-particle quantities are diagonal in spin space, so after performing sums over all the relevant Kronecker-δs, we have

$$\begin{aligned}\mathcal{C}_{ij}^{\mathrm{dd},(2)} &= \sum_{\sigma\sigma'}\sum_{\alpha\beta\gamma\delta}\sum_{\tilde{\mu}\tilde{\nu}\tilde{\rho}\tilde{\sigma}} V_{i\tilde{\mu}}^{\mathrm{ri}} V_{j\tilde{\nu}}^{\mathrm{ri}} \frac{1}{\tilde{\epsilon}_{\tilde{\mu}}+\tilde{\epsilon}_{\tilde{\nu}}-\tilde{\epsilon}_{\tilde{\rho}}-\tilde{\epsilon}_{\tilde{\sigma}}} \times \\ &\quad [n_{\mathrm{F}}(\tilde{\xi}_{\tilde{\sigma}})-n_{\mathrm{F}}(\tilde{\xi}_{\tilde{\mu}})][n_{\mathrm{F}}(\tilde{\xi}_{\tilde{\sigma}}-\tilde{\xi}_{\tilde{\mu}})-n_{\mathrm{F}}(\tilde{\xi}_{\tilde{\nu}})] \times \\ &\quad [n_{\mathrm{F}}(\tilde{\xi}_{\tilde{\mu}}+\tilde{\xi}_{\tilde{\nu}}-\tilde{\xi}_{\tilde{\sigma}})-n_{\mathrm{F}}(\tilde{\xi}_{\tilde{\rho}})] V_{\tilde{\rho}i}^{\mathrm{ri},-1} V_{\tilde{\sigma}j}^{\mathrm{ri},-1} \times \\ &\quad V_{\tilde{\mu}\alpha}^{\mathrm{in}} V_{\tilde{\nu}\beta}^{\mathrm{in}} \Gamma_{(\alpha,\sigma)(\beta,\sigma')(\gamma,\sigma)(\delta,\sigma')} V_{\gamma\tilde{\rho}}^{\mathrm{in},-1} V_{\delta\tilde{\sigma}}^{\mathrm{in},-1}. \end{aligned} \tag{1.97}$$

Inserting Eq. (1.53), we may perform the summation over the remaining spin indices and arrive at

$$\begin{aligned}\mathcal{C}_{ij}^{\mathrm{dd},(2)} &= \sum_{\alpha\beta\gamma\delta}\sum_{\tilde{\mu}\tilde{\nu}\tilde{\rho}\tilde{\sigma}} V_{i\tilde{\mu}}^{\mathrm{ri}} V_{j\tilde{\nu}}^{\mathrm{ri}} \frac{1}{\tilde{\epsilon}_{\tilde{\mu}}+\tilde{\epsilon}_{\tilde{\nu}}-\tilde{\epsilon}_{\tilde{\rho}}-\tilde{\epsilon}_{\tilde{\sigma}}} \times \\ &\quad [n_{\mathrm{F}}(\tilde{\xi}_{\tilde{\sigma}})-n_{\mathrm{F}}(\tilde{\xi}_{\tilde{\mu}})][n_{\mathrm{F}}(\tilde{\xi}_{\tilde{\sigma}}-\tilde{\xi}_{\tilde{\mu}})-n_{\mathrm{F}}(\tilde{\xi}_{\tilde{\nu}})] \times \\ &\quad [n_{\mathrm{F}}(\tilde{\xi}_{\tilde{\mu}}+\tilde{\xi}_{\tilde{\nu}}-\tilde{\xi}_{\tilde{\sigma}})-n_{\mathrm{F}}(\tilde{\xi}_{\tilde{\rho}})] V_{\tilde{\rho}i}^{\mathrm{ri},-1} V_{\tilde{\sigma}j}^{\mathrm{ri},-1} \times \\ &\quad V_{\tilde{\mu}\alpha}^{\mathrm{in}} V_{\tilde{\nu}\beta}^{\mathrm{in}} \Big[2\Gamma^{\mathrm{s}}_{\alpha\beta\gamma\delta} - 4\Gamma^{\mathrm{s}}_{\alpha\beta\delta\gamma}\Big] V_{\gamma\tilde{\rho}}^{\mathrm{in},-1} V_{\delta\tilde{\sigma}}^{\mathrm{in},-1}. \end{aligned} \tag{1.98}$$

At $T = 0$, the result is analogously given by

$$\begin{aligned} \mathcal{C}_{ij}^{\mathrm{dd},(2)} &= \sum_{\alpha\beta\gamma\delta} \left[\sum_{\tilde{\rho},\tilde{\sigma}\colon \mathrm{holes}}^{\tilde{\mu},\tilde{\nu}\colon \mathrm{electrons}} - \sum_{\tilde{\rho},\tilde{\sigma}\colon \mathrm{electrons}}^{\tilde{\mu},\tilde{\nu}\colon \mathrm{holes}} \right] \times \\ & V_{i\tilde{\mu}}^{\mathrm{ri}} V_{j\tilde{\nu}}^{\mathrm{ri}} \frac{1}{\tilde{\epsilon}_{\tilde{\mu}} + \tilde{\epsilon}_{\tilde{\nu}} - \tilde{\epsilon}_{\tilde{\rho}} - \tilde{\epsilon}_{\tilde{\sigma}}} V_{\tilde{\rho}i}^{\mathrm{ri},-1} V_{\tilde{\sigma}j}^{\mathrm{ri},-1} \times \\ & V_{\tilde{\mu}\alpha}^{\mathrm{in}} V_{\tilde{\nu}\beta}^{\mathrm{in}} \Big[2\Gamma^{\mathrm{s}}_{\alpha\beta\gamma\delta} - 4\Gamma^{\mathrm{s}}_{\alpha\beta\delta\gamma} \Big] V_{\gamma\tilde{\rho}}^{\mathrm{in},-1} V_{\delta\tilde{\sigma}}^{\mathrm{in},-1}. \end{aligned} \tag{1.99}$$

Spin-Spin Correlator

In contrast to the expectation value of $\mathbf{S}_i$, the expectation value of $\mathbf{S}_i \cdot \mathbf{S}_j$ does not automatically vanish in systems with SU(2) symmetry. Using

$$\mathbf{S}_i = \sum_{\sigma\sigma'} \hat{\mathrm{c}}_{i\sigma}^\dagger \vec{\tau}_{\sigma\sigma'} \hat{\mathrm{c}}_{i\sigma'}, \tag{1.100}$$

where $\vec{\tau}$ are the Pauli matrices. Using the identity

$$\sum_{k=0}^{3} \tau_{\sigma\sigma'}^k \tau_{\bar{\sigma}\bar{\sigma}'}^k = 2\delta_{\sigma\bar{\sigma}'}\delta_{\sigma'\bar{\sigma}}, \tag{1.101}$$

we may write

$$\begin{aligned} \mathcal{C}_{ij}^{\mathrm{ss}} &:= \Big\langle \mathbf{S}_i \cdot \mathbf{S}_j \Big\rangle \\ &= \sum_k \sum_{\sigma\sigma'} \sum_{\bar{\sigma}\bar{\sigma}'} \tau_{\sigma\sigma'}^k \tau_{\bar{\sigma}\bar{\sigma}'}^k \Big\langle \hat{\mathrm{c}}_{i\sigma}^\dagger \hat{\mathrm{c}}_{i\sigma'} \hat{\mathrm{c}}_{j\bar{\sigma}}^\dagger \hat{\mathrm{c}}_{j\bar{\sigma}'} \Big\rangle \\ &= 2\sum_{\sigma\sigma'} \Big\langle \hat{\mathrm{c}}_{i\sigma}^\dagger \hat{\mathrm{c}}_{i\sigma'} \hat{\mathrm{c}}_{j\sigma'}^\dagger \hat{\mathrm{c}}_{j\sigma} \Big\rangle - \Big\langle \hat{\mathrm{n}}_i \hat{\mathrm{n}}_j \Big\rangle \\ &= 2\sum_{\sigma\sigma'} \Big\langle \hat{\mathrm{c}}_{i\sigma}^\dagger \hat{\mathrm{c}}_{j\sigma'}^\dagger \hat{\mathrm{c}}_{j\sigma} \hat{\mathrm{c}}_{i\sigma'} \Big\rangle - \Big\langle \hat{\mathrm{n}}_i \hat{\mathrm{n}}_j \Big\rangle - 4\delta_{ij} \Big\langle \hat{\mathrm{n}}_i \Big\rangle \\ &= \mathcal{C}_{ij}^{\mathrm{ss},(2)} - \Big\langle \hat{\mathrm{n}}_i \hat{\mathrm{n}}_j \Big\rangle - 4\delta_{ij} \Big\langle \hat{\mathrm{n}}_i \Big\rangle \\ &\quad + 2\sum_{\sigma\sigma'} \left[\Big\langle \hat{\mathrm{c}}_{j\sigma'}^\dagger \hat{\mathrm{c}}_{j\sigma} \Big\rangle \Big\langle \hat{\mathrm{c}}_{i\sigma}^\dagger \hat{\mathrm{c}}_{i\sigma'} \Big\rangle - \Big\langle \hat{\mathrm{c}}_{i\sigma}^\dagger \hat{\mathrm{c}}_{j\sigma} \Big\rangle \Big\langle \hat{\mathrm{c}}_{j\sigma'}^\dagger \hat{\mathrm{c}}_{i\sigma'} \Big\rangle \right] \\ &= \mathcal{C}_{ij}^{\mathrm{ss},(2)} + 4\Big\langle \hat{\mathrm{n}}_{i\sigma} \Big\rangle \Big\langle \hat{\mathrm{n}}_{j\sigma} \Big\rangle - 8\Big\langle \hat{\mathrm{c}}_{i\sigma}^\dagger \hat{\mathrm{c}}_{j\sigma} \Big\rangle \Big\langle \hat{\mathrm{c}}_{j\sigma}^\dagger \hat{\mathrm{c}}_{i\sigma} \Big\rangle \\ &\qquad - \Big\langle \hat{\mathrm{n}}_i \hat{\mathrm{n}}_j \Big\rangle - 4\delta_{ij} \Big\langle \hat{\mathrm{n}}_i \Big\rangle. \end{aligned} \tag{1.102}$$

Inserting Eq. (1.81), quite a few terms cancel and we arrive at

$$\mathcal{C}_{ij}^{\mathrm{ss}} = \mathcal{C}_{ij}^{\mathrm{ss},(2)} - \mathcal{C}_{ij}^{\mathrm{dd},(2)} - 6\Big(\Big\langle \hat{\mathrm{c}}_{i\sigma}^{\dagger}\hat{\mathrm{c}}_{j\sigma}\Big\rangle\Big\langle \hat{\mathrm{c}}_{j\sigma}^{\dagger}\hat{\mathrm{c}}_{i\sigma}\Big\rangle + \delta_{ij}\Big\langle \hat{\mathrm{n}}_{i}\Big\rangle\Big). \tag{1.103}$$

The expression for $\mathcal{C}_{ij}^{\mathrm{ss},(2)}$ may be derived in the same manner as the expression for $\mathcal{C}_{ij}^{\mathrm{dd},(2)}$. At finite temperatures, it reads

$$\begin{aligned}
\mathcal{C}_{ij}^{\mathrm{ss},(2)} &= 2\sum_{\alpha\beta\gamma\delta}\sum_{\tilde{\mu}\tilde{\nu}\tilde{\rho}\tilde{\sigma}} V_{i\tilde{\mu}}^{\mathrm{ri}} V_{j\tilde{\nu}}^{\mathrm{ri}} \frac{1}{\tilde{\epsilon}_{\tilde{\mu}}+\tilde{\epsilon}_{\tilde{\nu}}-\tilde{\epsilon}_{\tilde{\rho}}-\tilde{\epsilon}_{\tilde{\sigma}}} \times \\
&\quad [n_{\mathrm{F}}(\tilde{\xi}_{\tilde{\sigma}}) - n_{\mathrm{F}}(\tilde{\xi}_{\tilde{\mu}})][n_{\mathrm{F}}(\tilde{\xi}_{\tilde{\sigma}}-\tilde{\xi}_{\tilde{\mu}}) - n_{\mathrm{F}}(\tilde{\xi}_{\tilde{\nu}})] \times \\
&\quad [n_{\mathrm{F}}(\tilde{\xi}_{\tilde{\mu}}+\tilde{\xi}_{\tilde{\nu}}-\tilde{\xi}_{\tilde{\sigma}}) - n_{\mathrm{F}}(\tilde{\xi}_{\tilde{\rho}})] V_{\tilde{\rho}i}^{\mathrm{ri},-1} V_{\tilde{\sigma}j}^{\mathrm{ri},-1} \times \\
&\quad V_{\tilde{\mu}\alpha}^{\mathrm{in}} V_{\tilde{\nu}\beta}^{\mathrm{in}} \Big[4\Gamma^{\mathrm{s}}_{\alpha\beta\gamma\delta} - 2\Gamma^{\mathrm{s}}_{\alpha\beta\delta\gamma}\Big] V_{\gamma\tilde{\rho}}^{\mathrm{in},-1} V_{\delta\tilde{\sigma}}^{\mathrm{in},-1}.
\end{aligned} \tag{1.104}$$

A more interesting quantity is the difference between $\mathcal{C}_{ij}^{\mathrm{ss},(2)}$ and $\mathcal{C}_{ij}^{\mathrm{dd},(2)}$,

$$\begin{aligned}
\mathcal{C}_{ij}^{\mathrm{ss}',(2)} &= \mathcal{C}_{ij}^{\mathrm{ss},(2)} - \mathcal{C}_{ij}^{\mathrm{dd},(2)} \\
&= 6\sum_{\alpha\beta\gamma\delta}\sum_{\tilde{\mu}\tilde{\nu}\tilde{\rho}\tilde{\sigma}} V_{i\tilde{\mu}}^{\mathrm{ri}} V_{j\tilde{\nu}}^{\mathrm{ri}} \frac{1}{\tilde{\epsilon}_{\tilde{\mu}}+\tilde{\epsilon}_{\tilde{\nu}}-\tilde{\epsilon}_{\tilde{\rho}}-\tilde{\epsilon}_{\tilde{\sigma}}} \times \\
&\quad [n_{\mathrm{F}}(\tilde{\xi}_{\tilde{\sigma}}) - n_{\mathrm{F}}(\tilde{\xi}_{\tilde{\mu}})][n_{\mathrm{F}}(\tilde{\xi}_{\tilde{\sigma}}-\tilde{\xi}_{\tilde{\mu}}) - n_{\mathrm{F}}(\tilde{\xi}_{\tilde{\nu}})] \times \\
&\quad [n_{\mathrm{F}}(\tilde{\xi}_{\tilde{\mu}}+\tilde{\xi}_{\tilde{\nu}}-\tilde{\xi}_{\tilde{\sigma}}) - n_{\mathrm{F}}(\tilde{\xi}_{\tilde{\rho}})] V_{\tilde{\rho}i}^{\mathrm{ri},-1} V_{\tilde{\sigma}j}^{\mathrm{ri},-1} \times \\
&\quad V_{\tilde{\mu}\alpha}^{\mathrm{in}} V_{\tilde{\nu}\beta}^{\mathrm{in}} \Gamma^{\mathrm{s}}_{\alpha\beta\gamma\delta} V_{\gamma\tilde{\rho}}^{\mathrm{in},-1} V_{\delta\tilde{\sigma}}^{\mathrm{in},-1}.
\end{aligned} \tag{1.105}$$

At $T = 0$, the expression reads

$$\begin{aligned}
\mathcal{C}_{ij}^{\mathrm{ss}',(2)} &= 6\sum_{\alpha\beta\gamma\delta}\left[\sum_{\tilde{\rho},\tilde{\sigma}:\,\mathrm{holes}}^{\tilde{\mu},\tilde{\nu}:\,\mathrm{electrons}} - \sum_{\tilde{\rho},\tilde{\sigma}:\,\mathrm{electrons}}^{\tilde{\mu},\tilde{\nu}:\,\mathrm{holes}}\right] \times \\
&\quad V_{i\tilde{\mu}}^{\mathrm{ri}} V_{j\tilde{\nu}}^{\mathrm{ri}} \frac{1}{\tilde{\epsilon}_{\tilde{\mu}}+\tilde{\epsilon}_{\tilde{\nu}}-\tilde{\epsilon}_{\tilde{\rho}}-\tilde{\epsilon}_{\tilde{\sigma}}} V_{\tilde{\rho}i}^{\mathrm{ri},-1} V_{\tilde{\sigma}j}^{\mathrm{ri},-1} \times \\
&\quad V_{\tilde{\mu}\alpha}^{\mathrm{in}} V_{\tilde{\nu}\beta}^{\mathrm{in}} \Gamma^{\mathrm{s}}_{\alpha\beta\gamma\delta} V_{\gamma\tilde{\rho}}^{\mathrm{in},-1} V_{\delta\tilde{\sigma}}^{\mathrm{in},-1}.
\end{aligned} \tag{1.106}$$

1.6 Reduction in the number of orbitals

We would like to emphasize that the flow equations for the self-energy and the vertex, even in their simplest form, Eqs. (1.31,1.41), are still challenging computationally. In

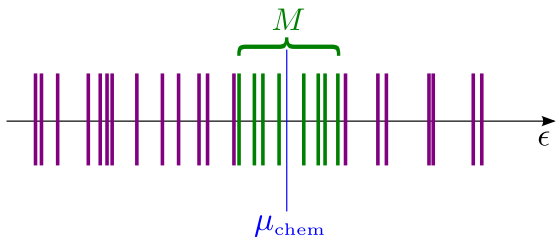

Figure 1.2: *Selection of M orbitals (green) around μ_{chem} for which the vertex will be renormalized. The self-energy will still be stored for all N orbitals, including the remaining (purple) ones.*

inhomogeneous systems, in general there are no further symmetries for us left to exploit, most notably there is no translational symmetry and hence no quasi-momentum conservation, which would simplify these equations greatly – in translationally invariant systems all single-particle quantities are diagonal in momentum space, and the vertex only depends on three momenta, the fourth given by momentum conservation.

Furthermore, in translationally invariant systems the approximation that only momenta on the Fermi surface are relevant is ubiquitously employed. The Brillouin zone is divided into patches that each contain one of the tracked momenta on the Fermi surface and the vertex is only calculated for those momenta. Whenever it needs to be evaluated for other momenta, it is replaced by the vertex evaluated at known momenta within the same patch. [10] This greatly decreases the degrees of freedom that need to be kept in homogeneous systems.

In our setup this is not possible, since there is no concept of a well-defined Fermi surface; the discrete orbitals of the inhomogeneous system can't (in general) be characterized in a systematic fashion. Therefore, we propose an alternative approach to reducing the degrees of freedom of the problem, compatible with inhomogeneous systems: we store and calculate the vertex only for a reduced set of M orbitals around the chemical potential, μ_{chem}, (typically half above and half below); see Fig. 1.2 for details. The external indices of the flow equation for the vertex, Eq. 1.41, now only span a reduced number of states. On the right hand side the vertex still needs to be evaluated for orbitals not included in the list of selected state, there we choose to replace it by the bare interaction,

$$\Gamma^{\Lambda}_{\alpha\beta\gamma\delta} \to \begin{cases} \Gamma^{\Lambda}_{\alpha\beta\gamma\delta} & \{\alpha,\beta,\gamma,\delta\} \subseteq S_M \\ U_{\alpha\beta\gamma\delta} & \text{otherwise} \end{cases} , \tag{1.107}$$

where S_M is the set of M selected orbitals. In the following, we will denote indices that are to be taken from S_M with bars, e.g. $\bar{\alpha}$, whereas indices that are to be taken from the set of all orbitals without bars, e.g. α.

The flow of the self-energy will still be calculated for all orbitals, as it does not increase the complexity of the calculation relative to the diagram of the vertex.

We note that at finite temperatures the approximation of choosing only M states close to μ_{chem} is only valid if $T \ll \Delta_M$, where Δ_M is the spacing between the lowest and highest states for which the vertex dependency is kept.

Finally, we would like to comment on the choice for M at a given system size. As long as the approximation holds that only physics close to the Fermi energy is relevant for the FRG flow (as is also assumed in applications of the FRG for translationally invariant systems), we can argue that the number of states for which the vertex is kept, M, should grow sub-linearly with the total number of orbitals, N. In a translationally invariant system, the Fermi surface is an object of dimensionality $d-1$ within the d-dimensional Brillouin zone. Since the number of states in the Brillouin zone grows as L^d, but the number of states on a surface within that space grows as L^{d-1}, we conclude that even for inhomogeneous systems, where we cannot define a clear Fermi surface, it is reasonable to expect that the number of states required should be proportional to L^{d-1}, which can be rewritten as $L^{d-1} = (L^d)^{(d-1)/d} = N^{1-1/d}$. This gives us some confidence that the number of states M we need to keep should grow as $\sqrt{N}$ in two-dimensional systems.

Note that this does not hold true for zero-dimensional systems (e.g. quantum dots, molecules), since the argument relies on taking the thermodynamic limit. We will revisit those types of systems in our outlook, Sec. 5.2.

In Chapter 3 we will demonstrate the efficacy of this approximation and also revisit the question of system size scaling.

1.6.1 Phase Transitions due to Interactions

One of the main applications of the functional renormalization group is the study of phase diagrams, because it provides an unbiased view of competing instabilities of the system. We will now discuss two cases: applying the FRG to a system in a parameter regime where no symmetry is spontaneously broken, and applying it to a system in a parameter regime where the ground state of the system has a spontaneously broken symmetry.

First we must note that our approach tackles finite size systems. We may therefore only extrapolate the behavior in the thermodynamic limit by increasing the system size. More importantly, however, if one considers a system that in the thermodynamic limit has a quantum critical point at $U = 0$, such that even with an infinitesimally small interaction the symmetry is broken, for finite system sizes there will be a finite $U^*(L)$. Below this value the system will still remain adiabatically connected to the non-interacting starting point, and only above that value will it start to show characteristics of the symmetry-broken phase. It is therefore important to study the behavior of $U^*(L)$ with increasing system size to determine whether there is a phase transition at finite U

or not. Finally, if there is a phase transition that the non-interacting system undergoes (e.g. Anderson transition), it must be detected using the non-interacting quantities instead of the method described for interaction-induced phase transitions.

In a parameter regime where the symmetries of the non-interacting system are intact is trivial: the interaction will renormalize certain quantities. The FRG flow will continue to the end and one has access to the full single and two-particle quantities of that system.

The more interesting case is when the ground state symmetry of a given system is broken. Then at a critical scale Λ_c during the flow the vertex will diverge. The drastic increase of the vertex with decreasing Λ is referred to as the flow to strong coupling. Once this happens, one needs to stop the flow, because the current scheme is not sufficient to describe the symmetry-broken phase. However, it is possible to infer a tentative phase diagram by comparing the strength of two-particle correlators at Λ_c. This is the reason why the FRG is considered to be an unbiased method, because there are no assumptions made a priori as to which correlator will diverge most strongly. This will be the method by which we will classify interaction-based phase transitions within our work.

There are cases in which competing order parameters influence each other (such as antiferromagnetism and d-wave superconductivity), so that if possible one should continue the flow to $\Lambda \to 0$ to obtain information about the true phase diagram of the system. This may be done via either the introduction of an infinitesimal symmetry-breaking term in the action that becomes finite during the flow, as has been done for superconductivity in [25]. Alternatively, one may calculate the flow for the combined Bose-Fermi system, where Fermions were decoupled via a Hubbard-Stratonovich transformation.[26] Due to the computational cost that these procedures incur already for translationally invariant systems, it is still an open question as to how to best adapt these schemes for inhomogeneous systems.

Chapter 2
2 Implementation

We discuss details of our implementation of the flow equations derived in previous chapters. We cover details on how to efficiently implement the diagrams for the vertex flow and the correlators, how to properly parallelize the code and our treatment of the chemical potential during the renormalization procedure.

We implement the FRG procedure in C++, using the Eigen linear algebra library [27] for matrix products and the HDF5 file format [28] for storage. We employ the OpenMP 3.1 standard [29] for parallelization.

2.1 Efficient Trace Evaluation

To discuss the computation complexity of the flow equations, we use N to denote the number of total single-particle orbitals and M the number of states for which the vertex flow is kept (see Section 1.6). With this in mind, the computational complexity of the self-energy flow, Eqs. (1.31,1.55,1.70), is given by $\mathcal{O}(N^4)$ – two loops for each of the outer indices, two loops for the contraction with the non-diagonal single-scale propagator. At first glance the flow of the vertex, e.g. Eq. (1.41) appears to have a complexity of $\mathcal{O}(N^8)$. However, one may define intermediate products, $I^{\mathrm{c},\pm}, I^{\mathrm{ph},\pm}$,

$$I^{\mathrm{c},+}_{\mu\rho\bar{\gamma}\bar{\delta}} = \sum_{\nu} P^{\Lambda,s}_{\mu\nu}(\Lambda)\Gamma^{\Lambda}_{\nu\rho\bar{\gamma}\bar{\delta}} \tag{2.1}$$

$$I^{\mathrm{c},-}_{\bar{\alpha}\bar{\beta}\rho\mu} = \sum_{\sigma} P^{\Lambda,s}_{\rho\sigma}(-\Lambda)\Gamma^{\Lambda}_{\bar{\alpha}\bar{\beta}\sigma\mu} \tag{2.2}$$

$$I^{\mathrm{ph},\pm}_{\bar{\alpha}\nu\bar{\gamma}\sigma} = \sum_{\rho} \Gamma^{\Lambda}_{\bar{\alpha}\nu\bar{\gamma}\rho} P^{\Lambda,s}_{\rho\sigma}(\pm\Lambda), \tag{2.3}$$

where each of these partial diagrams has a complexity of $\mathcal{O}(N^5)$. The flow equation for the vertex now reads

$$\begin{aligned}\frac{\mathrm{d}}{\mathrm{d}\Lambda}\Gamma^{\Lambda}_{\bar{\alpha}\bar{\beta}\bar{\gamma}\bar{\delta}} &= -\frac{1}{2\pi}\sum_{\mu\rho}\Big\{ I^{\mathrm{c},+}_{\mu\rho\bar{\gamma}\bar{\delta}} I^{\mathrm{c},-}_{\bar{\alpha}\bar{\beta}\rho\mu} \\ &\quad + I^{\mathrm{ph},+}_{\bar{\alpha}\mu\bar{\gamma}\rho} I^{\mathrm{ph},+}_{\bar{\beta}\rho\bar{\delta}\mu} + I^{\mathrm{ph},-}_{\bar{\alpha}\mu\bar{\gamma}\rho} I^{\mathrm{ph},-}_{\bar{\beta}\rho\bar{\delta}\mu} - I^{\mathrm{ph},+}_{\bar{\beta}\mu\bar{\gamma}\rho} I^{\mathrm{ph},+}_{\bar{\alpha}\rho\bar{\delta}\mu} - I^{\mathrm{ph},-}_{\bar{\beta}\mu\bar{\gamma}\rho} I^{\mathrm{ph},-}_{\bar{\alpha}\rho\bar{\delta}\mu} \Big\}, \quad (2.4)\end{aligned}$$

with a computational complexity of $\mathcal{O}(N^6)$. In the case of $M < N$, using the replacement in Eq. (1.107), this reduces to $\mathcal{O}(N^2M^3)$ for the calculation of the intermediates and to $\mathcal{O}(N^2M^4)$ for the trace.

Using our argument from Sec. 1.6 that $M \propto \sqrt{N}$, we expect a scaling of $\mathcal{O}(N^4)$ for two-dimensional systems.

2.1.1 GEMM kernels for Tensor evaluation

In order to evaluate the temporary products for the flow of the vertex, Eqs. (2.1,2.2,2.3), it is advantageous to rewrite the expression in terms of a matrix product, e.g.

$$I^{\mathrm{c},+}_{\mu,(\rho\bar{\gamma}\bar{\delta})} = \sum_{\nu} P^{\Lambda,s}_{\mu\nu}(\Lambda)\Gamma^{\Lambda}_{\nu,(\rho\bar{\gamma}\bar{\delta})}, \quad (2.5)$$

where we interpret $(\rho\bar{\gamma}\bar{\delta})$ as a single index, because modern generic matrix-matrix multiplication (GEMM) kernels are highly optimized and perform far better than a simple sum. For the cases where we calculate the renormalization of the vertex for all states, this is trivial. Note that for some equations one needs to retain a copy of the vertex with transposed indices to be able to do this. Since our implementation is typically not constrained by the available memory but rather the available processing power, this tradeoff is advantageous.

It is trickier to approximate the vertex according to Eq. (1.107). Instead of rewriting the entire expression in terms of a GEMM kernel, we need to perform the loop on the external indices explicitly. We may then split up the resulting matrix product into five parts. Taking for example Eq. (2.1) and using that S_M is the subset of states for which

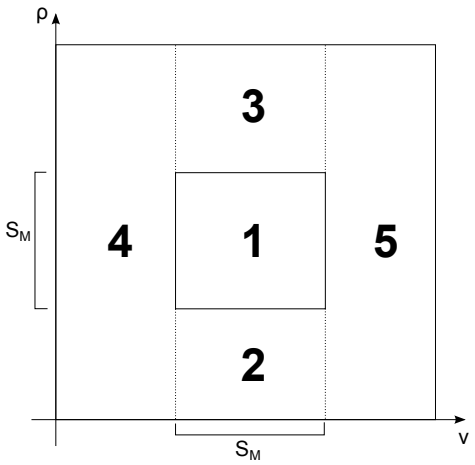

Figure 2.1: *The subdivision of the GEMM kernel for the intermediate product $I^{c,+}$ in the ν and ρ indices. The regions one to five in the diagram correspond to the terms of Eqs. (2.6,2.7,2.8,2.9,2.10), respectively.*

the vertex is renormalized, we have

$$
\begin{aligned}
I^{c,+}_{\mu\rho\bar{\gamma}\bar{\delta}} \;=\; & \sum_{\bar{\nu}\in S_M} P^{\Lambda,s}_{\mu\bar{\nu}}(\Lambda)\Gamma^{\Lambda}_{\bar{\nu}\rho\bar{\gamma}\bar{\delta}} \qquad [\rho \in S_M] && (2.6)\\
& + \sum_{\bar{\nu}\in S_M} P^{\Lambda,s}_{\mu\bar{\nu}}(\Lambda)U_{\bar{\nu}\rho\bar{\gamma}\bar{\delta}} \qquad [\rho < \min(S_M)] && (2.7)\\
& + \sum_{\bar{\nu}\in S_M} P^{\Lambda,s}_{\mu\bar{\nu}}(\Lambda)U_{\bar{\nu}\rho\bar{\gamma}\bar{\delta}} \qquad [\rho > \max(S_M)] && (2.8)\\
& + \sum_{\nu<\min(S_M)} P^{\Lambda,s}_{\mu\nu}(\Lambda)U_{\nu\rho\bar{\gamma}\bar{\delta}} && (2.9)\\
& + \sum_{\nu>\max(S_M)} P^{\Lambda,s}_{\mu\nu}(\Lambda)U_{\nu\rho\bar{\gamma}\bar{\delta}}. && (2.10)
\end{aligned}
$$

We assume here that the non-interacting states are ordered in energy. The five subexpressions may then be written in terms of GEMM kernels with rectangular blocks of the matrices $P^{\Lambda,s}$ and $U_{..\bar{\gamma}\bar{\delta}}$. Figure 2.1 shows the division into these terms in the plane of ν and ρ indices.

There are no standard kernels for trace evaluation, e.g. Eq. (2.4), hence we implement that directly in terms of a loop.

2.1.2 Parallelization

In the era of computer systems with multiple processor cores, parallel computation has become more and more important. We will now discuss how we exploit this in our implementation. Within our code we use a parallelization scheme based on a shared memory architecture, OpenMP [29]. It is in principle possible to utilize distributed memory methods, such as MPI (Message Passing Interface, [30]), which allow the usage of far more processor cores for the same calculation. However, it makes little sense to utilize a large number of computer nodes for a single system if this has to be performed multiple times if one keeps disorder averaging in mind. In the following we will discuss the two most expensive parts of the calculation and how parallelization applies to them: intermediate products for the vertex flow and trace evaluation.

The intermediate products offer a trivial way to parallelize: it is possible to use a parallel version of the GEMM kernel to calculate the matrix products. In the case we track the renormalization of the entire vertex, this would likely be the most efficient avenue. In our case, however, the effective matrix size that is fed into the GEMM kernel is relatively small (we want to calculate the vertex for as few states as possible), so it is unlikely that using a parallel matrix product kernel will scale well even for a low amount of processors. Instead, we parallelize the loops over the two outer indices in the intermediate products and perform serialized matrix products on each processor. This is trivially possible, since the calculations are independent of each other for any given pair of external indices.

Similarly, for the evaluation of the trace, we parallelize the loops over all four external indices and have each processor evaluate the trace for a given set of external indices serially.

Further details on the parallelization are explained in Appendix A.

2.2 Chemical Potential

We want to keep the number of particles fixed to study the system at a given filling fraction. Since our flow modifies the real part of the self-energy, we need to constantly adjust the chemical potential during the renormalization procedure. We have the advantage that disorder makes sure that we always have a finite level spacing.

2.2.1 Zero Temperature

At $T = 0$ we diagonalize the matrix $H_0 + \Sigma^\Lambda$ to obtain the new quasi-particle energies for a given Λ (including the initial Λ_0, since $\Sigma^{\Lambda_0} \neq 0$). We choose our chemical potential to be

$$\mu^\Lambda_{\text{chem}} = \frac{1}{2}(\tilde{\epsilon}^\Lambda_{N_e+1} + \tilde{\epsilon}^\Lambda_{N_e}), \tag{2.11}$$

where $\tilde{\epsilon}^{\Lambda}_{N_\mathrm{e}}$ is the energy of the highest occupied quasi-particle state and $\tilde{\epsilon}^{\Lambda}_{N_\mathrm{e}}$ the energy of the lowest unoccupied quasi-particle state. We choose this representation over the more $\tilde{\epsilon}^{\Lambda}_{N_\mathrm{e}} + 0^+$ to increase numerical stability and because it is value of μ_chem when taking the $T \to 0$ limit from finite temperature. Note that both choices become equivalent for the limit of large system sizes (as long as the chemical potential is within a band), as the mean level spacing goes to zero.

2.2.2 Finite Temperatures

At $T > 0$ we have to find the solution to the equation

$$N_\mathrm{e} = \sum_{\tilde{\epsilon}^{\Lambda}_{\tilde{\alpha}} < \mu^{\Lambda}_\mathrm{chem}} n_\mathrm{F}(\tilde{\epsilon}_{\tilde{\alpha}} - \mu^{\Lambda}_\mathrm{chem}), \tag{2.12}$$

where N_e is the number of electrons in the given system and $\tilde{\epsilon}^{\Lambda}_{\tilde{\alpha}}$ are the quasi-particle energies for a given Λ, i.e. the eigenvalues of $H_0 + \Sigma^{\Lambda}$, so the eigenvalues are needed here as well.

Our algorithm to solve this equation for μ_chem works in three stages: obtain an initial guess for μ_chem, $\mu^{(0)}_\mathrm{chem}$, (trivially) obtain a second guess, $\mu^{(1)}_\mathrm{chem}$, with $\mathrm{sgn}(N_\mathrm{e}(\mu^{\Lambda,(1)}_\mathrm{chem}) - N_\mathrm{e}) = -\mathrm{sgn}(N_\mathrm{e}(\mu^{\Lambda,(0)}_\mathrm{chem}) - N_\mathrm{e})$ and then use the secant algorithm [31] to iteratively find the final μ_chem.

The initial guess is taken to be the same as the value for $T = 0$, Eq. (2.11), since for low temperatures the value is a very good approximation. We then calculate

$$\mu^{\Lambda,(0)}_\mathrm{chem} + \mathrm{sgn}(N_\mathrm{e}(\mu^{(0)}_\mathrm{chem}) - N_\mathrm{e})\frac{\Delta}{4} i,$$

where Δ is the mean level spacing of the system and i is an integer that starts at 1 and is incremented until the condition $\mathrm{sgn}(N_\mathrm{e}(\mu^{(1)}_\mathrm{chem}) - N_\mathrm{e}) = -\mathrm{sgn}(N_\mathrm{e}(\mu^{(0)}_\mathrm{chem}) - N_\mathrm{e})$ is satisfied. In practice $i = 1$ or $i = 2$ will already satisfy that condition, which is why $\frac{\Delta}{4}$ is a good empirical choice here.[1]

Both initial guesses are then used as input for the secant algorithm. Since $N_\mathrm{e}(\epsilon)$ is monotonous and the value searched for is encompassed with both guesses, convergence will be quite fast (10 to 20 iterations in practice). We consider the chemical potential to be converged if the relative error of the number of electrons,

$$\left| \frac{N_\mathrm{e}(\mu^{(i)}_\mathrm{chem}) - N_\mathrm{e}}{N_\mathrm{e}(\mu^{(i)}_\mathrm{chem}) - N_\mathrm{e}} \right|,$$

[1] We cut this scheme off at $i = 10$, since it is only used to accelerate the convergence of the secant algorithm, which is likely to also work if the second value does not satisfy the condition, albeit more slowly.

is larger than the square root of the machine precision. While the smallest possible error here would be of the order of $\hat{\epsilon}N$, with $\hat{\epsilon}$ being the machine precision and N the number of orbitals in the system, the energies $\tilde{\epsilon}_{\tilde{\alpha}}$ only have a precision of $\sqrt{\hat{\epsilon}}$ due to the diagonalization procedure.

2.3 Correlators

Starting from Eq. (1.92), it is first necessary to transform the vertex into the Λ-dependent quasi-particle basis,

$$\tilde{\Gamma}^{\Lambda}_{\tilde{\mu}\tilde{\nu}\tilde{\rho}\tilde{\sigma}} = \sum_{\alpha\beta\gamma\delta} V^{\mathrm{in}}_{\tilde{\mu}\alpha} V^{\mathrm{in}}_{\tilde{\nu}\beta} \Gamma^{\Lambda}_{\alpha\beta\gamma\delta} V^{\mathrm{in},-1}_{\gamma\tilde{\rho}} V^{\mathrm{in},-1}_{\delta\tilde{\sigma}}. \tag{2.13}$$

We apply each basis transform sequentially, applying the outer transformations first. In between we transpose the vertex, so that we may apply the final two transformations as outer transformations as well. Due to the symmetry of the vertex the resulting expression is equivalent (even in the case of systems with $SU(2)$ symmetry, which is symmetric if both index pairs are swapped, as is the case here). This gives us the following sequence of basis transformation steps:

$$\Gamma^{\Lambda,(1)}_{\tilde{\mu}\beta\gamma\delta} = \sum_{\alpha} V^{\mathrm{in}}_{\tilde{\mu}\alpha} \Gamma^{\Lambda}_{\alpha\beta\gamma\delta} \tag{2.14}$$

$$\Gamma^{\Lambda,(2)}_{\tilde{\mu}\beta\gamma\tilde{\sigma}} = \sum_{\delta} \Gamma^{\Lambda,(1)}_{\alpha\beta\gamma\delta} V^{\mathrm{in},-1}_{\delta\tilde{\sigma}} \tag{2.15}$$

$$\Gamma^{\Lambda,(3)}_{\beta\tilde{\mu}\tilde{\sigma}\gamma} = \Gamma^{\Lambda,(2)}_{\tilde{\mu}\beta\gamma\tilde{\sigma}} \tag{2.16}$$

$$\Gamma^{\Lambda,(4)}_{\tilde{\nu}\tilde{\mu}\tilde{\sigma}\gamma} = \sum_{\tilde{\nu}} V^{\mathrm{in}}_{\tilde{\nu}\beta} \Gamma^{\Lambda,(3)}_{\beta\tilde{\mu}\tilde{\sigma}\gamma} \tag{2.17}$$

$$\tilde{\Gamma}^{\Lambda}_{\tilde{\mu}\tilde{\nu}\tilde{\rho}\tilde{\sigma}} = \sum_{\tilde{\rho}} \Gamma^{\Lambda,(4)}_{\tilde{\nu}\tilde{\mu}\tilde{\sigma}\gamma} V^{\mathrm{in},-1}_{\gamma\tilde{\rho}} \tag{2.18}$$

We utilize a standard generic matrix-matrix multiplication (GEMM) kernel as provided by the Eigen library for these products, interpreting the tensor as a matrix, e.g. $\Gamma^{\Lambda}_{\alpha,(\beta\gamma\delta)}$. When the scheme for reducing the number of states, Eq. (1.107), is applied, we employ rectangular submatrices of the V^{in}, since Γ is only of size $\mathcal{C}^{M^4}$ but $\tilde{\Gamma}$ needs to be of size $\mathcal{C}^{N^4}$.

Since there are also contributions from orbitals not included in the M selected states, we also need to perform the same basis transformation for the bare interaction, U. Note that it is faster to use a GEMM kernel for that multiplication as well, but due to the structure of the formula, in contrast to the flow of the vertex itself it precludes us from

easily separating out the contributions for which we utilize the renormalized interaction Γ. (The flow equation separates into 5 separate contributions, this would separate into far more.) It is thus easier to simply transform the full object U and then add the transform of $\Gamma - U$ to that expression.

We then proceed to multiply the transformed vertex by the energy denominator of Eq. (1.92),

$$\tilde{\Gamma}^{\Lambda,\mathrm{div}}_{\tilde{\mu}\tilde{\nu}\tilde{\rho}\tilde{\sigma}} = \tilde{\Gamma}^{\Lambda}_{\tilde{\mu}\tilde{\nu}\tilde{\rho}\tilde{\sigma}} \frac{1}{\tilde{\epsilon}_{\tilde{\mu}} + \tilde{\epsilon}_{\tilde{\nu}} - \tilde{\epsilon}_{\tilde{\rho}} - \tilde{\epsilon}_{\tilde{\sigma}}}. \tag{2.19}$$

Finally, we need to transform to real space and select the proper orbitals,

$$\mathcal{C}^{\mathrm{dd-pre},(2)}_{i\tilde{\nu}\tilde{\sigma}} = \sum_{\tilde{\mu}\tilde{\rho}} n_{\tilde{\mu},\tilde{\rho}} V^{\mathrm{ri}}_{i\tilde{\mu}} \tilde{\Gamma}^{\Lambda,\mathrm{div}}_{\tilde{\mu}\tilde{\nu}\tilde{\rho}\tilde{\sigma}} V^{\mathrm{ri},-1}_{\tilde{\rho}i} \tag{2.20}$$

$$\mathcal{C}^{\mathrm{dd},(2)}_{ij} = \sum_{\tilde{\nu}\tilde{\sigma}} n_{\tilde{\nu},\tilde{\sigma}} V^{\mathrm{ri}}_{j\tilde{\nu}} \mathcal{C}^{\mathrm{dd-pre},(2)}_{i\tilde{\nu}\tilde{\sigma}} V^{\mathrm{ri},-1}_{\tilde{\sigma}j}, \tag{2.21}$$

where $n_{\tilde{\epsilon},\tilde{\epsilon}'}$ is the factor required to ensure that the proper occupation is used, see Eqs. (1.92,1.96).

Because we transform into the basis of the quasi-particles for a given Λ, the transformation matrices V^{in} are Λ-dependent and that contribution cannot be calculated just once initially. This means that for each Λ the density-density correlator incurs a cost of $\mathcal{O}(N^5)$. Eq. (2.19) has a complexity of $\mathcal{O}(N^4)$ and Eq. (2.20) a complexity of $\mathcal{O}(N^5)$. This cannot be simplified further without additional approximations, making it the most expensive object to calculate.

Fortunately, it is not required for the flow of the vertex or the self-energy. Therefore, when we do not see a divergence in our flow in Λ, we calculate the density-density correlator only once at the very end of the flow. In case a divergence is seen, we perform a backtracking procedure: while we don't store the vertex for every single iteration step, we do keep it for the last n_{bt} iterations. Once we detect a divergence, we reset the system to the current iteration minus n_{bt} steps (typically 10) and calculate the density-density correlator at that iteration step and proceed to the next iteration again. This is performed for a total of $n_{\mathrm{dv}} \leq n_{\mathrm{bt}}$ iterations (typically 1 or 2), where we don't need to recalculate the flow but can just use the known self-energy and the vertex.

2.4 Restarting

Calculations for larger systems may take a relatively long time. In case of technical difficulties, we implement a restarting procedure that allows us to continue a calculation at the point where it last stopped. We save the initial Λ, the step size, the number of selected states M, the chosen target Λ. Furthermore, we keep the last self-energy and

vertex as well as the number of the last iteration to complete. These quantities suffice to reproduce the calculation at a later point in time.

Chapter 3
3 Application to disordered systems

In this chapter we compare our FRG approach to exact diagonalization (ED) in 2D and to the density matrix renormalization group (DMRG) in 1D and show that it provides us with the means to characterize the ground state of the system. We also compare our approximation that reduces the number of orbitals for which the vertex renormalization flow is calculated with results that take into account all orbitals and show that our approach for this type of approximation is justified.

3.1 Hamiltonian

One of the simplest possible models that includes both interactions and disorder is a tight-binding model on a lattice with nearest-neighbor hopping, nearest-neighbor interactions and on-site disorder, where we assume that the Fermions don't have a spin. The corresponding Hamiltonian reads

$$H = -t \sum_{<ij>} \hat{c}_i^\dagger \hat{c}_j + \sum_i \delta\epsilon_i \hat{n}_i + U \sum_{<ij>} \hat{n}_i \hat{n}_j, \tag{3.1}$$

where t is the hopping parameter, U the interaction strength and the $\delta\epsilon_i$ the on-site energies, which are chosen from a box distribution with width W centered around $\epsilon = 0$.

We have a look at this model in both $d = 1$ and $d = 2$. In principle the FRG should also be applicable in three dimensions, but the number of orbitals grows far greater with linear system size in three dimensions. Even just 6 sites in each direction already gives a total number of 216 orbitals.

In 2D this model could be realized in terms of a strongly screened two-dimensional electron gas with a strong in-plane magnetic field. This would polarize all of the spins due to the Zeemann effect, but have no orbital contribution.

3.2 Comparison with Exact Diagonalization (2D)

Our main goal is to apply this method to two-dimensional systems. We choose a simple square lattice with periodic boundary conditions for our calculations and compare our method to exact diagonalization for small enough system sizes (16 orbitals). In the following we will discuss our implementation of exact diagonalization and then compare results for some sample systems with the functional renormalization group to demonstrate its efficacy.

3.2.1 Methodology

For our implementation of exact diagonalization, we construct the full N_e-particle Hilbert space. Its dimension is $\begin{pmatrix} N \\ N_\mathrm{e} \end{pmatrix}$ and grows exponentially with the number of orbitals N. We systematically construct the basis states of that space and implement the action of the full many-body Hamiltonian on that basis (we do *not* explicitly construct the matrix elements of the Hamiltonian itself). An iterative eigensolver for sparse problems is employed to calculate the full many-body ground state for a given system. We utilize the standard ARPACK package [32] in direct mode.[1]

For simple observables, such as the density, we may then simply calculate expectation values with respect to the many-body ground state,

$$\left\langle \hat{\mathrm{n}}_i \right\rangle = \langle 0 | \, \hat{\mathrm{c}}_i^\dagger \hat{\mathrm{c}}_i \, | 0 \rangle \, . \tag{3.2}$$

We also want to calculate the single-particle density of states, $\rho(\epsilon)$. This is given by the expectation value

$$\rho(\epsilon) \;=\; -\frac{1}{\pi} \Im \, \mathrm{tr}_{ij} \left\langle \hat{\mathrm{c}}_i \frac{1}{\epsilon - \hat{H} + E_0 + i\eta} \hat{\mathrm{c}}_j^\dagger \right\rangle + \left\langle \hat{\mathrm{c}}_j^\dagger \frac{1}{\epsilon + \hat{H} - E_0 + i\eta} \hat{\mathrm{c}}_i \right\rangle , \tag{3.3}$$

which we arrive at by Fourier transforming the definition of the retarded Green's function. This expressions contains the inverse of a very large matrix, which needs to be done for every single energy at which the density of states is to be evaluated at. Furthermore, directly inverting such a large matrix is only possible using iterative algorithms, which would again have to be applied for every single energy. We therefore follow an alternative approach as outlined in the PhD thesis of Alexander Braun [33]. One may expand the denominator in terms of Chebyshev polynomials $T_n(x)$, such that we get

$$c_{ij,n}^{(+)} = \langle 0 | \, \hat{\mathrm{c}}_i T_n \Big(a(\hat{H} - E_0 - b) \Big) \hat{\mathrm{c}}_j^\dagger \, | 0 \rangle \, , c_{ij,n}^{(-)} = \langle 0 | \, \hat{\mathrm{c}}_i^\dagger T_n \Big(a(\hat{H} - E_0 - b) \Big) \hat{\mathrm{c}}_j \, | 0 \rangle \, , \tag{3.4}$$

[1] The shift-inverse mode is not required, since the eigenvalues we are interested in are taken from the spectrum edges, not the center.

where E_0 is the ground state energy. The variables a and b are scaling factors that arise due to the fact that the Chebyshev polynomials are only well-defined in the interval $[-1, 1]$, so the Hamiltonian needs to be scaled to fit into that range. We note that since we are calculating expectations in the Hilbert spaces for $N_\mathrm{e}+1$ and $N_\mathrm{e}-1$ particles, we need to take into account the extremal eigenvalues of the Hamiltonian in those spaces. To make sure we don't suffer from numerical artifacts, we scale the argument of the Chebyshev polynomials into the interval $[-0.9, 0.9]$.[2] This gives us

$$\begin{aligned} \delta &= 0.1, \qquad \text{(distance to interval boundaries)} \\ a &= \frac{2(1-\delta)}{(\epsilon_\mathrm{max} - E_0) - (\epsilon_\mathrm{min} - E_0)}, \qquad (3.5) \\ b &= \frac{(\epsilon_\mathrm{max} - E_0) + (\epsilon_\mathrm{min} - E_0)}{2} - \delta, \qquad (3.6) \end{aligned}$$

where $\epsilon_\mathrm{min,max}$ are the extremal many-body eigenvalues of the system with $N_\mathrm{e}+1$ ($N_\mathrm{e}-1$) particles and E_0 is the ground state energy for N_e particles.

We may then rewrite the single-particle retarded Green's function in terms of these coefficients,

$$\mathcal{G}_{ij}(\omega) = a \sum_{n=0}^{\infty} \left(\alpha_n^+ \Big(a(\omega + i\eta \mp b) \Big) c_{ij,n}^{(+)} - \alpha_n^- \Big(a(\omega + i\eta \mp b) \Big) c_{ji,n}^{(-)} \right). \qquad (3.7)$$

The density of states is then given by the imaginary part of this expression traced over the real space indices, which is why we only need to calculate the diagonal part of this expression. If we terminate the expansion at a finite n, the formula remains only valid for finite η, with

$$\eta \gtrsim \frac{1}{a n_\mathrm{max}}. \qquad (3.8)$$

For further discussion on this topic we would like to defer to Alexander Braun's thesis. [33]

Exact diagonalization has its limits: the many-particle Hilbert space grows exponentially with the system size. While it is in principle possible to increase the system size further, we restrict our calculations to systems with 16 orbitals ($L = 4$), because it is possible to perform the entire procedure (exact diagonalization, Chebyshev expansion) within a single day for a single system.

3.2.2 Results

In the following we will present results comparing the functional renormalization group method with exact diagonalization for the Hamiltonian of Eq. (3.1) on a square lattice

[2] Using exactly $[-1, 1]$ does not work, since the polynomials are fixed at the boundaries of the interval. One needs to distance oneself at least by relative error in the eigenvalues from the boundary.

with $4\times4 = 16$ sites and periodic boundary conditions. We start with the regime of very weak disorder and very weak interactions. We compare individual disorder configuration, because agreement on that level automatically implies agreement in averaged quantities.

We use an exponential parametrization for the flow equations, Eqs. (1.31,2.4),

$$\Lambda = \Lambda_0 \mathrm{e}^{-l\Delta s}, \qquad l \in \mathbb{N}, \tag{3.9}$$

where Λ_0 is the initial Λ at which the flow starts and l is our iteration number. This parametrization has the advantage that it captures the physics close to the Fermi energy well, as the integration mesh gets denser, while still being relatively fast in reaching that point (having a wider mesh initially while Λ is much larger than the system's energy scales). Both flow equations are of the form

$$\frac{\mathrm{d}}{\mathrm{d}\Lambda} A(\Lambda) = -\frac{1}{2\pi} B(\Lambda). \tag{3.10}$$

Performing the integral from $\Lambda(l)$ to $\Lambda(l+1)$, we arrive at the structure

$$A(\Lambda(l+1)) = A(\Lambda(l)) + \frac{\Lambda(l)\Delta s}{2\pi} B(\Lambda(l)) \tag{3.11}$$

for all of our flow equations, assuming that Δs is sufficiently small. In the following calculations we have chosen the parameters $\Delta s = 0.02$ and $\Lambda_0 = 40$. Unless we encounter a divergence in the flow, we stop as soon as $\Lambda < 10^{-4}$ (giving a total of $l_{\max} = 645$ iterations).

We monitor the flow for divergencies by looking at the 2-norm of the vertex,

$$|\Gamma^\Lambda| = M^{-4} \sqrt{\sum_{\bar\alpha\bar\beta\bar\gamma\bar\delta} (\Gamma^\Lambda_{\bar\alpha\bar\beta\bar\gamma\bar\delta})^2}. \tag{3.12}$$

We assume that our flow has started to diverge as soon as the current norm of Γ has exceeded a certain threshold relatively to the norm of Γ at the start of the flow, also taking into account the derivative of the norm of Γ with respect to the flow parameter. In that case we stop the flow, because this indicates an instability due to the interaction, as was discussed in Sec. 1.6.1.

We expect the clean model at half filling to exhibit a charge density wave (CDW) ordering for any finite $U > 0$ in the thermodynamic limit, in accordance with a renormalization group analysis by Shankar. [34] Remaining at half filling, if disorder is weak, the interaction strength should therefore be chosen to be much weaker to ensure we remain in a regime where finite size effects destroy the charge density wave ordering. Fig. 3.1 shows the comparison of the real space density, $n(\mathbf{r})$, and the density of states, $\rho(\epsilon)$, between both methods. As per Eq. (3.8) the broadening for ED is given by the

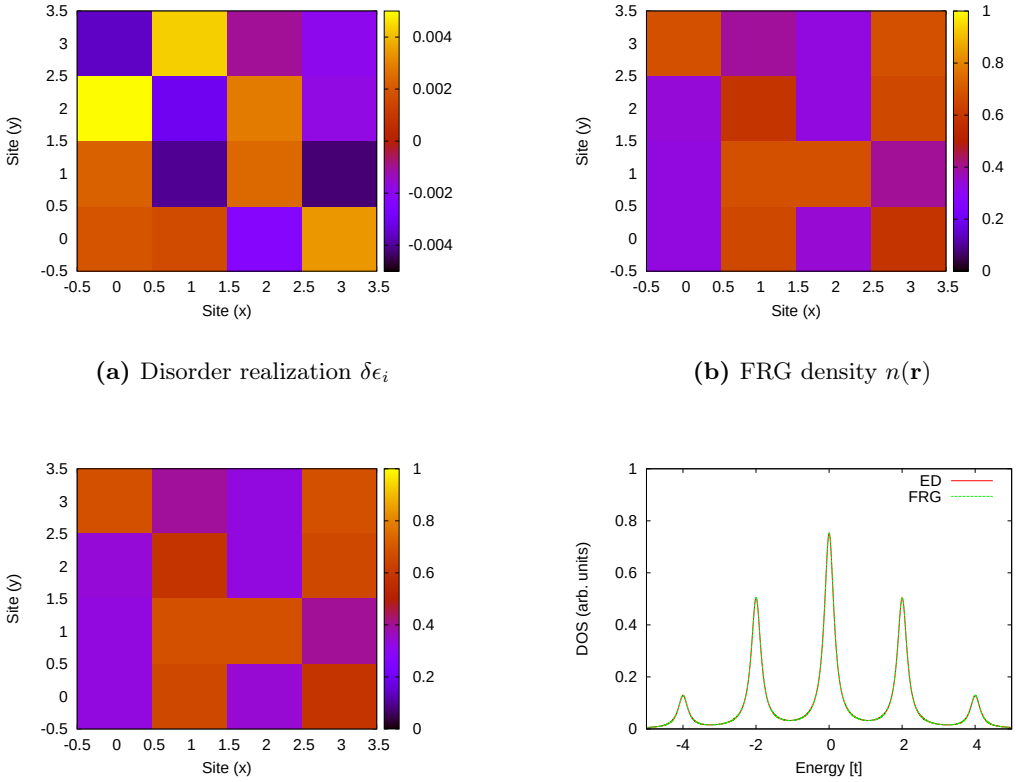

(a) Disorder realization $\delta\epsilon_i$

(b) FRG density $n(\mathbf{r})$

(c) ED density $n(\mathbf{r})$

(d) Density of states

Figure 3.1: *Comparison between the density $n(\mathbf{r})$ between (b) the functional renormalization group and (c) exact diagonalization for a given disorder realization (a) at $t = 1$, $U = 0.001$, $W = 0.01$, and $\nu = 1/2$. The mean square difference between both densities is 10^{-6}. (d) Comparison between the density of states from ED and FRG, with a broadening of $\eta = 0.16t$.*

number of Chebyshev moments calculated (here 10^5). The density of states for the FRG was broadened with the same η for ease of comparison. At these high values of η the individual levels are broadened to such a degree that the lifting of the degeneracies (a 4×4 clean square lattice with nearest-neighbor hopping has 5 eigenenergies, with degeneracies 1, 4, 6, 4 and 1) due to the weak disorder is not visible.

It is unsurprising that both methods agree for such a low interaction, because we expect even simple perturbation theory to hold for such low values of U, and even the non-interacting system is quite close. By increasing the disorder strength the degenera-

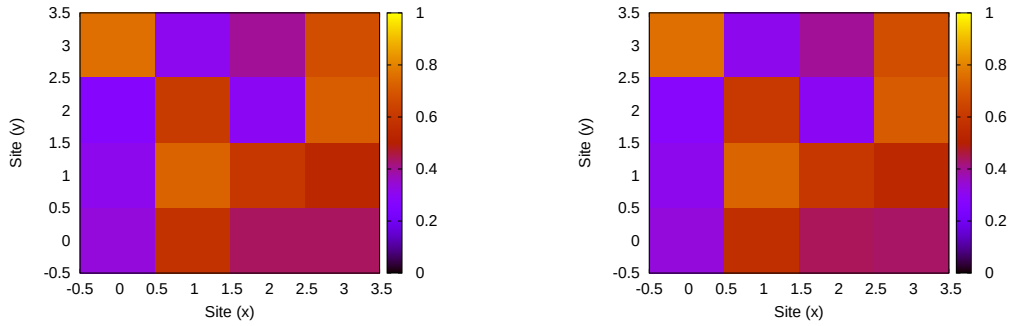

(a) FRG density $n(\mathbf{r})$ **(b)** ED density $n(\mathbf{r})$

Figure 3.2: *Comparison between the density $n(\mathbf{r})$ between (a) the functional renormalization group and (b) exact diagonalization for the same (but rescaled) disorder realization as in Fig. 3.1 but at $t = 1$, $U = 0.1$, $W = 1$ and $\nu = 0.5$. The mean square difference between both densities is $7.8 \cdot 10^{-4}$.*

cies between the non-interacting levels are further lifted. This allows us increase the interaction strength without entering the charge density wave regime. This can be seen in Fig. 3.2, where we have utilized the same disorder configuration, but have scaled the on-site energies by a factor of 100.

We can see a clear quantitative agreement for low enough U so that no instabilities occur. Remaining at weak to moderate disorder strengths, we will now look at an increase of the interaction. If the disorder is weak enough the interaction will now be strong enough to overcome finite-size effects and the system will establish CDW ordering. Due to the fact that disorder is present the system behaves differently to the clean system: without disorder the average density of a CDW state is still 0.5, because the system is translationally invariant. The CDW can only be seen by looking at higher-order correlators, such as the density-density correlator. This is not true in a

disordered system: as soon as an infinitesimal amount of disorder is present, it breaks the translational invariance of the system, causing the CDW to be pinned and the ground state not to be degenerate anymore.

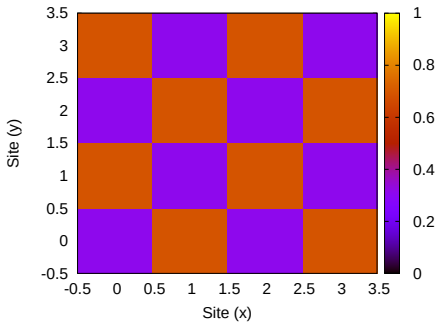

Figure 3.3: *Density $n(\mathbf{r})$ from exact diagonalization (ED) at $t = 1$, $W = 0.01$, $U = 0.01$ and $\nu = 0.5$ for the disorder realization in Fig. 3.1 rescaled, showing a pinned charge density wave.*

This means that the density itself will exhibit an ordering with a wave vector of $\mathbf{Q} = (\pi, \pi)$, i.e. a checkerboard pattern. We note that the density profiles of Figs. 3.1,3.2 are manifestly different. However, if we increase our interaction to $U = 0.01$ (for the case that $W = 0.01$) the density profile of the system under exact diagonalization does exhibit a checkerboard pattern, as can be seen in Fig. 3.3.

Recalling our discussion from Sec. 1.6.1, our implementation of the functional renormalization group will not be able to quantitatively access the charge density wave phase. However, we expect the flow equations to diverge as to indicate that an instability is present in the system. This is indeed what we see in our numerics, since our criterion for aborting the calculation is hit on this system. Fig. 3.4 visualizes the flow of the vertex norm up to that point, and we can clearly see the expected divergence.

Furthermore, the functional renormalization group allows us to determine the type of instability that dominates the system at that point in the flow, which is often an indication for the symmetry of the system's ground state. Since we expect a charge density wave in this system, we calculate the density-density correlator of the system at the point where we abort the calculation. The nontrivial part of the correlator is given by Eq. (1.92). Interpreting the real space indices as two-dimensional coordinates, we may define

$$\mathcal{D}(\mathbf{x}, \mathbf{x}') = \mathcal{C}^{\mathrm{dd},(2)}_{i=(x,y),j=(x',y')}, \tag{3.13}$$

which we may then Fourier transform and average over the entire sample to obtain a

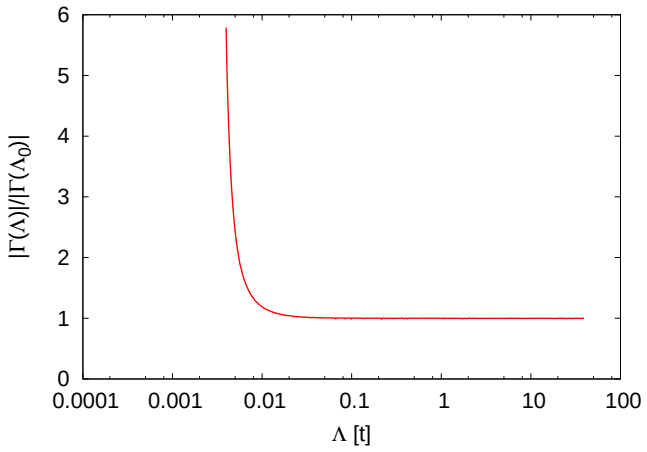

Figure 3.4: *FRG flow of the norm of* Γ^{Λ} *at* $t = 1$, $W = 0.01$, $U = 0.01$ *and* $\nu = 0.5$ *for the disorder realization in Fig. 3.1 rescaled. The flow diverges at* $\Lambda_c \approx 0.004t$.

k-space representation,

$$\mathcal{D}(\mathbf{k}) = N^{-1} \sum_{\mathbf{x}\mathbf{x}'} \mathrm{e}^{\mathrm{i}\mathbf{k}(\mathbf{x}-\mathbf{x}')} \mathcal{D}(\mathbf{x}, \mathbf{x}'). \tag{3.14}$$

We use the periodic nature of the lattice and look at the real part of the correlator is taken (the Fourier transform introduces an imaginary part). We expect this quantity to be strongly peaked at (π, π) because of the charge density wave, which is what can clearly be seen in Fig. 3.5. It is important to note that this is unbiased: we have not used the fact that we expect a charge density wave phase at all in our FRG flow – we have solved the flow equations numerically and once the flow starts to diverge the correlators give us information about the type of instability that dominates the system.

These results also hold true if we take a look at higher disorder strengths. For this small finite-size system increasing the disorder means that the CDW transition will happen at larger interaction strength U. Let us first look at the in the symmetric phase: at $W = 5$ and $U = 0.1$ the system does not exhibit a charge density wave. Fig. 3.6 shows the real-space density and the density of states for this system. We do not show the the plot for the real space density obtained via FRG, because the differences are minuscule; the mean square difference in real-space densities is 10^{-4}. Since disorder is strong, the degeneracies between individual levels are lifted enough to ensure that Overall we have a good agreement between the exact results and our method.

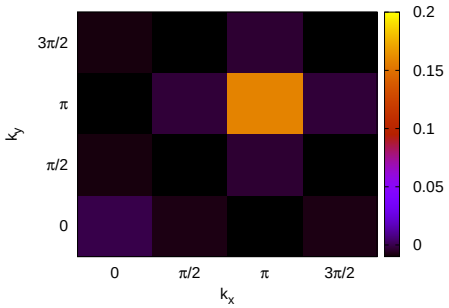

Figure 3.5: *The density-density correlator as defined in Eq.* (3.14) *at* Λ_c *for a system with parameters* $t = 1$, $W = 0.01$, $U = 0.01$ *and* $\nu = 0.5$. *Only the real part is shown. The peak at* (π, π) *indicates that the system has a CDW instability.*

If we increase the interaction further, we will also see a charge density wave phase, for example at $U = 5$. (In the finite system there will always be a CDW ground state as long as U is large enough.) Fig. 3.7 confirms that the functional renormalization group correctly predicts the dominating instability of the system due to interactions.

We have shown that we can successfully apply the functional renormalization group method to disordered 2D systems, for a large range of disorder strengths. It provides and unbiased view towards instabilities of the system due to interactions, while we can treat disorder exactly at the same time. There are two outcomes of a calculation with our formulation of the FRG: either we achieve convergence and we are able to obtain quantitative results in the phase that does not have a spontaneously broken symmetry, or our flow diverges and the leading instability in the FRG flow allows us to make an inference about the ground state of the system. We thus have a tool that allows us to study the phase diagram of disordered interacting systems, without being constrained by the disorder strength.

Note that while we have only shown a single disorder configuration here, we have verified our method with a multitude of random disorder realizations. The exact value of U at which the phase transition happens will vary slightly with the realization, but the agreement holds.

Since all of our calculations are done on finite-size systems, there are certain finite-size effects that we need to take into account. As already mentioned, as $L \to \infty$ the clean system will order in a charge density wave at half filling for even an infinitesimal interaction U. In every calculation we have seen, this only happens at finite U. We therefore need to go to larger systems in order to extrapolate the limit of $U_c(L)$. Only

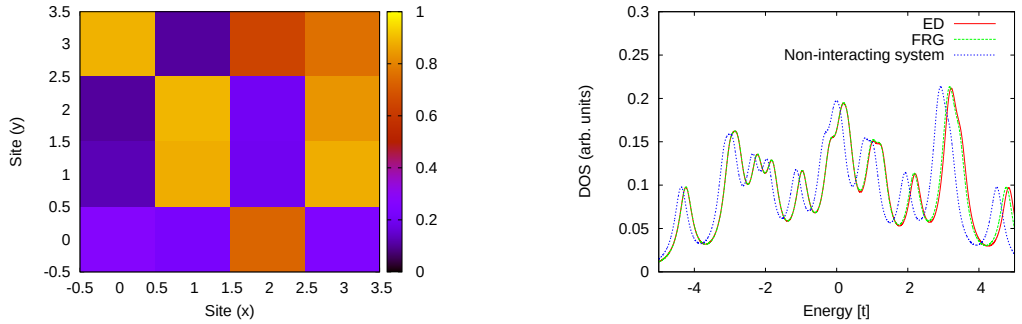

(a) ED density $n(\mathbf{r})$ **(b)** Density of states comparison

Figure 3.6: *The density as obtained by exact diagonalization (a) at $t = 1$, $W = 5$, $U = 0.1$ and $\nu = 0.5$ for the disorder realization in Fig. 3.1 rescaled, in the symmetric phase. The densities of states (b) for the same system are compared between ED, FRG and also against the non-interacting system.*

such a calculation will allow us to make statements about the effect of disorder on the phase transition.

3.3 Larger systems

We will now apply the functional renormalization group to larger systems, where ED is not feasible anymore. As has been discussed in Sec. 1.6, we have developed an approximation to reduce the number of degrees of freedom in the calculation. Instead of calculating the flow of the vertex for all orbitals of the system, we only keep the dependency on M orbitals close to the Fermi energy. This is in analogy to projecting the momenta of the vertex down onto the Fermi surface as done in clean system implementations of the FRG. Our difficulty lies in the fact that we do not have translational invariance and thus no quasi-momentum conservation. Whenever we need to evaluate the vertex for orbitals that are not included in the selected M, we cannot replace it by the vertex evaluated for other orbitals, because we know of no systematic way to set up such a mapping. Instead, we replace the vertex by the base interaction term of the Hamiltonian.

In this section we will demonstrate that this approximation works in practice. We do not compare our results to exact diagonalization, as that is unfeasible for larger system

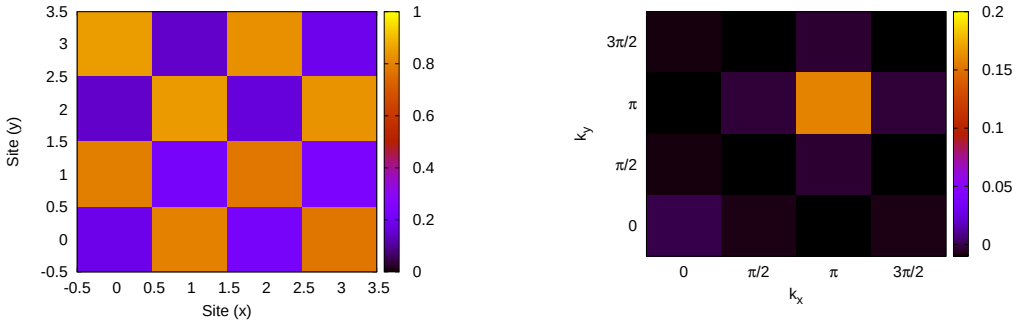

(a) ED density $n(\mathbf{r})$ **(b)** Density-density correlator from FRG

Figure 3.7: *The density as obtained by exact diagonalization (a) at $t = 1$, $W = 5$, $U = 5$ and $\nu = 0.5$ for the disorder realization in Fig. 3.1 rescaled, in the symmetry-broken phase, showing a pinned charge density wave. Near Λ_c the density-density correlator obtained via FRG (b) shows (π, π) ordering.*

sizes. Instead we compare our results to our own FRG implementation in the limit where the flow of the vertex is kept for all orbitals. (This was what has successfully been compared to exact diagonalization in the previous section for smaller systems.)

In the following we will use a 6×6 square lattice with periodic boundary conditions at half filling, giving us 36 orbitals in total. We then calculate each system twice: once where the flow of the vertex is calculated for all states of the system (our reference) and once where we only keep the flow of the vertex for 16 states around the Fermi energy.

Choosing a random disorder realization, at $W = 0.001t$ and $U = 0.01t$ the 36 site system exhibits a charge density wave. In both cases the norm of the vertex diverges, as can be seen in Fig. 3.8. The divergence occurs at the same point in the flow, supporting the rationale for our approximation. The true test, however, is whether the flow with less states allows us to infer the instability. For this we calculate the density-density correlator of that system, which has a contribution from Γ^{Λ} and U in the case where we reduce the number of states (this has been discussed in Sec. 2.3). Fig. 3.9 compares the density-density correlator near Λ_c obtained from both calculations. We clearly recognize the peak at (π, π) of the CDW instability in both calculations. Even with our approximation we are able to detect instabilities in the system. This is not surprising, because in a clean system the CDW instability relates to nesting of the Fermi surface; so the most relevant states to capture this in disordered systems will be those close to the Fermi energy, for which we explicitly keep the vertex.

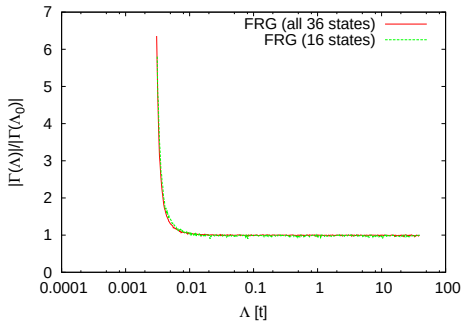

Figure 3.8: *FRG flow of the norm of* Γ^Λ *at* $t = 1$, $W = 0.001$, $U = 0.01$ *and* $\nu = 0.5$ *for a random disorder realization. The flow diverges at* $\Lambda_c \approx 0.003t$ *for both variants of the renormalization group.*

Finally, we perform the same comparison in the regime of the symmetric phase. This occurs at e.g. $W = 1$, $U = 0.01$. The real space density is shown in Fig. 3.10. We see that there is excellent agreement between the density profiles of both methods, validating our approach. We also compare the density of states as shown in Fig. 3.11. Since we are not comparing to exact diagonalization here, we have used a smaller η to resolve nearly all quasi-particle energies of the system. Even for states that are not within the M selected states both densities of states are in good agreement. (We do expect them to become less so if we increase the interaction.) Subtracting both curves from one another yields values of the order of 10^{-2} in these units.

3.4 Parallelization

In this section we will show the degree of parallelization of our code. This is necessary to estimate a system size limit for our method. With a test system with $N = 36$ sites and $M = 16$ states (so that the system size is sufficiently large that thread creation and work scheduling does not take up a significant amount of time) we repeatedly run the same calculation on a system with 12 cores, but each time with a different number of threads. Speedup is typically defined as the time it takes a single thread to execute a calculation divided the the time it takes N_t threads to execute a calculation. Fig. 3.12 shows the results. The linear scaling demonstrates that the strategy employed is close to optimal, but there is room for improvement. At least for systems with that size or larger, using up to 8 threads per calculation will speed up the calculation considerably. The data point for 12 threads is likely an anomaly (the calculation even took longer

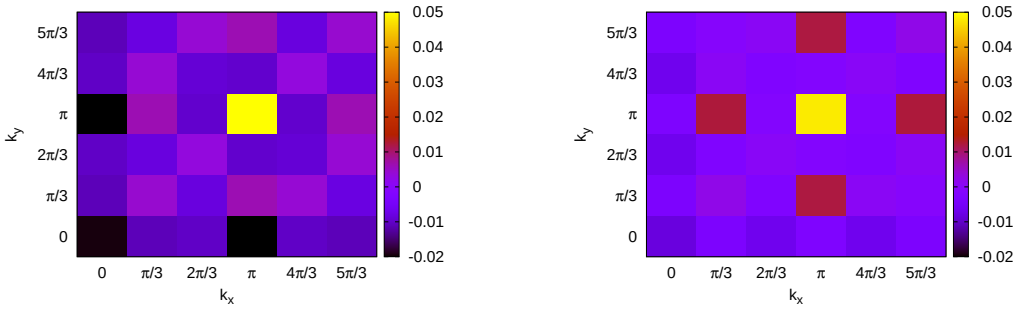

(a) Density-density correlator from 36-state vertex

(b) Density-density correlator from 16-state vertex

Figure 3.9: *The density-density correlator as obtained by the functional renormalization group near Λ_c for the same disorder realization as in Fig. 3.8 at $t = 1$, $W = 0.001$, $U = 0.01$ and $\nu = 0.5$. We compare the full calculation that includes the vertex flow for all states (a) and the calculation where the vertex flow is included only for states close to the Fermi energy (b). Both show a peak at (π, π), indicating a charge density wave instability.*

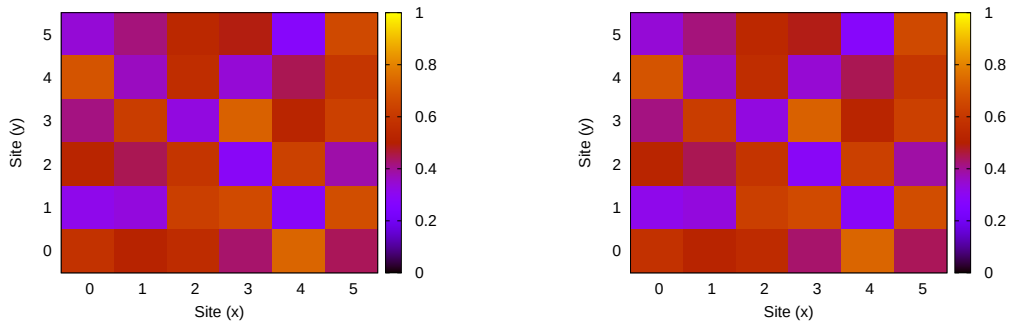

(a) Density $n(\mathbf{r})$ (all states)

(b) Density $n(\mathbf{r})$ (16 states)

Figure 3.10: *The density as obtained by the functional renormalization group for the same disorder realization as in Fig. 3.8 (rescaled) with* $t = 1$, $W = 1$, $U = 0.01$ *and* $\nu = 0.5$. *We compare the full calculation that includes the vertex flow for all states (a) and the calculation where the vertex flow is included only for states close to the Fermi energy (b). The mean square difference between the densities is* $2.8 \cdot 10^{-4}$.

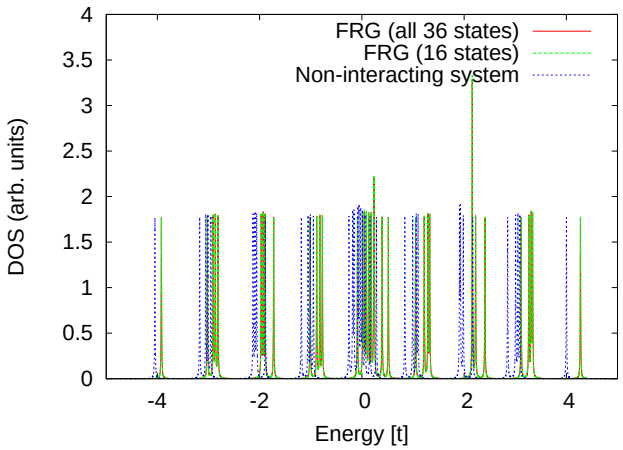

Figure 3.11: *Density of states of converged FRG flows at* $t = 1$, $W = 1$, $U = 0.01$ *and* $\nu = 0.5$ *for the (rescaled) disorder configuration of Fig. 3.9 with* $M = 16$ *and* $M = 36$ *states. The density of states of the non-interacting system is also shown for comparison.*

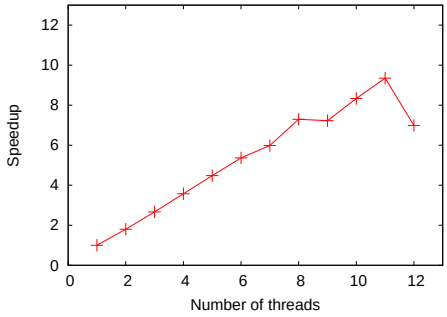

Figure 3.12: *Speedup of the FRG flow by parallelization. The scaling is linear but suboptimal (the slope is slightly lower than* 1*.*

than with 11 threads in absolute numbers). Possibly the system size is a little too small so that processor cores run idle more. It could also be that the shared processor cache is not large enough for all the data and it has to be fetched from memory excessively.

3.5 Scaling

We have seen previously that our method works well for a system with $N = 36$ sites and $M = 16$ states. A single calculation with eight threads in parallel takes not quite $160s$ to complete. If we assume a scaling of N^4 with the system size, see Sec. 2.1, this means that increasing the system size to 64 should increase the number of states taken into account to ≈ 21. The computation time for a single configuration should increase by roughly a factor of 10. In practice, even with keeping just 16 states in a system with 64 orbitals, the time required for a single run increases by a factor of 20. This is most likely due to cache locality, where (parts of) smaller systems might fit completely into the processor's cache and thus run faster. There is some room for optimization potential in the memory access patterns.

A single 8×8 system takes between one and five hours of computation time on 8 cores. (Depending on the number of states one stores the flow of the vertex for.) A 16×16 system (256 orbitals) would require a computation time at least 16 times as high (assuming that cache locality effects have no further deteriorating effect), increasing the computation time for a single system to a range of between 1 and 4 days.

These tests were done on reasonably modern hardware. Cutting-edge hardware might increase the speed by $10\% - 15\%$, but not much more.

While there is still room for optimization in the code, it is doubtful that an improve-

ment of more than a factor of 2 can be achieved. Therefore system sizes of $16x16$ seem to be the upper limit of what can sensibly done with our method for these systems. (Keep in mind that we need to perform multiple calculations to average over disorder and we need to test multiple parameter ranges, so while it might be possible to run a single larger system on even more cores, possibly using distributed memory parallelization, the total amount of needed computations is immense.)

3.6 Comparison with DMRG (1D)

We have also tested our method on one-dimensional systems. Our setup is the Hamiltonian in Eq. (3.1), i.e. spinless Fermions with nearest-neighbor hopping, nearest-neighbor interaction and on-site disorder, this time on a chain.

This time we compare our method to the density matrix renormalization group (DMRG). It was first introduced by Steven White in 1992 [35] and has been a highly successful tool in one-dimensional systems ever since. It is an iterative algorithm that tries to find an optimal subspace of the many-body Hilbert space to represent the many-body ground state of the system. The DMRG is equivalent to exact diagonalization if the size of the subspace that is taken into account is increased to the full size of the many-body Hilbert space. A review of the method may be found in [36]. The DMRG is more efficient computationally than brute-force exact diagonalization but can be considered a reference method for the system we want to test the FRG against.

3.6.1 Results

The DMRG results shown here have been provided by Felix Weiner using a DMRG code developed by Peter Schmitteckert.

For the comparison we consider a small chain of $L = 16$ sites. In our FRG we keep the flow of the vertex for all 16 states. At a given, fixed disorder configuration with $W = 0.2$ and $t = 1$ we compare our results for three different interaction strengths: $U = 0.2$, $U = 1.5$ and $U = 2.5$.

At $U = 2$ the clean system exhibits a CDW ($Q = \pi$) transition in one dimension. Even if disorder modifies this slightly, the system will exhibit a CDW phase at $U = 2.5$, which is not the case for the other two values we investigate. Fig. 3.13 shows the results when comparing the real space densities obtained from both methods. For the lower $U = 0.2$ the FRG reproduces the DMRG result quite well. However, while there is qualitative agreement at $U = 1.5$, there is a quantitative difference. We reason that U is already large enough that fluctuations of the CDW order parameter start to have a significant influence on the system. Since the truncation scheme used in our flow equations is not suited to enter the symmetry-broken phase, it stands to reason that it is unable to quantitatively capture the effect of order parameter fluctuations below the

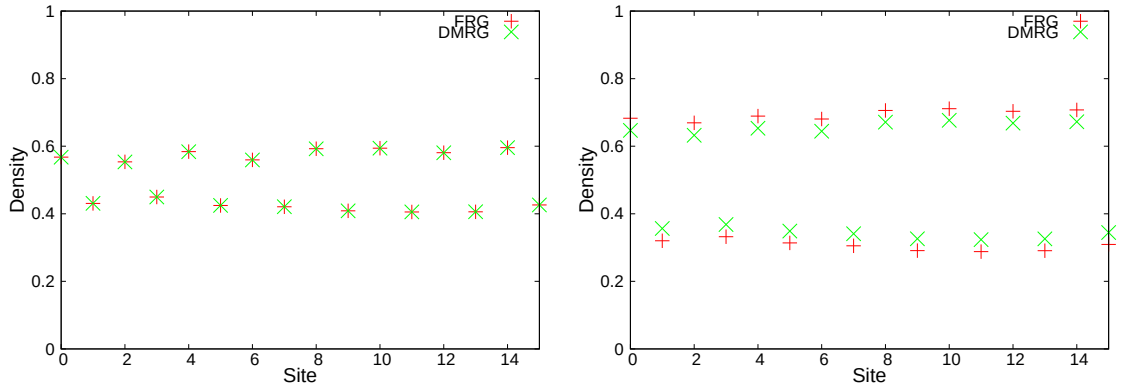

(a) Density $n(\mathbf{r})$ for $U = 0.2$ **(b)** Density $n(\mathbf{r})$ (16 states)

Figure 3.13: *Comparison between the real space density of a* 16 *site 1D chain between DMRG and FRG for* $U = 0.2$ *(a) and* $U = 1.5$ *(b). Both calculations did not exhibit a divergency in the FRG flow.*

phase transition. Nevertheless, the FRG still allows us to make qualitative predictions in this regime.

At $U = 2.5$ the DMRG shows that a pinned CDW with $Q = \pi$ is established. As expected the FRG flow diverges and we calculate the density-density correlator near the divergence. We plot the density-density correlator in Fig. 3.14. It clearly shows the peak at $k = \pi$, thus allowing us to infer the CDW ground state of the system in that parameter range.

There is a legitimate question to be asked regarding the application of our approach to one dimensional systems. When comparing it to DMRG, it is undoubtedly true that DMRG is far more flexible in what can be calculated in 1D. It is more expensive than our FRG formulation, but depending on which quantities are required, modern DMRG codes can handle hundreds of sites rather well, and we do not expect our method to be able to reach orders of magnitude more than that without further approximations. On the other hand, there have been other studies of one-dimensional systems with the help of FRG. Impurities and boundaries have been studied extensively, for example in [15]. More recently there also have been studies of disordered systems with FRG that are able to treat up to 10^5 sites [37]. In both cases additional constraints were imposed on the form of the vertex and the self-energy. Broadly speaking it is assumed that only matrix elements are allowed that are already present in the given Hamiltonian - those are then renormalized. This has the interesting property that it brings the FRG conceptually closer to the analytical renormalization group in that the flow equations describe the renormalization of couplings that are typically already present in the Hamiltonian. (As

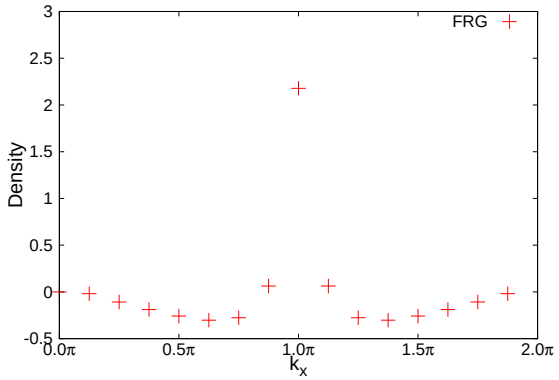

Figure 3.14: *Density-density correlator at $U = 2.5$, $t = 1$, $W = 0.2$ and $\nu = 0.5$ one a 16 site one-dimensional chain. The disorder configuration is the same as in Fig. 3.13. The correlator clearly shows a peak at $k = \pi$, hinting at the CDW ordered ground state of the system.*

always, the devil is in the details and we refer to the cited papers for a less simplified description.) While they are far more efficient than other methods, including our approach or the DMRG, if one constrains oneself to the systems for which those particular FRG schemes have been designed, we believe that these types of approximations will break down for systems with stronger disorder that is not just a single impurity, because we expect additional terms in the vertex and/or self-energy to be generated. Therefore we do believe that our approach could fit a niche even in one dimension, allowing it to access intermediate regimes too large for DMRG, but outside the scope of approximations made in other schemes.

That all said, the most promising application of our approach with regard to disordered systems lies in two dimensions, where DMRG loses its efficiency. Since our method treats disorder exactly and has no a priori bias with regard to the spontaneous symmetry breaking due to the interaction, it can provide a description of the interplay between disorder and interactions on the microscopic level.

3.7 Summary

We have demonstrated that it is possible to develop an FRG scheme that takes disorder into account exactly. By comparison with reference methods in two and one dimensions we have shown that we can make accurate qualitative and in many cases quantitative predictions about the ground state of the system at small system sizes in 2D and 1D. For slightly larger systems we have shown that our disorder version of the "Fermi surface

projection" scheme works by comparing the FRG with and without the approximation. This will enable us to reach comparatively large system sizes in the future, up to about 256 sites.

Chapter 4

4 Phase diagram of our model system

In this chapter we apply our method to the study of the phase diagram of our simple model system.

The Hamiltonian of the model, Eq. 3.1, describes spinless Fermions on a 2D square lattice with nearest-neighbor hopping, on-side disorder (from a box distribution with width W) and nearest-neighbor interactions (with strength U). All calculations are performed at a filling fraction of $\nu = 1/2$. We remind ourselves that in the clean thermodynamic limit an RG analysis [34] shows that for arbitrarily small U a CDW ground state is formed. At $U = 0$ Anderson's scaling analysis [3] tells us that the system will localize for arbitrarily small W.

We are now interested in the system when both U and W are finite. Fig. 4.1 illustrates possible scenarios that may occur: it could be that $U^*(W) = 0$ even for finite W, so that the system would undergo a CDW transition for any finite value of U. Alternatively, disorder could destroy CDW order at low U and there could be a phase boundary at finite U. The shape of the phase boundary is also in question, since it might help decide which (if any) of these scenarios is true: whether there is a finite U above which no Anderson insulator state survives, regardless of W, or whether there is a finite W above which no CDW state survives, regardless of the strength of U. The two nontrivial examples of possible $U^*(W)$ shown in Fig.4.1 illustrate this.

As we apply our method to finite size systems, we need to perform calculations for multiple system sizes in order to be able to extrapolate to the thermodynamic limit. Specifically, the transition to the CDW state will not happen at $U^* = 0$ but rather at $U^* > 0$. As the precise value for U^* for a given finite-size system at fixed W will depend on the specific disorder realization, we need to average over multiple configurations, otherwise our results could just be statistical anomalies.

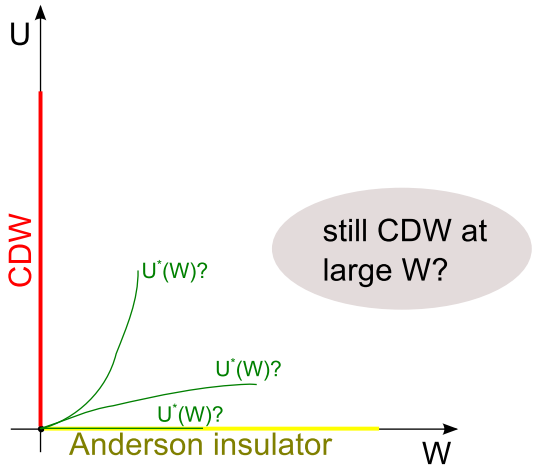

Figure 4.1: *Speculative phase diagram for the model we are studying. At the repulsive fixed point $U = W = 0$ the model reverts to a simple non-interacting clean tight-binding model. The axis for $W = 0$ shows a CDW transition in the ground state for arbitrarily small U, the axis for $U = 0$ shows an Anderson insulator for arbitrarily small W. Our interest lies in the features of the phase diagram at finite U and W.*

The following strategy is used: we take a fixed disorder strength W, generate multiple disorder configurations for different system sizes. For each combination of disorder and system size, we determine the value of U^* at which that specific system undergoes the CDW transition by performing multiple FRG calculations for different values of U. The values for U^* are subsequently averaged. We may now analyze the function $U^*(1/L^2)$ for any given disorder strength W in an attempt to extrapolate to $1/L^2 \to 0$.

Due to the amount of computer power required to perform these calculations, especially at large systems, the following results are averaged over only 5 disorder configurations each. (Note that we have *not* reused disorder configurations in these results, every configuration is uniquely generated with a truly random seed.) Figure 4.2 shows these results for five different values of W. The lack of statistics available in this data is precludes any attempt at extrapolating to $L \to \infty$. First of all, more configurations will need to be calculated to reduce the error bars. However, there is some analysis that is still possible with the data available.

First of all, we notice that $U^*(W) \approx W$. For small systems this is unsurprising: if we take a finite-size clean system, due to its symmetry many levels will be degenerate and the energies are not spread out evenly within the band width. Once disorder is added to the system, these degeneracies are lifted and the splitting is of the order of the disorder

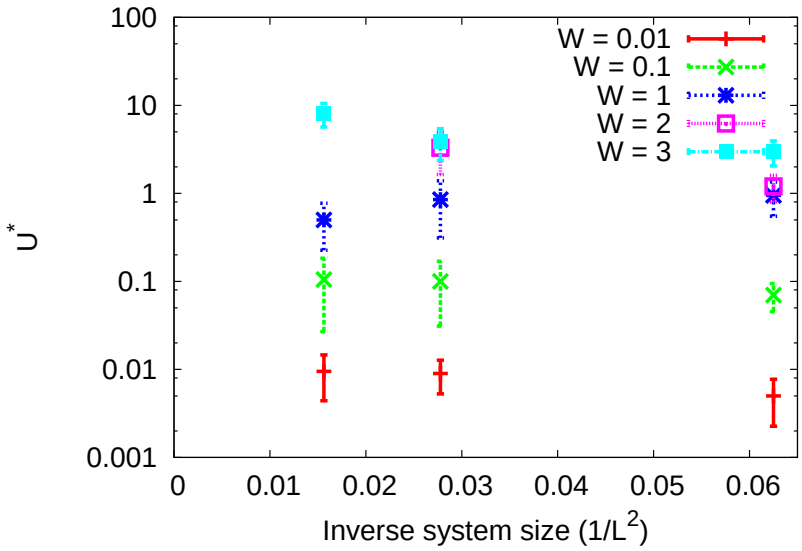

Figure 4.2: *The interaction strength U^* at which the transition from unordered to CDW state happens in our finite size system, plotted over the inverse system size $1/L^2$ for multiple different values of the disorder strength W. The results have been averaged over 5 disorder configurations (see text) and the standard deviation (1σ) is shown.*

strength W. If $U \gtrsim W$ it can overcome this splitting, restoring CDW ordering.

However, if the disorder strength W becomes larger than the level spacing in the clean case, which is certainly true for our calculations with $W = 2$ and $W = 3$ for the larger system sizes, this argument does not hold anymore. (Once the density of states is sufficiently smooth, we return to the classical RG understanding that effective disorder and interaction strengths influence each other as the system size increases.) If we take a look at the data points for $W = 2$ and $W = 3$, we do not see a decrease in $U^*(W)$ with the system size, as one would expect for very small W. This might be a hint that there is indeed a finite U^* for intermediate values of W. In fact, $U^*(W = 3)$ seems to increase with system size, which might even be an indication that CDW order does not survive this disorder strength. This scenario is plotted in Fig. 4.3, where we have used our results to infer parts of the phase diagram. Alternatively, if it turns out that the system sizes studied are still too small to perform an extrapolation, this could hint at a

transient finite-size regime worth to be studied.

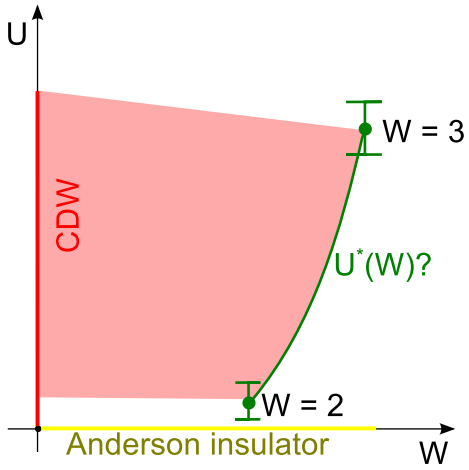

Figure 4.3: *The speculative phase diagram of our model, where we have plotted our results for $W = 2$ and $W = 3$. We see hints of the CDW transition not occurring at $U = 0$ anymore for finite W, and that disorder possibly even destroys CDW order for sufficiently large W.*

While this data does not allow us to draw definite conclusions about the phase diagram of the system, it does hint at interesting physics at intermediate W that merit further investigation, even in this relatively simple model. We have demonstrated that an analysis of the phase diagram is possible with our method, but more computations are required to complete the analysis.

Chapter 5
5 Conclusion and Outlook

We summarize the main results of our work and give an outlook on future research.

5.1 Summary

Historically the development of new numerical methods has often contributed to the understanding of phenomena in condensed matter systems. They may both provide backing for existing analytical results as well as inspiration as to how to tackle a problem from a different perspective. Very rarely do we see developments that revolutionize our understanding of a given problem, such as the way the numerical renormalization group (NRG) has allowed us to view Kondo systems in a new perspective [38] or the insights that density functional theory (DFT) has given us in using effective single particle pictures as descriptions for interacting systems. [39] Instead, most progress is typically made by incremental refinements of existing methods, allowing them to be applied in slightly different ways, gradually increasing our understanding. We hope that our work will help in such a manner when it comes to interacting disordered systems.

In this thesis we have demonstrated that the functional renormalization group can successfully be applied to disordered systems. Our approach takes disorder into account exactly, while treating the interaction in an unbiased way, enabling us to make inferences about the ground state behavior of the system we are studying. The method development was done investigating a relatively simple model of spinless Fermions with nearest-neighbor interaction and nearest-neighbor hopping. By comparing our results to reference methods (exact diagonalization and DMRG) for small system sizes, we have shown that our method works for these types of systems. Furthermore, we can scale our method to larger system sizes by reducing the number of states for which the flow of the vertex needs to be calculated. We have shown that this has no negative impact on the efficacy of our method and that scaling to larger systems is indeed possible. Fur-

thermore, we have confirmed that our implementation parallelizes well for a reasonable amount of processors.

We have shown that this may be applied to the study of the ground state phase diagram or a disordered interacting model. While further computations are required to perform a more detailed analysis of that phase diagram, we have seen hints that at intermediate disorder the CDW phase is suppressed, possibly being absent completely at large disorder concentrations.

5.2 Outlook

Especially with increasing system size it will be interesting to look at the localization length of the system (which can be calculated from the single-particle Green's function) and study how it is affected by interactions. This will open up another aspect of the phase diagram of this model for further investigation. It is also pertinent to study filling fractions other than $\nu = 1/2$, as there is nothing in our method that requires this.

Beyond the study of the phase diagram of this simple model, the next step is to apply our formulation of the FRG to more complex models. In non-interacting two-dimensional systems a true metal-insulator transition is expected for a finite disorder strength. Ostrovsky, Gornyi and Mirlin have argued [40] that the Coulomb interaction destroys the supermetallic phase that the non-interacting model predicts. They also state that this should not be the case for a short-range interaction that is weak enough, while the supermetallic phase is suppressed for stronger short-range interaction. While the long-range Coulomb interaction is inaccessible to our method (due to our truncation scheme of the higher-order terms in the FRG flow), our method could investigate the claim about short range interactions.

Another interesting application would be to study superconductor-insulator transitions in superconducting films. Since we are not constrained in the disorder strength, it should be possible to make statements about the transition point in such a system. (In clean systems, the functional renormalization group as a large track record of study of superconducting systems.)

Finally, an entirely different avenue of investigation is not directly related to disordered systems. The equations derived here are not specific to disordered systems; the only assumption made is that there is no (quasi-) momentum conservation. In principle, the should be applicable to any inhomogeneous system. This opens up the idea of applying the FRG to ab-initio calculations involving molecules. One of the goals of ab-initio methods is to make quantitative predictions of real molecules. A quantity of interest is the spectral gap and its exact position. The estimates obtained from ab-initio's workhorse Density functional theory (DFT) are often not accurate enough. Among the methods proposed to improve upon the DFT results is GW, which is an approximation

of the self-consistent Hedin equations [41] that neglects vertex corrections. However, it has been shown that for some systems vertex corrections do become important [42] and should not be neglected. Since the self-consistent GW cycle is already quite challenging computationally, it might be possible to use our inhomogeneous formulation of the FRG instead of or in addition to the GW cycle to include vertex corrections for the self-energy and hopefully improve upon existing results. One obstacle to overcome in this scenario is the Coulomb interaction: while a finite system provides a bound of the Coulomb interaction by definition, it will have to be investigated how well our approach to keep vertex corrections only for energies close to the Fermi energy will work in these kinds of systems. The answer to that question will give us a bound for the system size this can be applied to. (Since molecular calculations don't often include a huge multitude of different parameters – in contrast to a multitude of disorder configurations to average over – it is sensible to consider parallelizing the code further in order to be able to tackle larger systems.)

The development of this method and the demonstration of its efficacy has opened up a multitude of exciting possibilities for its application. Interaction effects in disordered systems remain an exciting topic and it is our hope that the tool we have created will help further understanding in this area.

A Appendix A
Implementation Details

This appendix provides further details about our implementation, discussing optimizations.

A.1 Symmetries of the Tensor

In the case of spinless Fermions, the vertex is antisymmetric with respect to exchange of any of the outermost pairs of indices, Eq. 1.22,

$$\Gamma^{\Lambda}_{\alpha\beta\gamma\delta} = -\Gamma^{\Lambda}_{\beta\alpha\gamma\delta} = -\Gamma^{\Lambda}_{\alpha\beta\delta\gamma} = \Gamma^{\Lambda}_{\beta\alpha\delta\gamma}.$$

Thus the flow equations for Γ^{Λ} need only be calculated for $\beta > \alpha$ and $\delta > \gamma$ and other elements of Γ^{Λ} follow directly. This saves slightly more than a factor of four of computing time. (Per pair of indices only half as many elements need to be calculated.) Listing 1 shows the associated pseudo-code.

It is still sensible to write the symmetry-connected elements at calculation time, though: if the symmetry were only to be used at read time and the tensor were only to be stored for an independent subset of indices, this would violate memory locality at read time, the tensor elements read during the evaluation of the flow equations would not necessarily lie close to each other in memory, causing cache misses and slowing down the calculation. [43] Since tensor elements are read far more often than written, the penalty incurred due to fact that writes are not memory local is minuscule compared to the potential read penalty otherwise. It should also be noted that while storing all elements of the vertex may require more memory, this is not the bottleneck: the size of the vertex scales with $\mathcal{O}(M^4)$, where M is the number of states in the subspace for which the renormalization of the vertex is kept, while the time required for computations scales at least with $\mathcal{O}(N^4)$ (see Chap. 3 for details), where N is the total number of single-particle states of the system, easily outgrowing any memory requirements.

```
for alpha = 0 .. (M - 1)
  for beta = (alpha + 1) .. (M - 1)
    for gamma = 0 .. (M - 1)
      for delta = (delta + 1) .. (M - 1)
        v = flowEquation(vertex, Lambda, alpha, beta, gamma, delta)
        vertex(alpha,beta,gamma,delta) += v
        vertex(beta,alpha,gamma,delta) -= v
        vertex(alpha,beta,delta,gamma) -= v
        vertex(beta,alpha,delta,gamma) += v
      end for
    end for
  end for
end for
```

Listing 1: *Pseudo-code that shows how the symmetries of the tensor may be used to speed up computation. The code shown here does not yet include parallelization.*

A.2 Parallelization

Using the OpenMP standard [29] many loops may trivially be parallelized by simple instructions that indicate to the compiler that a certain loop may be carried out in parallel. Simply parallelizing the outer-most loop in Listing 1 will not be optimal, however, since the workload is not distributed evenly. If we take just the α and β indices and parallelize the loop over the α index, we can see in Fig. A.1 how the workload is distributed unevenly among the different processors.

At first glance it might make sense to simply parallelize the loop over the β index, but that is not optimal either, as the size of the loop changes for each α ($\alpha - 1$ elements are traversed), which is frequently incommensurate with the number of processors - and while incommensurability cannot always be avoided when parallelizing, it should ideally only occur once at the end of an expensive loop, not multiple times within an expensive loop.

We therefore choose to parallelize all four loops at the same time: we know that the loop over a single pair of antisymmetric indices has $\frac{M(M-1)}{2}$ elements (simple triangular equation), thus we have $\left(\frac{M(M-1)}{2}\right)^2$ elements in total. Note that the flow for a given set of indices itself contains a loop over the inner indices of the equation, see Eq. 2.4, but the size of that loop is constant. If we do this, the workload will be distributed evenly among all processors – in the ideal case, where $\left(\frac{M(M-1)}{2}\right)^2$ is commensurate with the number of processors; otherwise some processors may experience a single instance less than the others.

We must now decompose the single loop index $i \in \left[0; \left(\frac{M(M-1)}{2}\right)^2 - 1\right]$ of the paral-

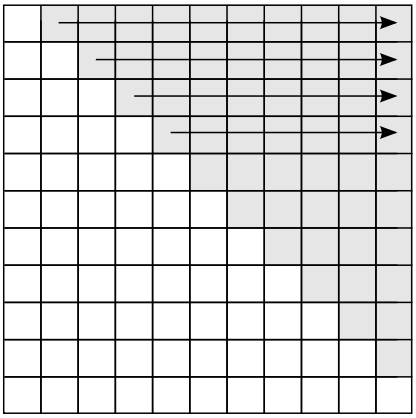

Figure A.1: *The inequality of workloads between different processors (here: four) when parallelizing the nested loops for the tensor elements, causing some processors to idle while others are still working.*

lelized loop back into the original indices in order to be able to know which elements of the vertex tensor to access. We first decompose it trivially into the left and right pairs,

$$i_L = i/\frac{M(M-1)}{2}, \tag{A.1}$$

$$i_R = i\%\frac{M(M-1)}{2}, \tag{A.2}$$

where % is the integer modulo operation and / the integer division (round towards zero). We must now decompose the index i_L into the original pair of indices (α, β) (the decomposition of i_R is analogous). For this we first take a look at how to combine (α, β) into a single index that continuously covers $\alpha < \beta$. Assuming that the indices grow first down and then right, see Fig. A.2, we can see that the number of index pairs we must traverse left of a column is given by the $c(c-1)/2$, where c is the column number starting at 0. Since we start counting at 0, the first index of a column is hence given by that number, and we may deduce the generic formula that maps a given column c and row r to a unique index j by

$$j = \frac{c(c-1)}{2} + r. \tag{A.3}$$

Simple algebra allows us to invert this formula and find the column c (we discard the second solution of the quadratic equation that yields negative indices):

$$c = \frac{1 + \sqrt{1 + 8j - 8r}}{2}. \tag{A.4}$$

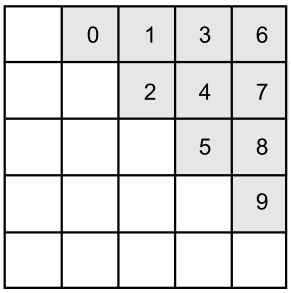

Figure A.2: *The scheme used to assign each point of the triangle in the matrix of indices (α, β) that indicates a traversed pair a continuous number. The other indices are not traversed due to the symmetry of the vertex.*

This still contains the unknown variable r for the row, but this can be eliminated easily, since we know that the column number has to be an integer. If we assume $r = 0$ for the first row, we can immediately write $c = \frac{1+\sqrt{1+8j}}{2}$. This is not valid anymore at $r > 0$, but we know that the resulting number must lie between the real column number and the next. Therefore, simply rounding down will yield the correct result here and we arrive at the formulas for column and row as

$$c = \left\lfloor \frac{1+\sqrt{1+8j}}{2} \right\rfloor, \qquad r = j - \frac{c(c-1)}{2}. \tag{A.5}$$

With this, we have

$$\alpha = \left\lfloor \frac{1+\sqrt{1+8i_L}}{2} \right\rfloor, \qquad \beta = i_L - \frac{\alpha(\alpha-1)}{2}, \tag{A.6}$$

$$\gamma = \left\lfloor \frac{1+\sqrt{1+8i_R}}{2} \right\rfloor, \qquad \delta = i_R - \frac{\gamma(\gamma-1)}{2}, \tag{A.7}$$

With that we have reduced the four outer loops of the flow equation for the vertex into an efficiently parallelizable loop over a single continuous index that we may then decompose back into the original indices.

A.3 Fast Division and Modulo in Inner Loops

In our implementation of the self-energy flow, we require the integer modulo operation with indices within the inner loop in order to more easily separate out the contributions

from the renormalized and the bare vertices: for the contribution where we replace the renormalized with the bare vertex, we traverse all $N - M$ indices in a single loop, by starting above the highest state we include in the renormalized vertex and wrapping around using modulo N.

The integer modulo operation is typically implemented with the help of the integer division operation. In current processor architectures, calculating an integer division is expensive however, on modern processors it can take over 100 cycles in latency to complete. [44, Table 15-4]

It is therefore advantageous to rewrite the integer division in terms of a multiplication with the inverse relative to the finite field of the integer data type. While most compilers do this for constant values of the divisor, values of the divisor that depend on run-time input (such as the system size one wants to calculate) are not affected. In our inner loop that calculates the self-energy flow, measurements showed that the modulo operation was more expensive than the product between the bare vertex and the propagator.

We therefore implement the optimization ourselves, following the outline of [45]. Before the loop starts, we compute the multiplicative inverse for the divisor (i.e. our current system size) and then use the much-faster multiplication instruction within the loop.

Bibliography

[1] P. Drude. Zur elektronentheorie der metalle. *Annalen der Physik*, 306(3):566–613, 1900. ISSN 1521-3889. doi: 10.1002/andp.19003060312. URL `http://dx.doi.org/10.1002/andp.19003060312`.
(Cited on page ix.)

[2] P. W. Anderson. Absence of diffusion in certain random lattices. *Phys. Rev.*, 109: 1492–1505, Mar 1958. doi: 10.1103/PhysRev.109.1492. URL `http://link.aps.org/doi/10.1103/PhysRev.109.1492`.
(Cited on page x.)

[3] E. Abrahams, P. W. Anderson, D. C. Licciardello, and T. V. Ramakrishnan. Scaling theory of localization: Absence of quantum diffusion in two dimensions. *Phys. Rev. Lett.*, 42:673–676, Mar 1979. doi: 10.1103/PhysRevLett.42.673. URL `http://link.aps.org/doi/10.1103/PhysRevLett.42.673`.
(Cited on pages x and 55.)

[4] Alexander Altland and Martin R. Zirnbauer. Nonstandard symmetry classes in mesoscopic normal-superconducting hybrid structures. *Phys. Rev. B*, 55:1142–1161, Jan 1997. doi: 10.1103/PhysRevB.55.1142. URL `http://link.aps.org/doi/10.1103/PhysRevB.55.1142`.
(Cited on page x.)

[5] M. Gell-Mann and M. Lévy. The axial vector current in beta decay. *Il Nuovo Cimento (1955-1965)*, 16(4):705–726, 1960. doi: 10.1007/BF02859738. URL `http://dx.doi.org/10.1007/BF02859738`.
(Cited on page x.)

[6] C. L. Kane and E. J. Mele. Z_2 topological order and the quantum spin hall effect. *Phys. Rev. Lett.*, 95:146802, Sep 2005. doi: 10.1103/PhysRevLett.95.146802. URL `http://link.aps.org/doi/10.1103/PhysRevLett.95.146802`.
(Cited on page xi.)

[7] Joseph E. Avron, Daniel Osadchy, and Ruedi Seiler. A topological look at the quantum hall effect. *Physics Today*, 56(8):38–42, 2003. doi: http://dx.doi.org/10.1063/1.1611351. URL `http://scitation.aip.org/content/aip/magazine/`

physicstoday/article/56/8/10.1063/1.1611351.
(Cited on page xi.)

[8] Ferdinand Evers and Alexander D. Mirlin. Anderson transitions. *Rev. Mod. Phys.*, 80:1355–1417, Oct 2008. doi: 10.1103/RevModPhys.80.1355. URL http://link.aps.org/doi/10.1103/RevModPhys.80.1355.
(Cited on page xi.)

[9] B.L. ALTSHULER and A.G. ARONOV. {CHAPTER} 1 - electron–electron interaction in disordered conductors. In A.L. Efros and M. Pollak, editors, *Electron–Electron Interactions in Disordered Systems*, volume 10 of *Modern Problems in Condensed Matter Sciences*, pages 1 – 153. Elsevier, 1985. doi: http://dx.doi.org/10.1016/B978-0-444-86916-6.50007-7. URL http://www.sciencedirect.com/science/article/pii/B9780444869166500077.
(Cited on page xi.)

[10] Christoph J. Halboth and Walter Metzner. Renormalization-group analysis of the two-dimensional hubbard model. *Phys. Rev. B*, 61:7364–7377, Mar 2000. doi: 10.1103/PhysRevB.61.7364. URL http://link.aps.org/doi/10.1103/PhysRevB.61.7364.
(Cited on pages xi, 1, and 24.)

[11] J. Reiss, D. Rohe, and W. Metzner. Renormalized mean-field analysis of antiferromagnetism and d-wave superconductivity in the two-dimensional hubbard model. *Phys. Rev. B*, 75:075110, Feb 2007. doi: 10.1103/PhysRevB.75.075110. URL http://link.aps.org/doi/10.1103/PhysRevB.75.075110.
(Cited on page xi.)

[12] Christoph J. Halboth and Walter Metzner. d-wave superconductivity and pomeranchuk instability in the two-dimensional hubbard model. *Phys. Rev. Lett.*, 85:5162–5165, Dec 2000. doi: 10.1103/PhysRevLett.85.5162. URL http://link.aps.org/doi/10.1103/PhysRevLett.85.5162.
(Cited on page xi.)

[13] R. Gersch, C. Honerkamp, and W. Metzner. Superconductivity in the attractive hubbard model: functional renormalization group analysis. *New Journal of Physics*, 10(4):045003, 2008. URL http://stacks.iop.org/1367-2630/10/i=4/a=045003.
(Cited on page xi.)

[14] A. A. Katanin. Two-loop functional renormalization group approach to the one- and two-dimensional hubbard model. *Phys. Rev. B*, 79:235119, Jun 2009. doi: 10.1103/PhysRevB.79.235119. URL http://link.aps.org/doi/10.1103/PhysRevB.

79.235119.
(Cited on page xi.)

[15] S. Andergassen, T. Enss, V. Meden, W. Metzner, U. Schollwöck, and K. Schönhammer. Functional renormalization group for luttinger liquids with impurities. *Phys. Rev. B*, 70:075102, Aug 2004. doi: 10.1103/PhysRevB.70.075102. URL http://link.aps.org/doi/10.1103/PhysRevB.70.075102.
(Cited on pages xi and 51.)

[16] Johannes Reuther and Peter Wölfle. J_1-J_2 frustrated two-dimensional heisenberg model: Random phase approximation and functional renormalization group. *Phys. Rev. B*, 81:144410, Apr 2010. doi: 10.1103/PhysRevB.81.144410. URL http://link.aps.org/doi/10.1103/PhysRevB.81.144410.
(Cited on page xi.)

[17] Johannes Reuther and Ronny Thomale. Functional renormalization group for the anisotropic triangular antiferromagnet. *Phys. Rev. B*, 83:024402, Jan 2011. doi: 10.1103/PhysRevB.83.024402. URL http://link.aps.org/doi/10.1103/PhysRevB.83.024402.
(Cited on page xi.)

[18] Johannes Reuther, Peter Wölfle, Rachid Darradi, Wolfram Brenig, Marcelo Arlego, and Johannes Richter. Quantum phases of the planar antiferromagnetic $J_1-J_2-J_3$ heisenberg model. *Phys. Rev. B*, 83:064416, Feb 2011. doi: 10.1103/PhysRevB.83.064416. URL http://link.aps.org/doi/10.1103/PhysRevB.83.064416.
(Cited on page xi.)

[19] Walter Metzner, Manfred Salmhofer, Carsten Honerkamp, Volker Meden, and Kurt Schoenhammer. Functional renormalization group approach to correlated fermion systems. *Rev. Mod. Phys*, 84:299, 2012. doi: 10.1103/RevModPhys.84.299. URL http://arxiv.org/abs/1105.5289v3;http://arxiv.org/pdf/1105.5289v3.
(Cited on pages xi, 2, 3, 5, 6, and 10.)

[20] Christian Seiler and Ferdinand Evers. Functional renormalization group approach to electronic structure calculations for systems without translational symmetry. *Phys. Rev. B*, 94:155102, Oct 2016. doi: 10.1103/PhysRevB.94.155102. URL http://link.aps.org/doi/10.1103/PhysRevB.94.155102.
(Cited on page xii.)

[21] Manfred Salmhofer. *Renormalization: An Introduction*. Springer, Berlin Heidelberg, 1999. ISBN 978-3-642-08430-0.
(Cited on page 2.)

[22] Tim R. Morris. The exact renormalization group and approximate solutions. *International Journal of Modern Physics A*, 09(14):2411–2449, 1994. doi: 10.1142/S0217751X94000972. URL `http://www.worldscientific.com/doi/abs/10.1142/S0217751X94000972`.
(Cited on page 7.)

[23] Manfred Salmhofer and Carsten Honerkamp. Fermionic renormalization group flows: Technique and theory. *Progress of Theoretical Physics*, 105(1):1–35, 2001. doi: 10.1143/PTP.105.1. URL `http://ptp.oxfordjournals.org/content/105/1/1.abstract`.
(Cited on page 11.)

[24] T. Enss, V. Meden, S. Andergassen, X. Barnabé-Thériault, W. Metzner, and K. Schönhammer. Impurity and correlation effects on transport in one-dimensional quantum wires. *Phys. Rev. B*, 71:155401, Apr 2005. doi: 10.1103/PhysRevB.71.155401. URL `http://link.aps.org/doi/10.1103/PhysRevB.71.155401`.
(Cited on page 14.)

[25] Manfred Salmhofer, Carsten Honerkamp, Walter Metzner, and Oliver Lauscher. Renormalization group flows into phases with broken symmetry. *Progress of Theoretical Physics*, 112(6):943–970, 2004. doi: 10.1143/PTP.112.943. URL `http://ptp.oxfordjournals.org/content/112/6/943.abstract`.
(Cited on page 26.)

[26] Tobias Baier, Eike Bick, and Christof Wetterich. Temperature dependence of antiferromagnetic order in the hubbard model. *Phys. Rev. B*, 70:125111, Sep 2004. doi: 10.1103/PhysRevB.70.125111. URL `http://link.aps.org/doi/10.1103/PhysRevB.70.125111`.
(Cited on page 26.)

[27] Gaël Guennebaud, Benoît Jacob, et al. Eigen v3. http://eigen.tuxfamily.org, 2010.
(Cited on page 27.)

[28] The HDF Group. Hierarchical Data Format, version 5, 1997-2015. URL `http://www.hdfgroup.org/HDF5/`. http://www.hdfgroup.org/HDF5/.
(Cited on page 27.)

[29] OpenMP Architecture Review Board. OpenMP Application Program Interface Version 3.1. http://www.openmp.org/mp-documents/OpenMP3.1.pdf, July 2011. URL `http://www.openmp.org/mp-documents/OpenMP3.1.pdf`.
(Cited on pages 27, 30, and 64.)

[30] Message P Forum. Mpi: A message-passing interface standard. Technical report, Knoxville, TN, USA, 1994.
(Cited on page 30.)

[31] William H. Press, Brian P. Flannery, Saul A. Teukolsky, and William T. Vetterling. *Numerical Recipes in FORTRAN 77: The Art of Scientific Computing*. Cambridge University Press, Cambridge, 1992. ISBN 978-0521430647.
(Cited on page 31.)

[32] Richard B. Lehoucq, Chao-Chih Yang, and Danny C. Sorensen. *ARPACK users' guide: solution of large-scale eigenvalue problems with implicitly restarted Arnoldi methods*. SIAM, Philadelphia, 1998. ISBN 0-89871-407-9. URL `http://opac.inria.fr/record=b1104502`.
(Cited on page 36.)

[33] Alexander Branschädel. Electronic transport in interacting nanostructures: time-dependent density-matrix-renormalisation-group approach, 2011. Dissertation, Karlsruher Institut für Technologie 2011.
(Cited on pages 36 and 37.)

[34] R. Shankar. Renormalization-group approach to interacting fermions. *Rev. Mod. Phys.*, 66:129–192, Jan 1994. doi: 10.1103/RevModPhys.66.129. URL `http://link.aps.org/doi/10.1103/RevModPhys.66.129`.
(Cited on pages 38 and 55.)

[35] Steven R. White. Density matrix formulation for quantum renormalization groups. *Phys. Rev. Lett.*, 69:2863–2866, Nov 1992. doi: 10.1103/PhysRevLett.69.2863. URL `http://link.aps.org/doi/10.1103/PhysRevLett.69.2863`.
(Cited on page 50.)

[36] Karen A. Hallberg. New trends in density matrix renormalization. *Advances in Physics*, 55(5-6):477–526, 2006. doi: 10.1080/00018730600766432. URL `http://dx.doi.org/10.1080/00018730600766432`.
(Cited on page 50.)

[37] C. Karrasch and J. E. Moore. Approaching many-body localization from disordered luttinger liquids via the functional renormalization group. *Phys. Rev. B*, 92:115108, Sep 2015. doi: 10.1103/PhysRevB.92.115108. URL `http://link.aps.org/doi/10.1103/PhysRevB.92.115108`.
(Cited on page 51.)

[38] Kenneth G. Wilson. The renormalization group: Critical phenomena and the kondo problem. *Rev. Mod. Phys.*, 47:773–840, Oct 1975. doi: 10.1103/RevModPhys.47.

773. URL http://link.aps.org/doi/10.1103/RevModPhys.47.773.
(Cited on page 59.)

[39] W. Kohn. Nobel lecture: Electronic structure of matter—wave functions and density functionals. *Rev. Mod. Phys.*, 71:1253–1266, Oct 1999. doi: 10.1103/RevModPhys.71.1253. URL http://link.aps.org/doi/10.1103/RevModPhys.71.1253.
(Cited on page 59.)

[40] P. M. Ostrovsky, I. V. Gornyi, and A. D. Mirlin. Interaction-induced criticality in F_2 topological insulators. *Phys. Rev. Lett.*, 105:036803, Jul 2010. doi: 10.1103/PhysRevLett.105.036803. URL http://link.aps.org/doi/10.1103/PhysRevLett.105.036803.
(Cited on page 60.)

[41] Lars Hedin. New method for calculating the one-particle green's function with application to the electron-gas problem. *Phys. Rev.*, 139:A796–A823, Aug 1965. doi: 10.1103/PhysRev.139.A796. URL http://link.aps.org/doi/10.1103/PhysRev.139.A796.
(Cited on page 61.)

[42] P. Romaniello, S. Guyot, and L. Reining. The self-energy beyond gw: Local and nonlocal vertex corrections. *The Journal of Chemical Physics*, 131(15):154111, 2009. doi: http://dx.doi.org/10.1063/1.3249965. URL http://scitation.aip.org/content/aip/journal/jcp/131/15/10.1063/1.3249965.
(Cited on page 61.)

[43] Peter J. Denning. The locality principle. *Commun. ACM*, 48(7):19–24, July 2005. ISSN 0001-0782. doi: 10.1145/1070838.1070856. URL http://doi.acm.org/10.1145/1070838.1070856.
(Cited on page 63.)

[44] Intel Corporation. *Intel 64 and IA-32 Architectures Optimization Reference Manual*. September 2015.
(Cited on page 67.)

[45] Henry S. Warren. *Hacker's Delight (2nd Edition)*. Addison-Wesley Professional, 2012. ISBN 978-0321842688.
(Cited on page 67.)